

# Fully Reactive 3D Inkjet Printing of Polydimethylsiloxane and Polyurethane

By

Craig Sturgess

A doctoral thesis submitted in partial  
fulfilment of the requirements for the award  
of doctor of philosophy of Nottingham  
University

Department of Mechanical, Materials, and  
Manufacturing Engineering

June 2017

## ***Abstract***

Additive Manufacturing (AM) encompasses several different technologies, such as inkjet printing, extrusion, and laser melting processes, to selectively transform a processable phase, such as a liquid or powder, to a solid phase, e.g. through solidification, chemical reaction or powder melting and solidification. The geometry is initially defined as a 3D CAD model, which is subsequently ‘sliced’ to create a geometrical representation suitable for the layer-wise manufacturing process. These layers are “printed” in series on a substrate and are additively stacked. Some AM processes can also include multiple materials or voids in this process to increase the design freedom and geometric complexity.

With any new process there are challenges, the key one for most AM processes is the limited material selection. Different processes have different material requirements and many current AM materials are sourced from other processes, for example a number of stereolithography processes use materials originally developed as finishes or coatings. The various AM processes have different criteria that must be met for a material to be suitable for processing, such as particle size and distribution, melting temperature and laser absorption in the case of laser-powder bed systems. This PhD is concerned with materials for ink jet printing, a major advantage of this process being the capability to co-deposit different materials.

As the materials in jetting are not fed from a single bed or on a platform, there is complete control over material placement. The basic technology behind material jetting is the same as that seen in desktop inkjet printers, and the major challenge in transforming this to a 3D printing method is in materials development. Currently, the process is dominated by fast curing UV based resins, which are primarily acrylate based, and solvent based inks. The solvent inks highlight their 2D printing origins as they have a low material

loading resulting in thin layers. These solvent systems are typically used to transport a conductive solute e.g. silver nanoparticles or graphene oxide.

The focus of this PhD was to develop new materials for AM jetting by combining reactive components during processing. This process, called Fully Reactive Inkjet Printing (FRIJP), is only possible because of the freedom of material jetting to use multiple materials. In this work two reactions were selected for the development of FRIJP inks. The first was the crosslinking of polysiloxane based polymers (PDMS), the second was the addition polymerisation of polyurethane. These two reactions schemes were chosen because they involve the combination of two different reactive species and produce no unwanted by-products.

For the FRIJP of PDMS a commercial two-part chemistry was used that separated the cross-linker and catalyst. When these two components are combined they produce a transparent PDMS rubber. The PDMS was found to have a viscosity that was too high for inkjet printing so a compatible solvent was selected and the concentration modified. Once a printable ink had been created, trials were conducted which involved printing the two components onto a substrate. It was found that by control of the mixing ratio and substrate heating, high reaction rates could be achieved and complex designs could be printed. These designs were then analysed using FTIR and Raman spectroscopy and it was found that there was comparable curing to the bulk mixing. It was also determined that for the selected PDMS there were no issues with substrate mixing which would result in concentration gradients.

The second reaction investigated was the addition polymerisation of polyurethane, which involves combination of the diol and diisocyanate. For this work, the inks were developed from monomers that had printable viscosities through thermal modification.

However, one ink used did contain a low concentration of solvent. For the polyurethane work the printing environment was controlled to minimise the moisture which could produce unwanted polyurea and amines. The metric used to determine how suitable the inks were for inkjet printing was the molecular weight of the polymer chain. The analysis was conducted using Size Exclusion Chromatography on the printed samples. It was found that after in development, it was possible to achieve an average molecular weight over 20,000, which was identified as the point whereby the polymer printing was successful.

This PhD also demonstrates that when printing these two chemistries, the small size of the droplets facilitates complete mixing of the inks. Importantly, with the immiscibility of the polyurethane monomers before reaction, it was found that the small droplet size allowed for the reaction and successive molecular diffusion to achieve the high degrees of conversion required for the production of functional polymers.

## *Acknowledgements*

Partner: Lauren Sturgess

Colleagues: Luke Parry  
Yinfeng He  
Fan Zhang  
Belen Begines  
Javier Ledesma  
Amanda Hüsler

Supervisors: Ricky Wildman  
Ian Ashcroft  
Chris Tuck

## ***Publications***

### *Manuscripts Published (Frist Author)*

#### **3D Reactive Inkjet Printing of Polydimethylsiloxane<sup>1</sup>**

Sturgess, C., Tuck, C. J., Ashcroft, I. A. & Wildman, R. D. 3D reactive inkjet printing of polydimethylsiloxane. *J. Mater. Chem. C* **5**, 9733–9743 (2017).

### *Manuscripts Published (Named Author)*

#### **3D Printing of Biocompatible Supramolecular Polymers and their Composites<sup>2</sup>**

Hart, L. R. et al. 3D Printing of Biocompatible Supramolecular Polymers and their Composites. *ACS Appl. Mater. Interfaces* **8**, 3115–3122 (2016).

#### **Inkjet printing of polyimide insulators for the 3D printing of dielectric materials for microelectronic applications<sup>3</sup>**

Zhang, F. et al. Inkjet printing of polyimide insulators for the 3D printing of dielectric materials for microelectronic applications. *J. Appl. Polym. Sci.* **133**, 43361 (2016).

### *Conference Presentations*

**A method for assessing the rates of mixing and reaction in Reactive Ink Jet Printing (RIJP)** - International Solid Freeform Fabrication Symposium An Additive Manufacturing Conference, August 2015, Austin Texas.

## ***Table of Contents***

Abstract .....	ii
Acknowledgements .....	v
Publications .....	vi
Table of Contents .....	vii
Table of Abbreviations .....	x
Table of Figures .....	xii
1 Introduction .....	1
1.1 Background .....	1
1.2 Aim of Research .....	5
1.3 Research Methodology .....	6
1.3.1 Statement of Novelty .....	7
1.4 Structure of Thesis .....	8
1.4.1 Thesis chapters .....	9
2 Literature Review .....	11
2.1 Introduction and Structure .....	11
2.2 Material Jetting .....	12
2.2.1 The 3D Material Jetting Process .....	14
2.2.2 Solidification Mechanisms .....	15
2.2.3 Ink Ejection .....	17
2.2.4 Ink Deposition .....	26
2.3 Chemistry .....	35
2.3.1 Polydimethylsiloxanes .....	35
2.3.2 Polyurethane .....	39
2.4 Fully reactive ink jetting .....	51
2.5 Gaps In Research .....	54
2.5.1 Statement Of Novelty .....	54
3 Materials and Methods .....	57
3.1 Materials .....	57
3.1.1 PDMS .....	57
3.1.2 Polyurethane .....	58
3.2 Methods .....	61
3.2.1 Material Rheology .....	63
3.2.2 Printability Assessment .....	67
3.2.3 FRIJP Printing .....	70
3.2.4 Chemical Analysis .....	72

3.2.5	Profile Analysis.....	76
3.3	Summary.....	77
4	Developed Jetting Methods.....	78
4.1.1	Print Head.....	79
4.1.2	Aerotech Printer.....	84
4.1.3	LP50 Printer.....	88
4.1.4	Line Printing.....	90
4.2	Discussion.....	95
5	FRIJP of Polydimethylsiloxane.....	96
5.1	Results.....	96
5.1.1	Printing on Setup 1.....	100
5.1.2	Printing on Setup 2.....	103
5.1.3	Printing on Setup 3.....	107
5.2	Discussion.....	116
6	FRIJP of Polyurethane: Immiscible Components.....	120
6.1	Results.....	121
6.1.1	Ink Development.....	121
6.1.2	Line Substrate Microscopy.....	124
6.1.3	Printed Sample Microscopy.....	130
6.1.4	Profile Analysis.....	133
6.1.5	SEC and NMR-FTIR Data.....	137
6.2	Discussion.....	142
7	FRIJP of Polyurethane: Miscible Components.....	144
7.1	Results.....	144
7.1.1	Ink Development.....	145
7.1.2	Printed Line Microscopy.....	146
7.1.3	Droplet volume microscopy.....	147
7.1.4	SEC and NMR Data.....	149
7.1.5	Profile Analysis.....	153
7.2	Discussion.....	155
8	Discussion.....	158
8.1	Mixing in FRIJP.....	158
8.2	Substrate heating.....	162
8.3	Evaporation.....	164
8.4	Printed Profiles.....	165
8.5	Unexpected Challenges.....	166

---

8.6	Summary and Novelty .....	167
9	Conclusions and Future Work.....	170
9.1	Conclusions .....	170
9.1.1	Conclusions: FRIJP .....	170
9.1.2	Conclusions: PDMS .....	171
9.1.3	Conclusions: PU.....	173
9.2	Future Work.....	174
9.2.1	Investigation of other poly-addition reactions .....	174
9.2.2	Conduct mechanical analysis.....	175
9.2.3	Droplet diameter .....	175
9.2.4	Monomers as a support .....	176
9.2.5	Functional grading.....	176
10	References.....	177

## *Table of Abbreviations*

### **Chemicals**

BDO	Butanediol
CNO	Carbon - Nitrogen - Oxygen (Isocyanate Group)
DBDT	Dibutyltin Dilaurate
DMF	Dimethylformamide
DMSO	Dimethyl Sulfoxide
HDI	Hexamethylene Diisocyanate
HMDI	Hydrogenated MDI
IPA	Isopropyl Alcohol
MDI	Methylene Diphenyl Diisocyanate
OH	Oxygen Hydrogen (Hydroxyl Group)
PDMS	Polydimethylsiloxane
PEG	Polyethylene Glycol
PFOTS	1H,1H,2H,2H-perfluorooctyltriethoxysilane
PTFE	Polytetrafluoroethylene
PU	Polyurethane
PUR	Polyurea
TPG	Tripropylene Glycol
TPU	Thermoplastic Polyurethane

### **Devices**

AFG	Arbitrary Function Generator
ATR	Attenuated Total Reflection
AUX	Auxiliary
CCD	Charge-Coupled Device
DMC	Dimatix Material Cartridge
DMP	Dimatix Material Printer
FPGA	Field Programmable Gate Array
FTIR	Fourier Transform Infrared Spectroscopy
GND	Ground
GPC	Gel Permeation Chromatography
NMR	Nuclear Magnetic Resonance
MOSFET	Metal Oxide Semiconductor Field Effect Transistor
OP-AMP	Operation Amplifier
PGM	Program
PSO	Position Synchronised Output
PZT	Piezoelectric ceramic
SEC	Size Exclusion Chromatography
SEM	Scanning Electron Microscope

### **Processes**

AM	Additive Manufacture
CIJ	Continuous Inkjet Printing
FRIJP	Fully Reactive Inkjet Printing
GOF	Goodness Of Fit
PID	Proportional Integral Differential (Control Algorithm)

PWM	Pulse Width Modulation
RIJP	Reactive Inkjet Printing
TTL	Transistor Transistor Logic
UV	Ultraviolet
<b>Software</b>	
BMP	Bitmap
CAD	Computer Aided Design

## ***Table of Figures***

Figure 1-1 Flow chart showing the process of research during this doctoral thesis. Showing the development of the RIJP ink and printer with final work on RIJP of polyurethane immiscible and miscible chemistries. ....	8
Figure 2-1 - The process of material jetting to build three-dimensional object.....	12
Figure 2-2 - CIJ and DoD process of ink ejection. Left: CIJ, Right: thermal (a) and PZT (b). Figure reproduced from Derby <sup>12</sup> . ....	13
Figure 2-3 - DoD piezoelectric operation modes, figure taken from Wijshoft <sup>11</sup> , reproduced with permission of rights holder. ....	14
Figure 2-4 – Generation of short liquid jet in the DoD process. This image was capture with a single exposure camera, with a duration of 8 nS, image taken from Bos <sup>25</sup> , in this case the tail re-joins the primary droplet so no satellites are formed. Reproduced with permission from rights holder. ....	18
Figure 2-5 - Results of the study conducted by Ohnesorge, the X axis is the Reynolds number, whereas the Y axis is now called the Ohnesorge number (Taken from the doctoral thesis). <sup>26</sup> .....	19
Figure 2-6 - Velocity of droplet ejecting a nozzle, left is the experimental, right is the numerical result. Figure from Van Der Bos, <sup>25</sup> reproduced with permission from rights holder.....	22
Figure 2-7 - "Drop volume normalized to the volume displaced by the actuator..." studying the relationship between $Oh$ ( $1/Z$ ) and the dispensed droplet volume. From Reis <sup>40</sup> reproduced with permission from license holder.....	23
Figure 2-8 - Left: Newtonian fluid printed at 32V (a) and 35V (b). Right: Non-Newtonian fluid printed at 32V (a) and 35V (b). Observed is the apparent "beads-on-a-string" phenomena. Reproduced from Hoath. <sup>42</sup> .....	24

- Figure 2-9 – Change in molecular weight of polystyrene solutions before (solid) and after (dashed) inkjet printing. Dimatix 10 pL cartridge was used with a 21  $\mu\text{m}$  nozzle diameter. Figure reproduced from A-Alamry<sup>43</sup> with permission of rights holder. .... 25
- Figure 2-10 - Surface profile analysis of a printed solvent based ink. The 1 %wt polystyrene was in ethyl acetate solution, printed onto perfluorinated glass. Evaporation and successive coffee-staining was observed. Figure taken from Gans,<sup>59</sup> reproduced with permission of rights holder. .... 29
- Figure 2-11 - The results from the experimental and numerical investigation of printing liquid lines by Thompson.<sup>50</sup> a-d) are the drop spacings as a function of droplet diameter. Model I is the case with no resistance, Model II resists flow through the viscosity term. Reproduced with permission from rights holder. .... 31
- Figure 2-12 - Hydrolysis reaction of a dichlorosilane to produce a polysiloxane and hydrochloric acid. <sup>14,71</sup> ..... 35
- Figure 2-13 - Crosslinking reaction schemes for polysiloxanes. a) peroxide free radical crosslinking, b) addition crosslinking between silicone hydride and vinyl functional polysiloxane in the presence of a platinum catalyst, c) condensation crosslinking between polysiloxane and acid based cross-linker in the presence of tin catalyst. .... 37
- Figure 2-14 - Phase mixed to phase separated polyurethane. Showing the soft segments and hard segments in the polyurethane network. Figure reproduced with permission from the rights holder.<sup>82</sup> ..... 40
- Figure 2-15 - Addition reaction between an isocyanate and hydroxyl end groups. The urethane linkage is typically formed in the presence of a suitable catalyst. .... 40
- Figure 2-16 - The result of varying the percent conversion, or the monomer ratio, on the final polymer average molecular number.  $r$  is the actual mixing ratio, where  $r=1$  is the ideal stoichiometric case. 43
- Figure 2-17 - Reaction of isocyanate with water, forming an amine, which can then react with isocyanate and form a urea linkage. This

reaction produces CO<sub>2</sub> gas, and is key in the production of rigid and flexible PU foam..... 44

Figure 2-18 “Schematic diagram showing the different regions and physicochemical processes considered in the modelling of interfacial polycondensation. Note the regions in which external mass transfer, molecular diffusion, and reaction kinetics operate and the use of the partition coefficients to treat phase equilibria for HMDA at the interfaces”. HMDA is an amine (instead of a diol in a urethane), organic phase is isocyanate subscript O, aqueous phase is amine (diol in urethane) subscript A. Figure reproduced from Dhumal<sup>90</sup> with permission from the right holder. .... 46

Figure 2-19 - "Interfacial polymerization at 25°C: top phase, BDO + 0.1 %wt catalyst; bottom phase, diisocyanate. Time (a) 0s; (b) 10 min;(c) 20 min; (d) 20 min (crossed polarizers)” Figure reproduced with permission from Fields 1986.<sup>91</sup> BDO = Butanediol, Catalyst = Dibutyltindilaurate..... 47

Figure 2-20 - Confocal laser scanning microscopy tracking a fluorescent dye included into the polyol components. Images represent an unknown time series, top is reflectance, bottom is fluorescence. Reproduced from Kröber<sup>9</sup> with permission from rights holder..... 51

Figure 3-1 – The components of the PDMS purchased as Polytek Platsil 71-Siliglass, the formula are estimated and the molecular weight unknown..... 58

Figure 3-2 - H<sub>12</sub>MDI chemical structure, *cis-cis*, isomer..... 58

Figure 3-3 - Chemical structure of Hexamethylene Diisocyanate... 59

Figure 3-4 - Chemical structure of 1,4 Butanediol. .... 59

Figure 3-5 - Chemical structure of Tripropylene Glycol..... 59

Figure 3-6 - The chemical structure of Polyethylene Glycol. The molecular weight used in this study was M<sub>n</sub> = 1000. .... 60

Figure 3-7 - Geometries used in rheological measurements. First the cone and plate, secondly the concentric cylinder. .... 64

Figure 3-8 - Example of data when the scan is conducted over a shear rate of  $1 - 1000 \text{ s}^{-1}$ . Sample is Tripropylene glycol ..... 65

Figure 3-9 - KRUSS DSA100, pendant drop of  $\text{H}_{12}\text{MDI}$  (diisocyanate). Red region defines the analysis zone, blue lines are user specified limits, and the green line is calculated profile fit. .... 66

Figure 3-10 - Dimatix Material Cartridge, the cartridge is shown in the two pieces, on the top the fluid bladder and pressure chamber, on the bottom the nozzle plate and connector. From the DMP 2800 User Guide.<sup>117</sup> ..... 68

Figure 3-11 - The Dimatix software, the three windows used when developing a new ink. Top-left, the waveform editor where the voltage controlling the PZT can be changed. Top-right, the voltage for each nozzle, to balance velocity of droplets each nozzle can have its own voltage. This page has multiple tabs to also control the pressure and temperature. Bottom, the dropwatcher view, in this menu you can toggle the nozzles, change the jetting frequency, switch from still to video, and run cleaning cycles. .... 69

Figure 3-12 - LP50 Printer inside the glove box. The front panel is currently off but when in place access is through the side chamber. .... 71

Figure 4-1 - Layer and line printing strategy, yellow = ink A, blue = ink B, green = product. .... 79

Figure 4-2 - Dimatix DMP Cartridge. (a) Image of an actual cartridge showing the assembly of fluid bladder and nozzle plate. (b) Function of each contact on the print head. (c) Disassembled cartridge where all structural components are removed. (d) Destroyed nozzle plate exposing the fluid channels, these pass over the PZT and to the nozzles. .... 80

Figure 4-3 - Schematic of the control of Dimatix nozzles with the Dimatix printer. .... 81

Figure 4-4 - Schematic of the Print Head Controller designed to take a single trigger input and output a complex waveform.....	81
Figure 4-5 - Dimatix Print Head Controller, a device which accepts a 0-2.5 V waveform, amplifies it to 30V (Gain 15) and control the internal heater. ....	83
Figure 4-6 - Printer stage 1 Aerotech stage with Dimatix print heads .....	84
Figure 4-7 - Result of using the WINDOW and DISTANCE command to control droplet placement. Where $C = 30$ , $A_1 B_1 A_2 B_2 = 300,500,650,800$ respectively. A value of 1 reflect a print signal.....	85
Figure 4-8 - Process for creating Aerobasic PGM file from a BMP..	86
Figure 4-9 - Generated code snippet from the Labview software for driving the print head.....	87
Figure 4-10 - Un-modified LP50 printer. a) Print head carriage, translation in X and Z. b) Pressure feed and overflow resevoir. c) Substrate camera. d) Print substrate, heated and vacuum chuck, translation in Y. e) Cleaning station. f) Dropview area. ....	88
Figure 4-11 - Dual Dimatix assembly for the LP50 printer. Heads A and B are interfaced through the actual Dimatix interface device (sourced as spares). These are mounted on a metal plate, connected to a laser sintered hub. The whole assembly can rotate up to 90° counter clockwise. ....	89
Figure 4-12 - Aligning the print head nozzles through rotation of the print assembly. With a zero $X_{\text{offset}}$ in a single pass both materials can be printed. ....	91
Figure 4-13 - Creating a line printed sample through the manipulation of the printing pattern. The printing pattern has two duplicate patterns with an offset equal to that of the nozzle spacing. ....	92
Figure 4-14 - Creating fractional droplet spacing through supersampling printing pattern. Achieving a droplet ratio of 1:3.5364.	

Without this method only 1:3.5 could be achieved, an error of over 1%. In this image the space between the two patterns has been reduced.  
..... 93

Figure 5-1 - Crosslink reaction of PDMS in the presence of a platinum catalyst, the silicone hydride bond Si-H is replaced with a Si-C bond when the C=C bond opens, and the hydrogen relocates to the new carbon. The compounds in each component of the PDMS formulation are labelled, as specified in the MSDS..... 96

Figure 5-2 - PDMS, and PDMS ink viscosity versus temperature. A printable viscosity was achieved when using 40% Octyl Acetate as a solvent..... 97

Figure 5-3 - Jetting process of Ink A. Duration of the capture is 100  $\mu$ s, droplet diameter is 20  $\mu$ m. Image series captured using the Dimatix drop watcher camera. .... 98

Figure 5-4 – A printed droplet grid comprising both Ink A and Ink B, resulting in cured PDMS spherical caps. The three substrates are a) cleaned glass slide b) on a pre-prepared PTFE coated slide and c) PFOTS-glass. It was found that the most circular and smallest droplet size was produced on the PFOTS glass. .... 101

Figure 5-5 - Image of printed film. The substrate temperature was 80 °C, the solid material was observed immediately. .... 101

Figure 5-6 – Substrate microstructuring, disconnected droplet printing to maximise the effect of pinning on a substrate where single PDMS ink does not pin. (a) a single layer of each component, Ink A and B is deposited, the initial spacing of the ink is such that the Ink A does not coalesce. (b-d) additional layers printed onto the grid, controlled spreading occurs and finally a continuous film is produced.  
..... 102

Figure 5-7 – (a) Microscope (Nikon ECLIPSE LV100ND) image of a printed film, and (b) SEM (Hitachi Analytical Benchtop SEM TM3030) image of a printed film, sample platinum coated for 90 s, printed on a polished PTFE substrate heated to 80 °C. High sample wavyness was caused by the initial microstructured film process, visible in the microscope image, the SEM image however. To confirm that the sample was a continuous film the top left corner was peeled.  
..... 103

Figure 5-8 – 4 mm<sup>2</sup> PDMS samples consisting of 50 reacted layers printed on a PDMS microstructured, PFOTS coated glass slide. The images show that the printed films are still very transparent despite being produced in discrete layers and lines. .... 104

Figure 5-9 - Profiles of the printed PDMS using the layer method. (a) printed at substrate temperature of 40 °C, (b) 60 °C, (c) 80 °C. Missing data is due to either high angles that are unscannable or the replication process causing incorrect replication..... 105

Figure 5-10 – (a) total spectra for printed samples and the liquid inks (b) quantified residual crosslink component in each printed sample in relation to uncured part A also included are cast samples created at 1:1 2:1 3:1 A:B ratio, data is shown as mean ± standard deviation (XY: n = 75, Z: n = 50). .... 107

Figure 5-11 - Samples printed using setup 3 with PDMS..... 108

Figure 5-12 - Determination of the minimum drop spacing for stable line formation of printed PDMS. Ten layers of five lines were printed at different drop spacings. Number of layers increasing from left to right. .... 109

Figure 5-13 - FRIJP Line strategy printing directly onto the PFOTS-glass. The substrate temperature is 80 °C..... 110

Figure 5-14 - Stepped ziggurat, 4x4 mm PDMS consisting of 5 steps, each printed with 30 reactive layers. .... 110

Figure 5-15 - Printing PDMS directly onto PDMS substrate. First step in the ziggurat design. Substrate heated to 80 °C..... 111

Figure 5-16 - Profile analysis of the stepped ziggurat printed design conducted on the Alicona. (a) line scans immediately before a step in X, (b) line scans in Y, (c) area profile, with highlights where line scans were taken from. .... 113

Figure 5-17 - Gaussian curve fitting to the FTIR spectra. The sample was the 1:1 calibration, scan 1. a) the calibration peak fitting b) the

fit at  $912\text{ cm}^{-1}$ , used for determination c) alternative low intensity peak at  $2150\text{ cm}^{-1}$  not used due to increasing noise..... 114

Figure 5-18 - Residual cross link component Si-H in the calibration and printed samples. The bond at  $912\text{ cm}^{-1}$  was used to determine the residual. The errors are from the curve fitting GOF of both the calibration and residual combined. .... 115

Figure 6-1 - Viscosity modification of the polyethylene based ink. There was a noticeable reduction in viscosity upon adding the butanediol, but further reduction was required. The final formulation contained 15 %wt DMF, achieving a printable viscosity at temperatures above  $60^{\circ}\text{C}$ . The data was selected from the stable shear rate range and the exponential model was used to fit the points (as described in 3.2.1 Material Rheology) ..... 122

Figure 6-2 - The viscosity temperature profiles for the inks chosen for immiscible PU printing. HDI ink has a printable viscosity over the total temperature range, the other inks require heating above  $50^{\circ}\text{C}$ . The data was selected from the stable shear rate range and the exponential model was used to fit the points (as described in 3.2.1 Material Rheology)..... 123

Figure 6-3 - Post printing reaction of  $\text{H}_{12}\text{MDI}$  and butanediol printed at  $30^{\circ}\text{C}$ . Suspected satellite formation produced single droplets.. 125

Figure 6-4 - Post printing reaction of  $\text{H}_{12}\text{MDI}$  and butanediol printed at  $30^{\circ}\text{C}$ . Repeated without the satellite formation. .... 125

Figure 6-5 - Post printing of  $\text{H}_{12}\text{MDI}$  and butanediol printed at a)  $50^{\circ}\text{C}$ , b)  $70^{\circ}\text{C}$ . There is apparent increase in uniformity of the printed lines. .... 126

Figure 6-6 - Post printing of a)  $\text{H}_{12}\text{MDI}$ , and b) butanediol, both monomers are printed at  $50^{\circ}\text{C}$ . It is observed that considerable evaporation of the butanediol occurs, with no visible reaction or evaporation of the  $\text{H}_{12}\text{MDI}$ . .... 127

Figure 6-7 - Post printing reaction of HDI and butanediol. Printed at  $30^{\circ}\text{C}$ ..... 127

Figure 6-8 - Multiple layer printing and imaging of HDI and butanediol. Printed at 30 °C. The time units are from the first capture of an image after printing a layer. .... 128

Figure 6-9 – Three successive layers of printed H<sub>12</sub>MDI and PEG BDO. Printed at 30 °C. Drop spacing set to 45 μm to increase separation. Showing how the initial printed layers segregated and how the later layers did not..... 129

Figure 6-10 - The last three layers of a five layer print of H<sub>12</sub>MDI and PEG BDO. Printed at 30 °C. Drop spacing set to 40 μm. Print, refers to image capture immediately after printing; while Cure, is an image taken immediately before printing the next layer..... 129

Figure 6-11 - Nucleation and growth of a phase separation was observed in the printed lines. A three layer print of H<sub>12</sub>MDI and PEG BDO. Printed at 30 °C. Drop spacing set to 40 μm..... 130

Figure 6-12 - Difference between printing a) line by line and b) layer by layer. The line stability is increased due to the reaction between each deposited line. Printed at 30 °C, with H<sub>12</sub>MDI and butanediol. .... 131

Figure 6-13 - Comparison of printing H<sub>12</sub>MDI and BDO at different substrate temperatures. a) 30 °C, b) 50°C, c) 70 °C. Pore size is seen to reduce and disappear on increased heating. .... 131

Figure 6-14 - Residual unmixed monomer on top of the printed PU. a) unwashed printed sample, b) sample washed with IPA. Sample printed at 30 °C. .... 132

Figure 6-15 – Cross polarisation imaging of printed PEG based PU. Sample was printed at 70 °C, a) unwashed - unpolarised, b) washed – unpolarised, c) unwashed - polarised, d) washed - polarised. It was found that only the PEG polarised light, whilst the PEG-PU did not. .... 133

Figure 6-16 - Surface profile data from the printed H<sub>12</sub>MDI and butanediol, substrate temperatures were (a) 30 °C, (b) 70 °C. The elevated substrate temperature reduced pore formation but resulted in large volume reduction. Samples were printed in the positive Y direction..... 134

Figure 6-17 – The samples of PEG-BDO-PU were the only samples which could be removed from the substrate. They were also shown to be flexible.....	135
Figure 6-18 – Surface profile data from the printed H <sub>12</sub> MDI and PEG-BDO, substrate temperatures were (a-c) 30 °C, 50 °C, and 70 °C. Samples were washed to remove any residual unreacted components. ....	136
Figure 6-19 - Surface profile data from the printed H <sub>12</sub> MDI and PEG-BDO, samples were unwashed (a) and washed (b), printed at 70 °C. NM stands for not measured, and was caused by bubble formation in the replica, for the case of the washed sample the NM data was 0 μm height.....	137
Figure 6-20 - Chromatogram from the SEC analysis of the inkjet printed polyurethane sample. Specific sample was Fast Printing 70 °C.....	140
Figure 6-21 - Chromatogram from the SEC analysis of the inkjet printed polyurethane sample. Specific sample was PEG 1 30 °C. .	140
Figure 6-22 - Chromatogram from the SEC analysis of the inkjet printed polyurethane sample. Specific sample was PEG 1 50 °C. .	140
Figure 6-23 - Chromatogram from the SEC analysis of the inkjet printed polyurethane sample. Specific sample was PEG 1 70 °C. .	141
Figure 7-1 - Viscosities of the inks used in printing the miscible polyurethane polymer. Both inks required only thermal modification to achieve a printable viscosity. The data was selected from the stable shear rate range and the exponential model was used to fit the points (as described in 3.2.1 Material Rheology) .....	145
Figure 7-2 - Determination of suitable drop spacing for the H <sub>12</sub> MDI and TPG polyurethane on glass. (a-e) 35, 50, 65, 80, 95 μm.....	147
Figure 7-3 - Result of optical droplet volume analysis conducted on TPG. Multiple layers of TPG were printed in a grid on glass.....	148

Figure 7-4 - Example image of a grid of TPG printed onto glass slides. On the right of the glass the contact angle is different, this causes issues in optical drop volume determination. .... 149

Figure 7-5 - Chromatogram from the SEC analysis of the inkjet printed polyurethane sample. Specific sample was B 100 °C. .... 151

Figure 7-6 - Chromatogram from the SEC analysis of the inkjet printed polyurethane sample. Specific sample was A 30 °C. .... 151

Figure 7-7 - Printed miscible polyurethane sample profiles obtained through Alicona. Samples are: (a) 50 °C (b) 50 °C + 100 °C (c) 100 °C (d) 100 °C + 100 °C..... 154

Figure 7-8 – Total volumes of printed samples for the miscible polyurethane profiles. Samples were printed onto a substrate of either 50 °C or 100 °C and post treatment at 100 °C was carried out on a subset..... 155

# *1 Introduction*

## **1.1 Background**

Additive manufacturing (AM), also known as 3D printing, is an advanced processing method for fabricating complex components consisting of one or more materials. Through the addition of many layers initially exposed surfaces later become internal features of the component. Additional functionality or complexity can be achieved through the combination of many materials on this exposed surface and this affords AM processes increased design freedom over conventional manufacture. Finally, without the need for tooling this design freedom is provided with no impact on the marginal cost of manufacture.

There are many AM technologies but it is the material jetting process, with the ability of including multiple components in a highly scalable manner, which is the focus of this research. Material jetting is an AM process whereby liquid inks are ejected from printing heads onto a substrate, after which the ink becomes solid through a range of possible mechanisms. Until solidification the process is identical to a desktop inkjet printer, the difference being that in 3D inkjet printing the previous ink layers support the next and a structure is assembled. In this manner, the process can change materials (colours of ink) and design (text on a page) at each layer. The total process offers a design freedom not experienced in conventional manufacture.

At the core of material jetting are the print heads, which are complex devices with many jetting nozzles. A single print head has the capability of outputting  $30 \text{ g}\cdot\text{min}^{-1}$  of material with 0% wastage (if solvent is not used).<sup>4</sup> The process is highly scalable, and with additional print heads there are directly increased build volumes and

processing speeds. Industrially the material jetting process has seen adoption in large scale manufacture, for example, semiconductors, printed electronics, displays, PCBs, and photovoltaics. These two-dimensional products involve a small number of layers which produce thin structures.

The AM process, however, requires the deposition of many layers so roll-to-roll processing is not currently employed. Instead small-scale manufacture has seen adoption of free standing printers such as PolyJet (Stratasys), and ProJet (3D Systems) machines. These printers can have build volumes around 1000 mm x 800 mm x 500 mm (Objet1000 Plus), but are limited in their material capabilities. They primarily use photo-curable resins designed for prototyping, which only have a very limited end use capability.

*“RM [AM] will become more of a reality when the properties of the materials that are produced become more acceptable and consistent”<sup>5</sup>*

**- N Hopkinson, R Hague, P Dickens – pg 18**

This quote highlights what the main barrier to AM currently is, and this is found across all seven<sup>6</sup> AM techniques. There is a limitation on the range of materials available, and particularly for AM polymers the process of manufacture can reduce their performance (e.g. are mechanically inferior). Material jetting is dominated by Reactive Inkjet Printing (RIJP), where a liquid undergoes a chemical change after deposition. The reaction scheme is usually UV initiated cross-linking, and free radical polymerisation occurs using a UV initiator. These materials include an acrylate group, which when initiated, reacts to form highly cross-linked 3D networks. Acrylate based polymers are used due to their fast curing rate and ease of processing, however, shrinkage is between 10-20%.<sup>7</sup> Part shrinkage during printing can lead to part deformation and high internal residual stresses. The residual stresses in material jetting photo-curable parts

can lead to poor high temperature stability, where prolonged heating can cause excessive warpage.

For these reasons, there is a desire for a larger range of materials, which has been pushing research into liquid-solid transition mechanisms. Where RIJP provided an alternative to melt and solvent based inks, now Full Reactive Inkjet Printing (FRIJP) aims to further increase the range of processable materials.<sup>8</sup> Using the FRIJP method the materials consist of two inks, where the contact between these causes a reaction. Without the need for acrylate monomers, FRIJP allows for reaction schemes other than free-radical polymerisation. This research involves the addition cross-linking of polydimethylsiloxane (PDMS) and the addition polymerisation of polyurethane (PU). The primary difference between these reactions and the acrylate group is that the functional groups only react with one monomer. This means monomers need to have two or more functional groups to form chains, and when these chains are produced the monomer becomes part of the polymer backbone. For acrylate based polymers the reactive groups open to react with two monomers, therefore the primary backbone is only formed of repeated acrylate links. This freedom to control how the backbone is structured allows for increasing variety in the final polymer.

The reaction schemes of PU and PDMS are understood for conventional manufacturing, where mechanical stirring in controlled reactors occurs. However, it is not known if FRIJP can yield desirable mixing in these cases. Material jetting printers cannot include stirring on the substrate, so it is only through dispersion of the two materials in small droplets that this mixing can be achieved. There are many processes in play: ejection of these reactive monomers, deposition onto solid or liquid surfaces, surface tension and contact angle driven flows, mixing of the components, and the reaction to produce solid polymers. Whilst some of these processes are

understood and discussed in the literature section, there are no examples available that sufficiently examine the total FRIJP process.

The first preliminary FRIJP of PU was conducted by Kröber<sup>9</sup>, but the work conducted contained no chemical analysis of the produced samples with no indication of the polyurethane reaction occurring. The PU printing aspects also looked at a highly crosslinked network which would already be possible through acrylate monomers. This PhD aims to investigate linear polyurethane without chemical cross-links. One formulation used is for thermoplastic polyurethane (TPU). The produced polymer would therefore be soluble in some solvents and able to be processed with heat. This system is particularly challenging as mechanical properties are highly dependent on the degree of mixing, with only very high conversion leading to a solid with desirable properties.

The printing of PDMS has recently been demonstrated,<sup>10</sup> but this consisted of premixed chemical components, which leads to limited ink stability. The inks were also highly viscous leading to a large nozzle size, and a low feature resolution. AM processing was not developed and the individual drops were used as lenses. In this study, the cross-linker and catalyst are deposited in separate inks. Once mixed, they react to form a highly cross-linked polymer. Although obtainable through acrylate modification of siloxanes this process would reduce the chemical resistance of the polymer. FRIJP instead allows for a pure PDMS solid, with high chemical resistance and light stability. This ink was used to produce complex geometries in three dimensions.

Demonstrating the FRIJP of PU and PDMS adds two new materials to the catalogue of practical 3D ink-jetting materials. The work involving the PU also shows that high levels of mixing are possible, which facilitates the use of other PU formulations already developed in industry. PU polymers can have various properties dependent on

the constituent monomers, and in this study the FRIJP of a thermoplastic polyurethane is demonstrated. However, PU is not limited to thermoplastics as there are thermosets, foams, elastomers, and plastics all available through changing the monomers or using additives.

Although FRIJP is a solidification mechanism, the required separation of reactive components facilitates the printing of functionally graded solids. Through variation of the mixing ratio or the addition of another ink, continuous solids with varying chemistry can be achieved. In the simplest case this could be variation in the cross-linker to achieve a hardness profile. In complex cases it could be the variation of monomers to produce both hard and flexible plastics. Components such as toothbrushes are produced using a two-shot injection moulding method, whereby a hard plastic is first cast and then placed inside a secondary mould. FRIJP has the capability to produce this variation in a single process, this reduces manufacturing complexity and facilitates increasing design complexity.

## 1.2 Aim of Research

The aim of this PhD is to identify the process conditions to enable FRIJP of polymeric materials. The following objectives were identified for this PhD;

- Create a printer for the FRIJP process to better understand the process requirements of the manufacturing method.
  - A research focused printing setup, based on industrial piezo-driven inkjet print heads.
- Investigate FRIJP formulations to determine what parameters, past the rheological requirements of jetting, are required for a successful ink.
  - Formulations that are jettable, but are also selected to achieve high degrees of mixing and reaction.

- Show, through FRIJP, what advantages the process brings over conventional 3D inkjet printing.
  - Achieving structures from polymers that are not processable through solvent, phase change or UV modification.
- Characterise the printed specimens, to determine what are the boundaries of successful FRIJP, to quantify how successful the process is.
  - To determine the degree of mixing and reaction, and the profiles or shape of the part.

### 1.3 Research Methodology

A printer was developed that would afford complete control over the FRIJP process. The printer used exchangeable print heads on a highly customisable printing platform. This allowed for both material and process development on a single platform.

In parallel to the printer development, a FRIJP ink of PDMS was developed. The development process started with selection of a suitable base chemistry. An addition cross-linking reaction was chosen due to the lack of by-products that would result in additional processes and part shrinkage. Once the chemistry was chosen the components were modified to produce a printable viscosity. The work then focused on characterising the printed parts in both geometric and chemical terms.

Once the successful FRIJP of PDMS was achieved, the new printer was exploited to create samples of linear polyurethane. The polymerisation reaction occurs with no by-product, and has been shown to work for FRIJP.<sup>9</sup> The work previously conducted, however, only demonstrated low conversion, low material loading (~25-50% solvent), low resolution (~100  $\mu\text{m}$  nozzle), and importantly no direct information on the printed polymer. Specifically, the chemical analysis was conducted off the printer and the reaction was only

proven by the liquid to solid transition of the printed parts, a change that could occur through several chemical routes. In this study, not only was the PU polymerisation confirmed by Nuclear Magnetic Resonance (NMR) spectroscopy but a value for the molecular weight was also achieved using Size Exclusion Chromatography (SEC), which led to an estimation of mixing degree.

### 1.3.1 Statement of Novelty

This PhD has shown the capability of the FRIJP printing process in producing both high molecular weight linear polyurethane and polysiloxanes, which has been accomplished by the careful control and consideration of both the chemistry involved and the FRIJP additive process. Specifically, this thesis demonstrates novelty in the following areas;

1. Incorporation of disposable Dimatix material inkjet cartridge into a two head FRIJP research printer.
2. Processing of PDMS with an industrial inkjet print head.
3. Producing solid PDMS samples with the FRIJP process.
4. Cure analysis of FRIJP printed samples to determine whether there is any spatial dependency.
5. Producing solid linear polyurethane samples with the FRIJP process.
  - Low weight monomers with mixing issues
  - High weight monomers which showed increased mixing
  - High compatibility monomers which led to bulk reaction
6. Optical analysis of the curing mechanism during/immediately after printing
7. Bulk chemical analysis of FRIJP linear polyurethane samples.
  - SEC to determine molecular weights
  - NMR to determine the degree of cure

## 1.4 Structure of Thesis

The thesis is structured so that the results of FRIJP are presented in three chapters: PDMS, immiscible PU, and miscible PU. The development of the setup was conducted throughout the printing of the PDMS, and the chronological order of work is shown in Figure 1-1.

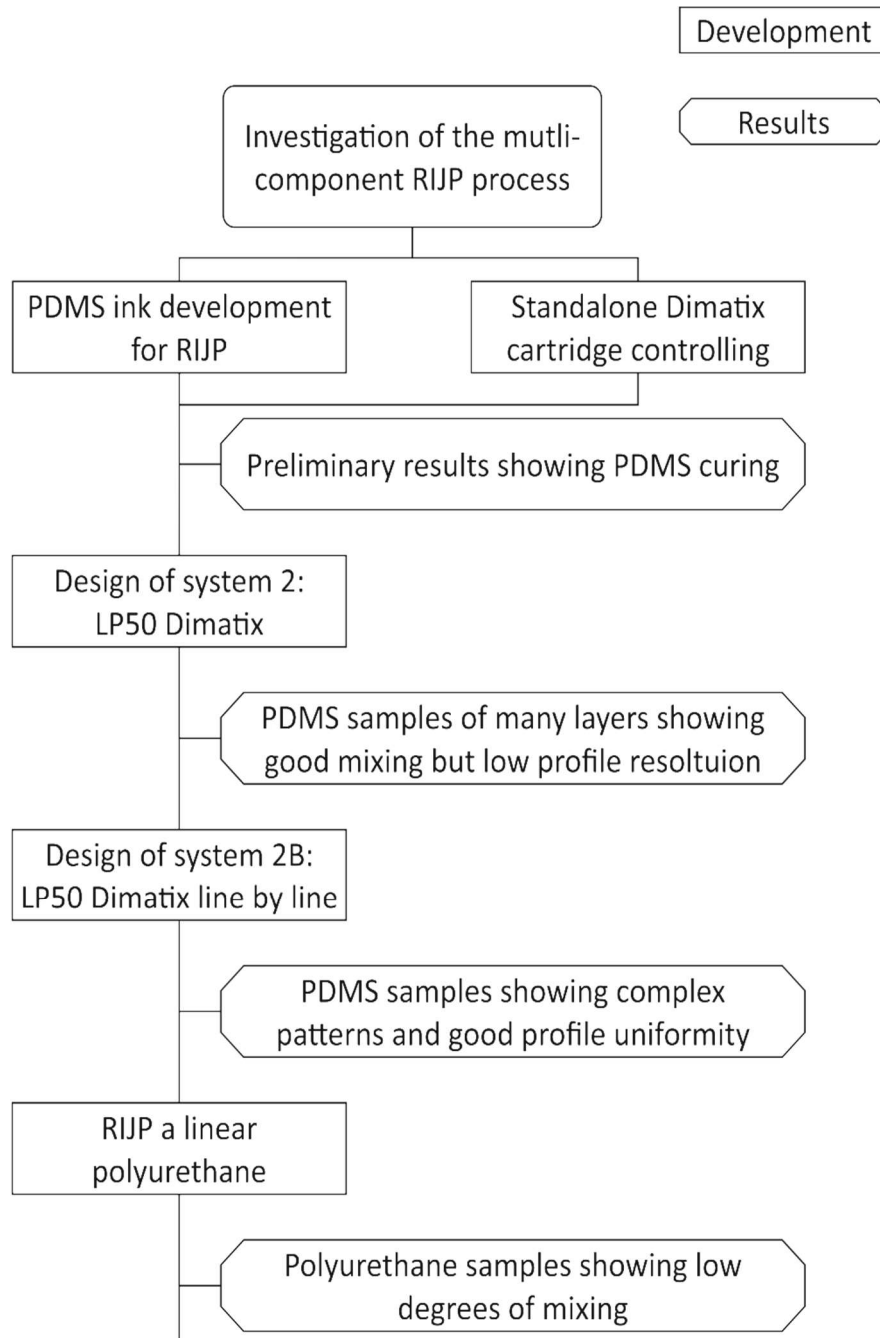


**Figure 1-1** Flow chart showing the process of research during this doctoral thesis. Showing the development of the RIJP ink and printer with final work on RIJP of polyurethane immiscible and miscible chemistries.

### 1.4.1 Thesis chapters

A description of the content of each chapter in the thesis is listed below.

**Chapter 2: Literature Review** provides a review of the relevant studies on jetting, and looks at jetting as a manufacturing technique. The literature is split into the different material jetting stages; ink development, jetting, liquid impact, and ink mixing. The second half studies the chemical reactions occurring during the FRIJP process. These are the addition reactions of polyurethane and polydimethylsiloxane. Finally, the current AM work relating to FRIJP is discussed.

**Chapter 3A: Materials and Established Methods** details the established methods and equipment used in this study, this involves: ink development, characterisation, and jetting. It also details the processes used to analyse the samples: spatial and bulk cure analysis, determination of molecular weight, and determination of printed sample profiles.

**Chapter 4: Developed Jetting Methods** discusses in detail the process of creating and improving the research focused FRIJP setup. It details the three stages of the setup, and how the line printing and droplet ratios were achieved.

**Chapter 5: FRIJP Polydimethylsiloxane** presents the work relating to the development and printing of the FRIJP PDMS ink. Firstly, results related to the development of the PDMS FRIJP ink, then results related to the initial film printing, and finally results with the completed research printer. The results from this chapter are closely related to the developments made in Chapter 4 and were carried out in parallel.

**Chapter 6: FRIJP Polyurethane: Immiscible Components** demonstrates FRIJP of two immiscible monomer components. It

highlights the effect of the material development, with in-process optical microscopy. The results show that using increasingly larger hydroxyl groups increases mixing, and the printing yields a high molecular weight thermoplastic polyurethane.

**Chapter 7: FRIJP Polyurethane: Miscible Components** details the second strategy for increasing the mixing in FRIJP of PU. Through the careful selection of the hydroxyl containing monomer, a miscible FRIJP ink is created. This miscible ink affords a greater degree of mixing over the immiscible monomers.

**Chapter 8: Discussion** discusses the findings of the PhD, and compares results from the three FRIJP inks. These findings will be compared to the literature surveyed, and used to highlight the novelty of this PhD.

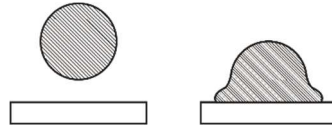
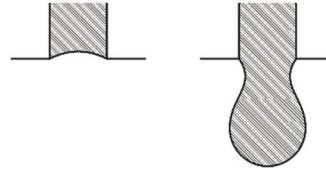
**Chapter 9: Conclusions and Future Work** highlights the main conclusions of this research, and identifies how the investigations in this study are novel. It will also highlight areas where this PhD has not been able to fully investigate the process, and outline how this can be carried out.

**CHAPTER TWO*****2 Literature Review*****2.1 Introduction and Structure**

This PhD's focus is the research and analysis of the FRIJP process for the creation of cross-linked and linear polymer materials, specifically PDMS and PU. The literature was reviewed to understand the jetting process, with a specific focus on the constraints which limit the range of processable materials. In this way, the advantages of FRIJP methods over other material jetting techniques can be highlighted.

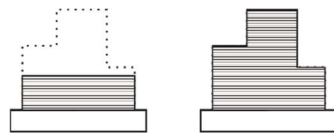
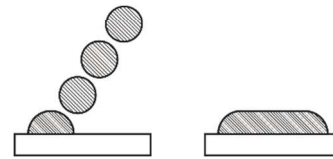
This literature review is separated into two sections; 1) the inkjet printing process, and 2) the relevant polymer chemistries. In the first section a brief background of the jetting technologies are discussed. After this, how material jetting in two dimensions has developed into an Additive Manufacturing technique is discussed, including an overview of the solidification mechanisms. Finally, the available literature is then reviewed in detail, following the material jetting AM process in the order: ink ejection, ink deposition, and ink coalescence (Figure 2-1). The material chemistry section highlights why the PU and PDMS reactions were chosen, what processing steps may have the largest impact, and any research currently related to material jetting of these materials. Finally, available examples of FRIJP are discussed.

Ink Ejection



Ink Deposition

Ink Coalescence



Layer Addition

Figure 2-1 - The process of material jetting to build three-dimensional object.

## 2.2 Material Jetting

There are two methods for ejection in material jetting processes: continuous inkjet (CIJ), and drop-on-demand (DoD). They are named due to the nature of droplet generation, either continuously during printing, or on demand, i.e. printing only when desired.

The first use of ink ejection to record information was seen in 1858 by William Thompson.<sup>11</sup> A continuous jet of liquid was ejected through a nozzle, and due to Plateau-Rayleigh instabilities the in-flight jet broke up into droplets. The droplets were deviated by the use of electric fields, and through selective deviation of droplets data was able to be recorded. A schematic of a modern CIJ printer is shown in Figure 2-2.

The CIJ process directs ink droplets into the desired position, deflecting undesired material away from the substrate. The continuous flow of fluid through the nozzle offers process advantages, but without collection and re-use the ink wastage can be high. The

high ejection speed of the CIJ process reduces the chance of nozzle blockage and machine downtime. It also allows CIJ print heads to be further away from the substrate than DoD, although this is associated with decreased print accuracy. CIJ is still used today in industry; the best known use is on expiry date printing in the food industry. A more comprehensive history of CIJ and the ink ejection process can be found in the review of Wijshoff<sup>11</sup>.

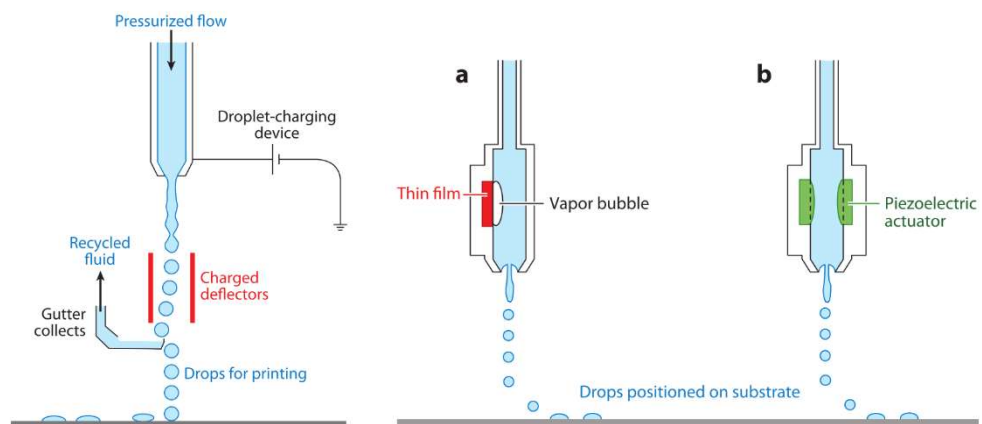


**Figure 2-2 - CIJ and DoD process of ink ejection. Left: CIJ, Right: thermal (a) and PZT (b). Figure reproduced from Derby<sup>12</sup>.**

During drop-on-demand printing, the ink is only ejected when required. There are two main ejection mechanisms: thermal and piezoelectric, as shown in Figure 2-2. Thermal inkjet, also called bubble jet, uses a print head which contains a small heater. The heater vaporises a small volume of ink, creating a vapour bubble, the formed bubble increases the chamber pressure causing fluid ejection from the nozzle. The ink is used in the ejection process as a thermal conductor, which reduces the selection of compatible solvents. The extreme heat of vaporisation could also have an adverse effect on the chemicals used in RIJP inks. Despite the issues with thermal DoD print heads, they are widely used in home desktop printers. This is because of the low cost compared to piezoelectric methods.

Instead of creating a bubble, piezoelectric transducer (PZT) print heads use electric current to deform a piezoelectric element. This change in geometry causes internal pressure waves which generate

the droplet at the nozzle. The arrangement of the piezoelectric elements in print heads is not always fixed, different configurations are shown in Figure 2-3, and these can be pushing, shearing, squeezing, and bending. The design of the print head can affect the operating range of the inks, the propensity for nozzle blockage, and the density of the nozzles, it is however not the focus of this review or work. In DoD printing the ink trajectory is unchanged; instead, the print head or substrate is translated. As DoD heads do not require downstream ink guiding, the heads are very compact, which allows for a greater density of nozzles for a given area.

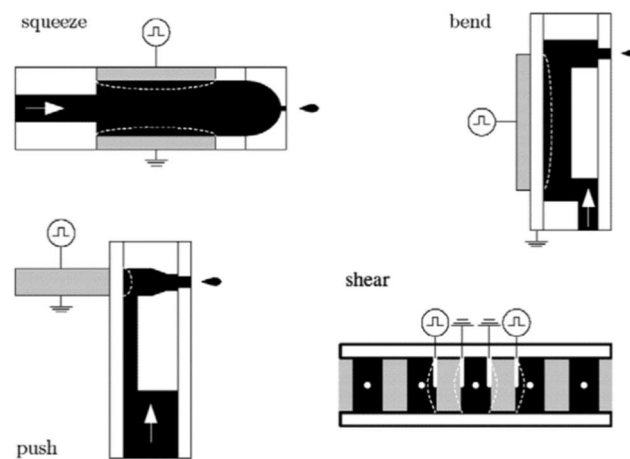


Figure 2-3 - DoD piezoelectric operation modes, figure taken from Wijshoft<sup>11</sup>, reproduced with permission of rights holder.

### 2.2.1 The 3D Material Jetting Process

To use material jetting to build three dimensional objects it is required that multiple layers are printed into the same build area. As objects are built in the Z direction, detail or materials can be placed “inside” a part during fabrication. Material jetting is one of the few Additive Manufacturing methods that offers multi-material processing in a single step, whilst also offering a high scalability.

In addition to the ability to process different build materials, commercial material jetting printers often employ a sacrificial support material. This material is made to be removed after printing is finished for increased resolution and part complexity. Also

employed in some commercial printers is a flying-cut, a process where each layer is mechanically planed flat prior to successive layers being deposited.<sup>7</sup>

### **2.2.2 Solidification Mechanisms**

The end goal of material jetting is achieving a solid part with minimal processing outside the printer. This means that the deposited ink needs to both quickly and reliably transition to a solid. Inks are commonly categorised by how they are modified for printing, and how after deposition they solidify. These categories are: phase change inks, solvent based inks, and reactive inks.

#### *Phase Change*

A phase change ink is one where the desired ink is melted inside the print head, creating a liquid that has been designed with a printable viscosity. Once deposited the ink rapidly cools and solidifies. This process was first commercialised with wax inks, the ModelMake (Sanders Prototype) in 1994, followed by the Actua2100 (3D Systems) in 1996. These early commercial printers used wax in the production of design concepts and forms for investment casting.<sup>7</sup> There has recently been renewed interest in this material for less traditional applications, including for example, pharmaceutical products.<sup>13</sup>

The phase change method is desirable due to the fast solidification, and high material loading of the inks. The polymers which are desirable in industry typically have a high molecular weight, as mechanical properties are dependent on polymer chain length.<sup>14</sup> High molecular weight polymers result in high melt viscosities, and these liquids are typically not jettable.<sup>14</sup> Alternative methods are then required to print these mechanical polymers, such as, solvent and reactive inks.

#### *Solvent Suspension*

The viscosity modification of polymer based inks can be achieved by dissolution in a suitable solvent. Through manipulation of concentration and type of solvent, inks with viscosities in the printable range can be achieved. The solidification mechanism in solvent based inks is typically evaporation, although the precipitation mechanism has also been used.<sup>15</sup> The solvent method has been used for a variety of polymers e.g. Polycaprolactone,<sup>16</sup> Biocompatible supramolecular polymers<sup>2</sup>, and Polyimide<sup>3</sup> and is a versatile method for polymer processing.

This method has also been used for the printing of conductive inks. Printed electronics is a very large area of research, focusing on achieving low resistance at high processing speeds. Copper,<sup>17</sup> Graphene,<sup>18</sup> and Silver<sup>19</sup> inks have been printed.

Despite the versatility of the solvent method, suspensions typically have a low solid loading. For example, a recently developed polyimide formulation was measured to contain a 1 %wt fraction of polymer.<sup>3</sup> Low solid loading in an ink directly effects the processing speeds, and the solvent waste is an undesirable feature, with both environmental and economic impact. Solvent inks also have issues when a thin continuous film is desired, as evaporation and fluid flows inside a droplet lead to a phenomena called the “coffee-ring” effect. This effect redistributes the material to the extents of the printed droplet or line and increases thickness variation of printed thin films.<sup>3</sup>

### *Reactive Inks*

Reactive inks undergo a chemical structure change during the solidification process. Smith<sup>8</sup> describes two different schemes. Firstly Single Reactive (SR), where a single component is printed and reacts; secondly Fully Reactive (FR), where two or more inks are printed together. The curing mechanism can be initialised through an external excitation, or occur due to the mixing of the two components.

The commercial 3D jetting printers available now, Objet (Stratasys) and Projet (3D Systems), make wide use of photopolymer inks. Photopolymer inks are single reactive inks, where a cross-linking reaction occurs once exposed to UV light. These materials are able to be jetted in a fully loaded acrylate based ink containing a photoinitiator. Once printed, exposure to a UV light initiates the cross-linking reaction. These inks are very attractive because of their full loading and high curing speeds.<sup>7</sup>

An issue with photopolymer inks is that during the printing of successive layers, previously printed layers are also exposed to the UV radiation. This overexposure causes changes in the mechanical properties.<sup>20</sup> Acrylate based inks are susceptible to both light and thermal degradation.<sup>14</sup>

Fully reactive inks offer a new route to the fabrication of solid components, as they increase the range of processable materials. Research has started to explore this method in relation to depositing multiple components of inks to produce copper,<sup>21</sup> nylon,<sup>22</sup> and polyurethane.<sup>9</sup> A desirable feature of FRIJP is that the inks can be based on multi-component chemistries already used in industry, as opposed to delaying the reaction of single chemical inks through acrylate modification.<sup>23,24</sup> Monomers and pre-polymers typically have a printable viscosity which does not require solvent modification. The reaction can occur from the mixing of the two components, and in this way no exterior stimuli is required. Through FRIJP it is possible to mimic the formulations used today in the polymer industry, utilising the many years of research and understanding already developed.

### **2.2.3 Ink Ejection**

In this study an ink refers to any liquid passed through the material jetting process. To develop a suitable ink it is not satisfactory to just eject a droplet, but to reliably eject, at high frequencies, a droplet with a constant volume and speed. This means there are requirements of

the ink in regards to fluid properties, reaction speed, and solvent evaporation rates. In this section the different conditions for reliable ink droplet formation are discussed.

Instead of the constant generation of a fluid jet, as found in CIJ, DoD is the process of generating short jets. Therefore, the research studying the breakup of fluid jets still applies, and through investigation of continuous jet breakup the DoD ink requirements can be understood. In the development of an ink the end goal is to achieve a single in-flight droplet, avoiding the formation of any satellite droplets, as shown in Figure 2-4. The higher the print reliability, the longer the head can run without running a cleaning cycle (purging, wiping, spitting) increasing material throughput. The maximum frequency of printing is limited by the time it takes for the ink to flow into the nozzle, and how quickly the dissipation of acoustic waves from the other jetting events occur. As these parameters are all interlinked, and depend heavily on material properties and nozzle design, the best way to develop an ink is to take an empirical approach through trial and error.

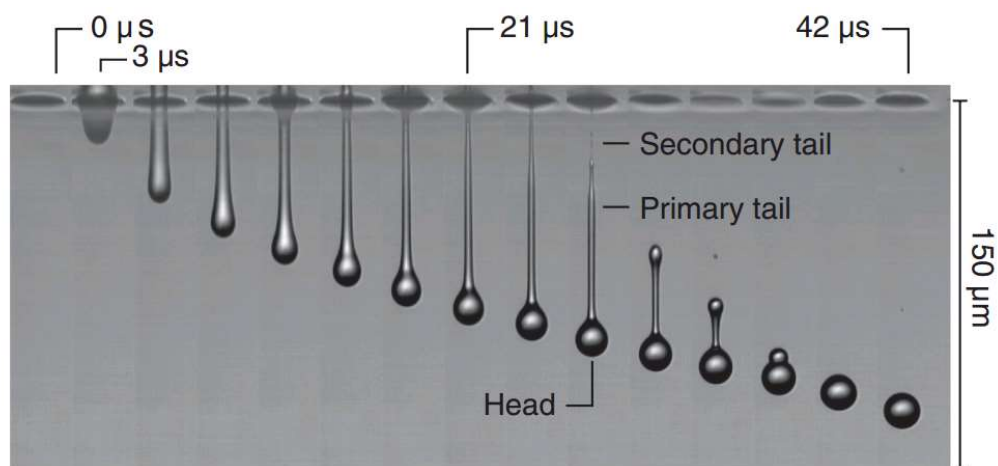


Figure 2-4 – Generation of short liquid jet in the DoD process. This image was capture with a single exposure camera, with a duration of 8 nS, image taken from Bos<sup>25</sup>, in this case the tail re-joins the primary droplet so no satellites are formed. Reproduced with permission from rights holder.

### *Ink Viscosity and Surface Tension*

Experimentally, the work of Ohnesorge has had a large impact on understanding droplet breakup and generation. In his thesis he developed an apparatus that used flash lighting to capture the dynamic process,<sup>26</sup> his thesis was later published and presented in a paper.<sup>27</sup> In his work he imaged droplets on a small time scale categorising the observed phenomena into four distinct behaviours: 0) Gravity driven dripping 1) Axisymmetric breakup 2) Screw-like breakup 3) Atomisation.

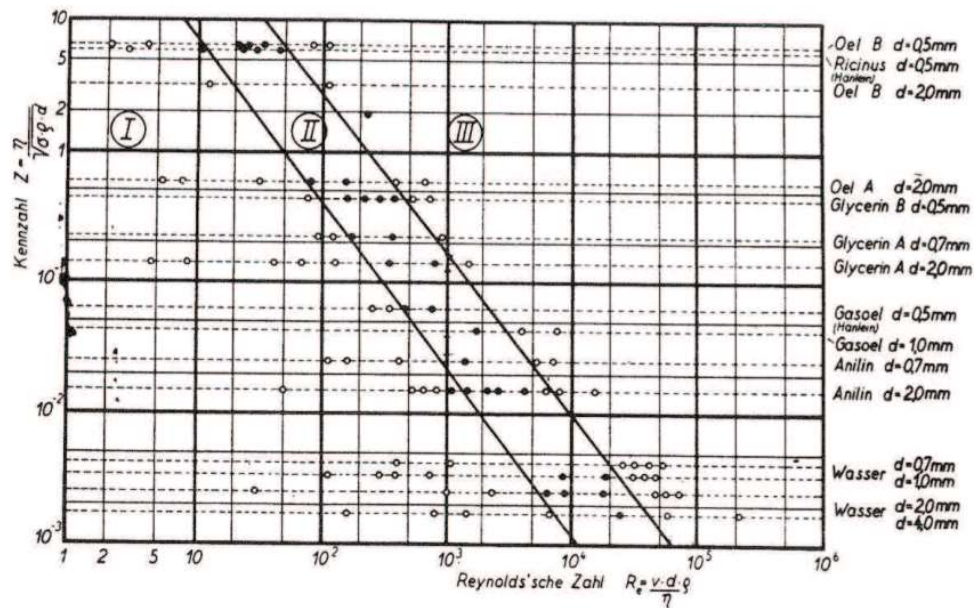


Figure 2-5 - Results of the study conducted by Ohnesorge, the X axis is the Reynolds number, whereas the Y axis is now called the Ohnesorge number (Taken from the doctoral thesis).<sup>26</sup>

The work of Ohnesorge produced the data shown in Figure 2-5, with the conclusion stating that the Ohnesorge number could be used to determine the regime. There are two additional non-dimensional numbers related to the understanding of the Ohnesorge number, the Weber number, and the Reynolds number;<sup>28</sup>

$$Oh = \frac{\mu}{\sqrt{\rho\sigma L}} = \frac{\sqrt{We}}{Re} \quad (2-1)$$

$$We = \frac{\rho v^2 L}{\sigma} \quad (2-2)$$

$$Re = \frac{\rho v L}{\mu} \quad (2-3)$$

where  $\mu$ ,  $\rho$ ,  $\sigma$ ,  $L$ , and  $v$  are the dynamic viscosity, density, surface tension, characteristic length, and velocity respectively. The Weber number is seen as the balance of inertia and surface tension, while the Reynolds number is the balance of inertia and viscous forces. Together they form the Ohnesorge number, which can be considered the balance of surface and viscous forces. It was in the work of Fromm<sup>29</sup> that the first steps were taken in relating the Ohnesorge number to DoD inkjet printing.

Of the parameters involved in the Ohnesorge number only the material viscosity, surface tension, and density are readily tuneable. The characteristic length and nozzle diameter are fixed for a given print head. To reduce the number of variables in ink development a number of authors have attempted to define a range for the Ohnesorge number. The initial work conducted by Fromm<sup>30</sup> and Reis,<sup>31</sup> used numerical simulations to narrow the range of the printable ink conditions. Fromm<sup>30</sup> suggests a  $Oh < 0.5$  for printable inks, whereas in a review paper by Derby<sup>12</sup> a different range of  $0.1 < Oh < 1$  is attributed to the work of Reis.<sup>31</sup> The  $Oh$  number represents a balance between the viscous and capillary timescales, therefore values outside these ranges suggest print issues due to ink viscosity ( $Oh > 1$ ) and surface tension ( $Oh < 0.1$ ).

Recently other authors have further investigated the range of the Ohnesorge number, with a consideration of the head design.<sup>32</sup> Basaran<sup>33</sup> removed satellites with a complex waveform including a negative pulse. Tai reports a larger range of  $0.02 < Oh < 1.5$ , and also mentions that fluids outside this range are jettable with decreasing reliability. Finally Jang<sup>34</sup> redefines a lower range of  $0.071 < Oh < 0.25$ , but it is specified that this range is for stable, accurate jetting with no satellite formation.

The  $Oh$  number has been shown to relate directly to the problem of jet breakup; however, the accuracy required affects the acceptable range. This review of literature reinforces the idea that for the ink development an empirical approach is required.

### *Shear Rate Dependent Viscosity*

The apparent viscosity of liquids that are non-Newtonian is dependent on the shear rate applied.<sup>28</sup> The Ohnesorge number includes a term for ink viscosity to predict ink printability. An assumption made by various authors is that the viscosity measured at low shear rates is suitable for use in printability prediction. Despite the process of inkjet deposition occurring at an estimated rate of  $\sim 1 \times 10^5 \text{ s}^{-1}$  Wang<sup>35</sup> reports that most inkjet printing research discusses viscosities at shear rates lower than  $1000 \text{ s}^{-1}$ . Specifically the following authors, Hong<sup>36</sup>  $< 300 \text{ s}^{-1}$ , Zhang<sup>3</sup>  $< 1000 \text{ s}^{-1}$ , and El-Molla<sup>23</sup>  $< 250 \text{ s}^{-1}$ , all report of no problems related to predicting printability from the viscosity measured at low shear rates. Hoath<sup>37</sup> measured viscoelastic materials with both a low ( $< 1000 \text{ s}^{-1}$ ) and medium shear ( $5000 \text{ s}^{-1}$ ) rheometer. He discovered that for these known non-Newtonian fluids ink printability could not be predicted using the low shear rheometer, instead it was necessary to understand the shear-viscosity relationship to estimate printability. It should be noted that Oath's work did not reach the theoretical shear rate of inkjet printing, and he suggests that further research in to higher shear viscosity measurement is required.

### *Stable Ejection*

DoD inkjet printing accuracy is dependent on the positioning stage used, and the minimum feature size is dependent on the droplet volume. If drop ejection, formation, or velocity is unstable the printing accuracy is reduced. To achieve accurate deposition during the DoD process a single in-flight ink droplet is required. Any velocity

variation between ejections affects the time of flight, reducing the accuracy of deposition.<sup>38</sup> Figure 2-6 shows the experimental and numerically calculated velocity of an in-flight droplet-ligament. Over the course of 35  $\mu\text{s}$  this ligament re-joins the droplet head, forming a single in-flight droplet. It is necessary for this process to complete before impact to achieve a circular droplet on the substrate. It is possible to increase the time of flight by increasing the print distance, but this can result in increased variation in droplet placement.

There are cases where the ligament does not re-join, but will instead separate, due to capillary breakup, producing a satellite droplet.<sup>39</sup> Satellite formation does not necessarily reduce droplet accuracy, as long as the satellite re-joins with the primary droplet before impact. Therefore the velocity of this satellite is important, if it is greater than the primary droplet it can also recombine in-flight, otherwise it will cause inaccuracies and material placed erroneously.

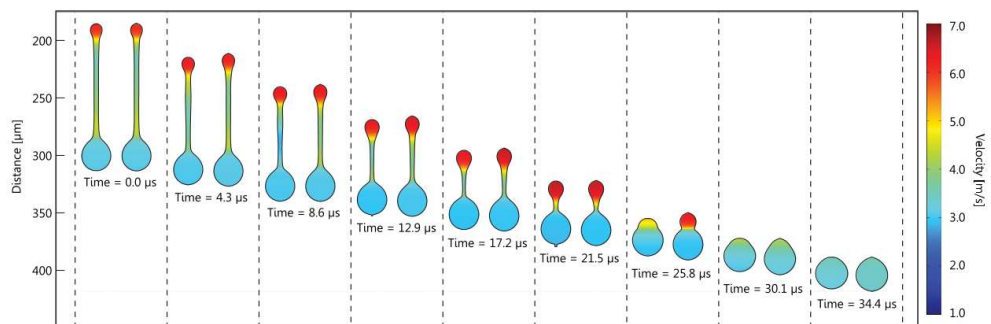


**Figure 2-6 - Velocity of droplet ejecting a nozzle, left is the experimental, right is the numerical result. Figure from Van Der Bos,<sup>25</sup> reproduced with permission from rights holder.**

### *Droplet Volume*

It is important in FRIJP to achieve the correct ratio between reactants. This ratio is achieved by knowing the droplet volume, and printing a correct droplet ratio. The dispensed droplet volume was investigated by Reis<sup>40</sup> who found that it was not only a function of PZT actuation, but also the Ohnesorge number. He found it was possible to vary the volume and droplet velocity by modifying the

electrical pulse driving the PZT, specifically the amplitude and rise time. There was an observed maximum volume, where further increasing the amplitude has no effect, the result of this analysis is in Figure 2-7.

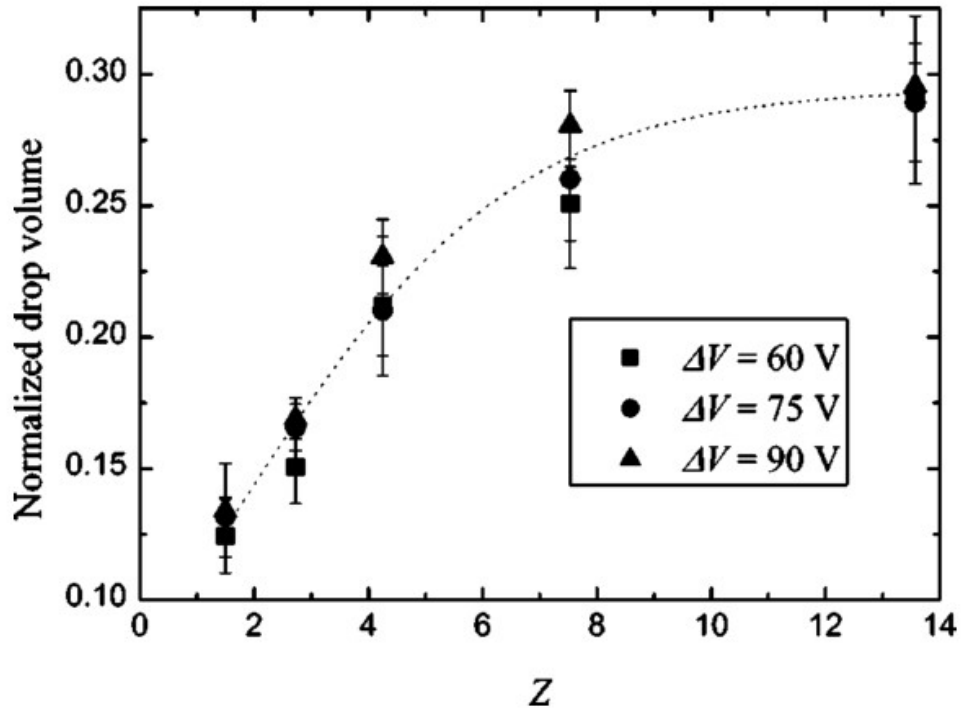


Figure 2-7 - "Drop volume normalized to the volume displaced by the actuator..." studying the relationship between  $Oh$  ( $1/Z$ ) and the dispensed droplet volume. From Reis<sup>40</sup> reproduced with permission from license holder.

### *High Molecular Weight Inks*

The ability to process high molecular weight polymers is an advantage of the solvent ink method, but as chain length increases long range interactions can occur. These molecular interactions manifest as viscoelasticity, which becomes the limiting factor when printing higher weight polymers. For inkjet printing this viscoelasticity has been found to affect not only droplet speed, but breakup of a jet into droplets.<sup>41</sup> This, as previously discussed, will also affect the measuring of viscosity data for printability assessment.

The work of Hoath<sup>42</sup> investigated high molecular weight solvent inks. Through varying the polymer weight and concentration he analysed

multiple inks with similar viscosities. He found that inks with polymers of higher molecular weight caused a reduction in the droplet speed, and increased the break-off time. The observed phenomena was likened to “beads-on-a-string”, shown in Figure 2-8. Hoath suggests that when printing high molecular weight polymers there are two additional dimensionless parameters, the Weissenberg and Deborah number. The Weissenberg number relates to the deformation rates of the solution in the process, and the Deborah number represents the capillary thinning. These results suggest that like the phase change method, there is a limit to the molecular weight of processable polymers using solvent inks.

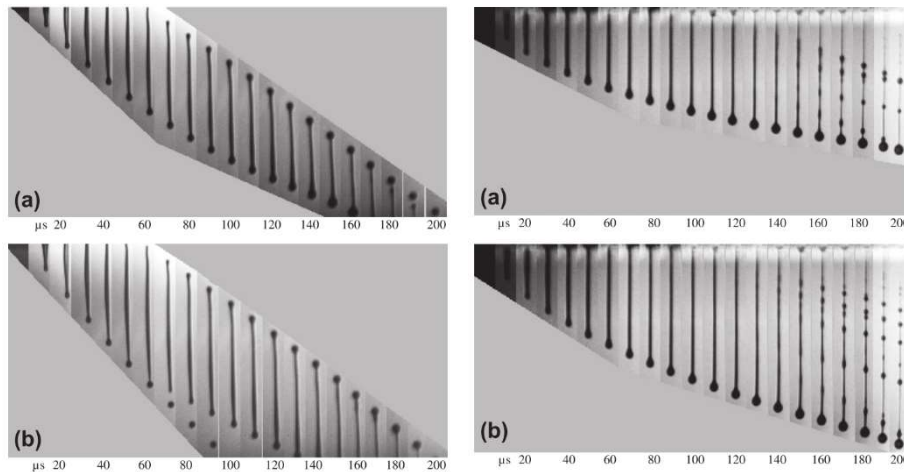


**Figure 2-8 - Left: Newtonian fluid printed at 32V (a) and 35V (b). Right: Non-Newtonian fluid printed at 32V (a) and 35V (b). Observed is the apparent "beads-on-a-string" phenomena. Reproduced from Hoath.<sup>42</sup>**

A significant issue with printing high molecular weight inks was recently discovered by A-Alamry.<sup>43</sup> In his paper he describes that polymers with weights between 100 kDa and 1 MDa were found to degrade during the inkjet process (Figure 2-9). The results showed that for a polystyrene ink with a pre-printing weight of  $M_w = 772$  kDa, that the post-printing degraded weight was  $M_w = 380$  kDa. Subsequently this phenomenon was modelled by McIlroy<sup>44</sup> who found full extension, followed by scission could occur in polymer chains at the nozzle exit. Wheeler<sup>45</sup> found that degradation could be reduced when using hyper branched polymers, which increases polymer

weight without greatly effecting chain length. This finding is in agreement with McIlroy, in that the degradation is caused when linear polymer chains are fully extended. McIlroy's modelling predicted this full extension occurs at the nozzle exit.

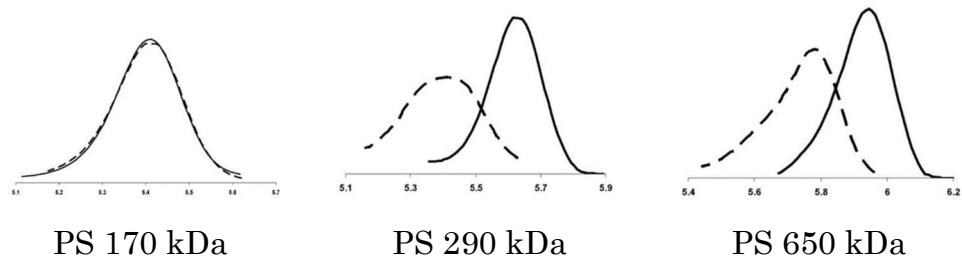


**Figure 2-9 – Change in molecular weight of polystyrene solutions before (solid) and after (dashed) inkjet printing. Dimatix 10 pL cartridge was used with a 21  $\mu\text{m}$  nozzle diameter. Figure reproduced from A-Alamry<sup>43</sup> with permission of rights holder.**

### *Summary of Inkjet Ejection*

In summary, correct ink ejection is highly dependent on the viscosity and surface tension of the fluid. Attempts have been made to determine the printable range of ink in terms of the Ohnesorge number. However, practically it has been shown that there are a variety of operating ranges depending on equipment used which it is better to define experimentally. When printing low weight polymers only the ink viscosity and surface tension are important; however, as increasing molecular weight polymers are used the consideration of chain interactions is crucial. Regardless of the polymer concentration and solution viscosity, polymer weight can become the limiting factor. Work involving solvent inks has identified that it is not an ideal solution for the printing of mechanical polymers with issues relating to high shear rate viscosity, viscoelasticity, and polymer degradation.

The method of FRIJP is then interesting as a means of printing low weight polymers or monomers to then polymerise on the substrate. The process would then be able to produce the high molecular weight

polymers, which are otherwise unprintable through solvent or phase change methods.

It has been found that the ink properties, nozzle parameters, and driving waveform all affect droplet volume. For FRIJP it is required that the mixing ratio is constant, and that it can be controlled during the process.

#### 2.2.4 Ink Deposition

The impact of a drop onto a substrate involves a complex relationship between the substrate, the air, and the ink. Primarily research into substrate interaction has focused on printing only the first layer onto a prepared substrate, as found in textile and conductive track inkjet printing. In additive manufacturing only the first layer involves an interaction between the ink and the prepared substrate, all subsequent layers are printed onto a previously deposited layer. Only recently with RIJP and FRIJP has research started to investigate what happens when a second liquid ink is printed onto a printed film or droplet.

##### *Single Ink Substrate Interaction*

The field of a single ink droplet impacting on a substrate has been well explored with numerical and experimental research techniques. It has been found that the impact adopts one of six morphologies; deposition, prompt splash, corona splash, receding break-up, rebound, and partial rebound.<sup>46</sup>

The process of droplet impact can exhibit multiple stages; impact, spreading, receding, and relaxation. The different morphologies are characterised by how they behave in these phases. The **rebound** and **partial rebound** case occur when the droplet recedes after impact, depending on the contact angle, either full or partial rebound may occur. **Receding break-up** occurs during the receding phase, if the contact angle is low enough the receding fluid breaks up leaving

behind droplets. **Corona splash** is observed during spreading, it is where fluid in contact with the surface spreads slower than the bulk, leading to breakup. **Prompt splash** also occurs during impact, it is caused by a high surface roughness. **Deposition** is the case of droplet impact with no break-up, and throughout the process of deposition the single droplets spreads in a controlled manner.

The dimensionless groups, Ohnesorge, Reynolds, and Weber have been used to determine when splashing or deposition will occur on smooth surfaces (defined as around  $R_t = 2.8 \mu\text{m}$ ).<sup>47</sup> It was found that using the relationship;

$$K = Oh Re^{1.25} \quad (2-4)$$

that when  $K < 57.7$  complete deposition will occur, and above this value the impact would result in splashing. It was also found that this boundary coincides with the generation of spraying from inkjet nozzles found by Ohnesorge.<sup>27,47</sup> This means when reliable inkjet generation is achieved the most likely impact morphology is deposition, assuming smooth substrate surfaces.

Deposition impact is where the inertia of the droplet is dissipated in the controlled spreading of the droplet. Once all inertia is dissipated the liquid spreads to achieve the equilibrium contact angle. The final shape is that of a spherical cap, described by the droplet volume and ink-substrate contact angle.<sup>48-52</sup>

The Bond number is a dimensionless number to predict the dominant forces between gravity and surface tension.

$$Bo = \frac{\Delta\rho g L^2}{\sigma} \quad (2-5)$$

Where  $\rho$ ,  $g$ ,  $\sigma$ , and  $L$  are the density, gravity, surface tension, characteristic length, and velocity respectively. For the length scales of the inkjet printing process individual droplets have a bond number

$Bo \cong 1E - 6$ , far below the critical value of 1. As gravity has a negligible effect, the spherical cap shape is then the lowest energy state for liquid droplets. At this small scale the dominant property is the surface energy, which takes the form of the ink surface tension and the ink-substrate contact angle. The ink surface tension is described by the Young-Laplace equation;<sup>28</sup>

$$\Delta P = \gamma \left( \frac{1}{R_1} + \frac{1}{R_2} \right) \quad (2-6)$$

where  $\Delta P$ ,  $R_1$ ,  $R_2$ , is the pressure drop across the liquid interface, and the principal radii of curvature respectively. The ink-substrate contact angle is a function of the solid-liquid-gas triple line. Young's equation relates the contact angle to liquid, solid, and gas surface energies in the following way;<sup>28</sup>

$$\cos \theta = \frac{\gamma_{SG} - \gamma_{SL}}{\gamma_{LG}} \quad (2-7)$$

where  $\theta$  is the ink-substrate contact angle, and the subscripts  $SG$ ,  $SL$ , and  $LG$ , are the solid-gas, solid-liquid, and liquid-gas interfacial tensions. Due to the controlled spreading during **deposition** impact, these properties are then the sole parameters required to describe the profile of an inkjet droplet.

Receding or dewetting is a process whereby the contact line, the point where the solid liquid and gas meet, moves to reduce coverage on the substrate. Movement occurs when either the contact angle is not at equilibrium, or when there is high surface curvature.<sup>53</sup> There are forces that resist the contact line movement, leading to the advancing and receding contact angles. For a contact line to advance it needs to reach an angle greater than the advancing contact angle, and for it to recede it must decrease below the receding contact angle. In this way there is a contact angle hysteresis, a range between the receding and advancing angles where movement does not occur.<sup>54,49</sup> As the forces

that restrict movement increase, so does the hysteresis. With large forces it is possible to achieve a receding contact angle of  $0^\circ$ , which means receding will no longer occur. A fixed contact line is called pinned, and at this point if any change in volume occurs the contact line does not move and instead the contact angle changes.<sup>55</sup> The effect of pinning on solvent based inks has been well explored, as it is one of the causes for the “coffee-ring” effect often observed,<sup>3,49,56,57</sup> and shown in Figure 2-10. This occurs due to the evaporation of a solvent, driving internal fluid flow to the contact line, transporting the solute.<sup>49,58</sup> The deposition of the solute at the contact line then increases the liquid pinning.

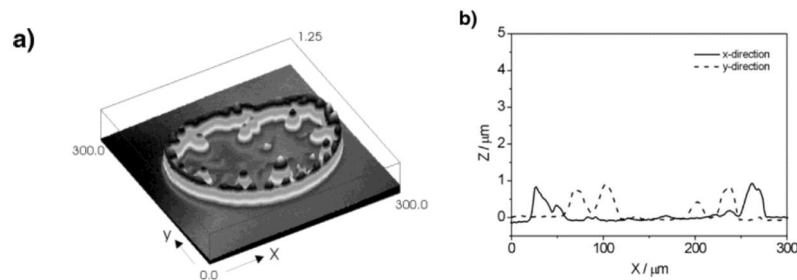


**Figure 2-10 - Surface profile analysis of a printed solvent based ink. The 1 %wt polystyrene was in ethyl acetate solution, printed onto perfluorinated glass. Evaporation and successive coffee-staining was observed. Figure taken from Gans,<sup>59</sup> reproduced with permission of rights holder.**

### *Printed Lines and Films*

When using material jetting it is necessary to achieve lines and films of constant thickness, as this is the only way to build objects in multiple layers. The printing of lines and films lacks the stability found in single droplet profiles. The lack of stability results in a time dependent profile, where the time to cure and viscosity of the ink are important. Movement in the printed ink occurs during and after the printing process, driven by the surface tension and the printed geometry.<sup>50</sup> The velocity fields inside neighbouring droplets have been investigated by Castrejón-Pita;<sup>53</sup> using high speed velocimetry he found there was negligible cross flow during impact.

Thompson<sup>50</sup> conducted an experimental and numerical investigation into printing lines. She assumed that impact flow was negligible, that liquid only redistributes from the drive to minimise curvature, and that a maximum contact angle was never exceeded. In the paper a modelling method is developed based on the assumptions of an impacting spherical cap of zero velocity, an infinite time for redistribution between droplets (no resistance), and a receding contact angle of zero (pinned) (Model I). It is later extended to include resistance to redistribution by including the viscosity term, and reducing settling time between jetting events for redistribution (Model II). The results of the numerical model are shown in Figure 2-11.

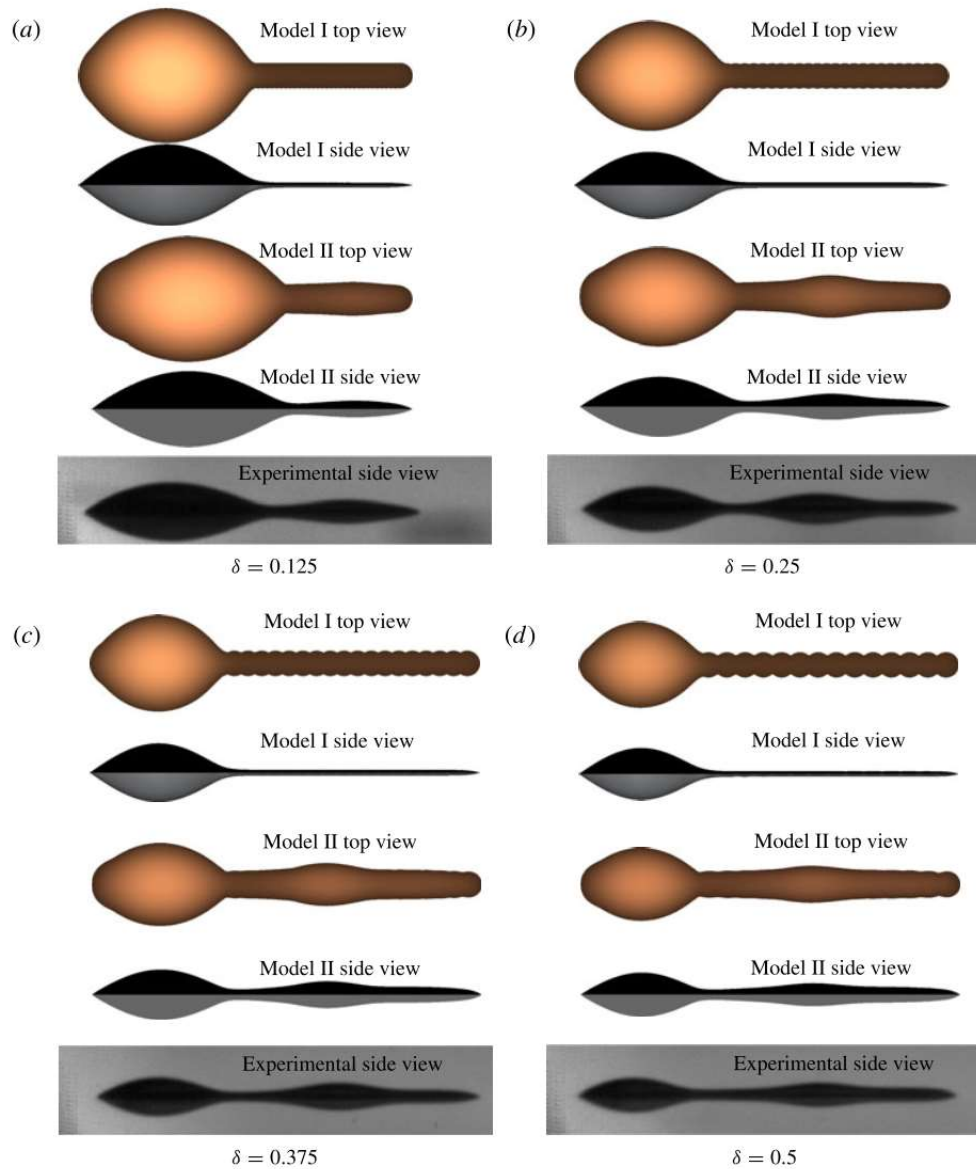


**Figure 2-11 - The results from the experimental and numerical investigation of printing liquid lines by Thompson.<sup>50</sup> a-d) are the drop spacings as a function of droplet diameter. Model I is the case with no resistance, Model II resists flow through the viscosity term. Reproduced with permission from rights holder.**

From the results of the model, validated with the experimental observations, it is clear to see the role of both surface tension and viscosity in producing a stable liquid line. When considering the case of no viscosity there is nothing opposing the transport of the liquid. In these cases a primary bulge is seen to develop and continually grow, but when the viscosity is implemented this transport is limited. In the cases of limited transport the primary bulge reaches a maximum, and secondary bulges appear along the printed line. As Thompson modelled an ideal fluid, with no curing mechanism, it isn't

possible to produce a completely stable ink line. This PhD uses an ink with a viscosity of 6.25 mPa.s, and a surface tension of 44 mNm<sup>-1</sup>; these values are consistent with solvent formulations used in inkjet printing.

Stringer<sup>51</sup> suggests two limits on the drop spacing for stable lines. The theory is consistent with the work of Thompson; there is a maximum drop spacing where ink droplets do not coalesce, and a minimum case. In the minimum case there is a maximum amount of ink that can be deposited before uncontrolled spreading (which leads to bulging) can occur. Stringer also investigated the effect of the solidification mechanism speed, which in this case was the evaporation of a solvent. He found that when a slower evaporation rate was used the range of drop spacings that produced stable lines was reduced.

The literature that discuss the creation of stable liquid lines are typically those where a solvent or wax ink has been deposited. In these cases the rapid increase in viscosity results in the creation of stable geometry. In solvent and phase change inks it is possible that this solidification can occur on a similar time scale to printing. For reactive curing mechanisms the rates of curing are related to mixing or reaction, and these are likely to be longer than phase change or solvent inks.

### *Multiple Ink Deposition*

For the study of FRIJP the understanding of how an ink droplet can interact on top of a liquid droplet is important. In solvent or wax based material jetting this does not occur, as delays are added for full solidification before successive layers are printed. In fully reactive, the reaction can only occur once both inks have mixed on the substrate. The problem of two in-flight droplets colliding is well investigated numerically and experimentally. Through the use of a high speed camera and dye the convective flow is tracked, and the

mixing monitored.<sup>60,61</sup> When collision occurs in flight it was found that impact and free-surface driven flows were capable of mixing the two droplets.<sup>62</sup> In the case of inkjet printing the droplet is contacting a solid surface, where the triple line becomes important. For droplets in contact with the substrate the free surface movement is greatly reduced. From the work of neighbouring droplet analysis Sellier<sup>63</sup> states that convective mixing is negligible, leaving molecular diffusion as the only mixing process.

Castrejón-Pita<sup>64</sup> conducted work directly focusing on FRIJP. His experimental and numerical analysis focused on the problem of coaxial printed droplets, through the use of high speed video, lattice Boltzmann modelling, and coloured dyes. He used non-dimensional numbers to relate the millimetre sized droplets to the micron droplet scale,<sup>65</sup> this method increased the resolution of the results and reduced the experimental setup cost. The non-dimensional numbers used were the Reynolds number, the Ohnesorge number, and the Weber number. The investigation agrees with the results of previous studies related to sequential neighbouring droplets, in all cases of drop on drop impact a laminar flow was observed. Due to this laminar flow and lack of free surface movement there was no observed mixing. The paper describes that this flow is likely absent due to the lack of stretching, and folding of the free surface. Castrejón-Pita also reaches the conclusion that FRIJP mixing is driven purely by molecular diffusion.

### *Summary of Ink Deposition*

Material jetting can offer increased design freedom and complexity over conventional manufacturing methods, but to achieve this, single inks need to be accurately placed onto the substrate. Once deposited these inks need to cure at a high rate to achieve continuous layers. The research until now has focused on producing stable lines with

solvent and phase change inks, these inks solidify at a high rate allowing for the production of these features.

When using fully reactive jetting the curing cannot occur until both inks are deposited, once this has occurred they need to mix and then react. Research has studied this impact mixing, and has found that the only mechanism for mixing in FRIJP is molecular diffusion. Despite this limitation the small length scales associated with inkjet printed droplets may facilitate full mixing. Currently in the literature there has been no reported work involving the creation of specific three dimensional objects using FRIJP, only lines and uncontrolled films. This is the next step, achieving a controlled three dimensional shape, demonstrating high rate mixing and curing in FRIJP.

## 2.3 Chemistry

This PhD studied the FRIJP of two materials, polydimethylsiloxane and polyurethane. Polydimethylsiloxane has been chosen as it can be a transparent polymer, which exhibits high thermal and oxidative stability.<sup>14</sup> It is also a reaction that can occur in normal atmosphere, reducing the printing process complexity. Polyurethane was chosen as it is a single reaction step which can produce a varied range of polymers, the range of material properties can be selected by changing the constituent monomers. In the FRIJP process as monomers are only combined on the substrate this could facilitate chemical grading in the printed part.

### 2.3.1 Polydimethylsiloxanes

Polydimethylsiloxane (PDMS) is a silicone elastomer that is widely used due to its low cost, biocompatibility, and optical transparency. One principle use of PDMS is the fabrication of microfluidic devices.<sup>66</sup> The transparency of PDMS in visible light has led to developments in integrated optics.<sup>67</sup> Recently optical waveguides have been fabricated, these show increased mechanical compatibility with microfluidic channels over conventional devices.<sup>68–70</sup>

#### *Chemical Reaction*<sup>14,71</sup>

Polysiloxanes are chemicals with the Si-O repeat backbone, they can be prepared through the hydrolysis of dichlorosilanes, and this reaction scheme is shown in Figure 2-12.

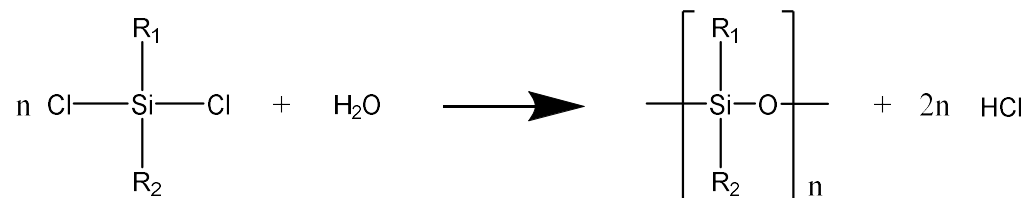


**Figure 2-12 - Hydrolysis reaction of a dichlorosilane to produce a polysiloxane and hydrochloric acid.** <sup>14,71</sup>

This reaction typically forms cyclic polysiloxanes, these then undergo ring-opening polymerisation to form linear polysiloxanes.<sup>14</sup> To cross-

link polysiloxanes, functional groups, such as carbon double bonds, are required. These functional groups are introduced into the polymer chain during the polymerisation process. In the case of vinyl (carbon double bonds) termination this occurs during the initial hydrolysis of chlorosilane. Through the addition of vinyl functional silane to the dichlorosilanes the vinyl termination is achieved.<sup>14</sup>

To form solid polysiloxanes cross-linking is carried out, there are a number of reaction schemes to achieve this, listed in Figure 2-13. Of the cross-linking reactions only one is an addition reaction, the platinum catalysed cross-linking of polysiloxane Figure 2-13b. Addition reactions are desirable for the FRIJP process as they produce no by-products, producing only a pure cross-linked product.<sup>8</sup>

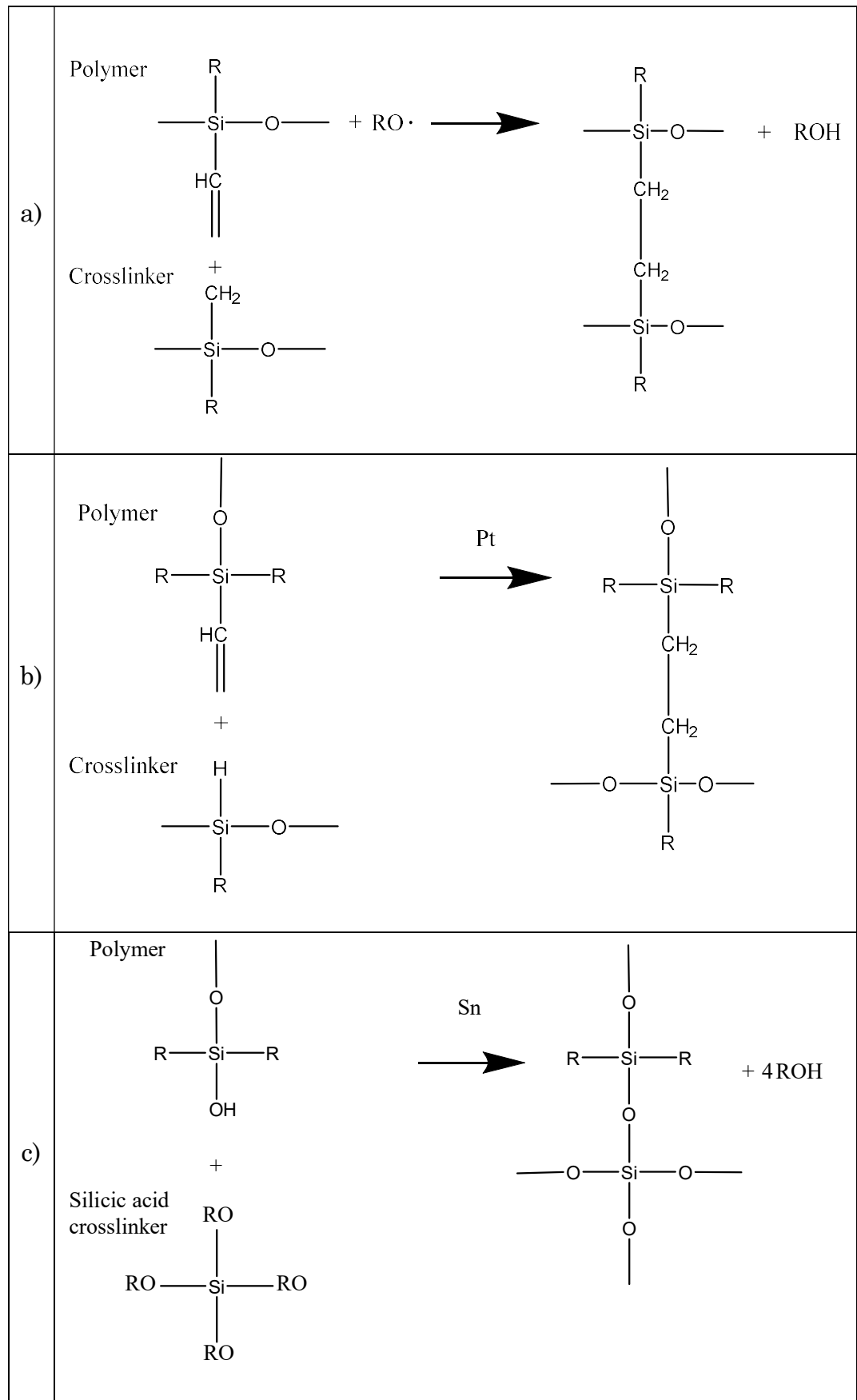


**Figure 2-13 - Crosslinking reaction schemes for polysiloxanes. a) peroxide free radical crosslinking, b) addition crosslinking between silicone hydride and vinyl functional polysiloxane in the presence of a platinum catalyst, c) condensation**

**crosslinking between polysiloxane and acid based cross-linker in the presence of tin catalyst.**

Prior to the chemical cross-linking, the constituent materials can be in a liquid, high viscosity liquid, or gel form depending on the molecular weight of the polymer. The ratio between the hydride and vinyl terminated siloxanes can be varied to change the material properties, with more crosslinking producing a less flexible, more rigid polymer.

### *Manufacturing method for PDMS*

The conventional method for producing PDMS devices is through casting in a mould produced with photolithography. The ability of PDMS to replicate features down to the micron scale is very desirable in the production of microfluidics. However to produce designs with closed channels or features, complex moulds are required. These complex moulds have parts that can be disassembled or dissolved, so the cast PDMS can be removed.

To create assemblies involving PDMS the surface needs to be modified. This modification can be chemical or physical, and it allows the fabrication of more complex designs, incorporating sensors, valves, etc.<sup>72</sup>

### *AM of PDMS*

The only demonstrated work involving the additive manufacture of PDMS devices is by Sung.<sup>10</sup> Despite the author calling the process “inkjet”, the devices are produced through extrusion dispensing of premixed PDMS. This method has two obvious disadvantages, the short work time before permanent nozzle blockage, and the low feature resolution of the extrusion method.

Despite not being for the fabrication of polymer objects, the work of Kirikova<sup>73</sup> shows interesting results in printing a polysiloxane based layer for adhesion of conductive tracks. In the paper they demonstrate

that they can polymerise (3-mercaptopropyl)trimethoxysilane (MPTS : similar to a dichlorosilane, but without the chlorine) in-situ to produce oligomers. The self-assembled layers (SALs) are produced using a MPTS ink in an alcohol based solvent. The SALs produced have a thickness of  $250 \pm 50$  nm, and were found to increase the conductive track adhesion on flexible substrates. In the work of Sun<sup>74</sup> PDMS was again used to aid conductive tracks. Conductive ink was printed onto an uncured PDMS substrate, after printing the PDMS was cured and the printed track was conductive over an increased range of curvatures.

### *Summary*

Despite the lack of inkjet printed PDMS parts, there has already been material jetting work involving PDMS. These cases have shown that printed PDMS could greatly benefit the conductive track printing process. The addition crosslinking scheme of pre-polymerised PDMS produces no by-products making it a suitable chemistry for fully reactive inkjet printing. Once a method for fabricating PDMS through jetting is achieved complex parts containing different materials and functions are possible.

### **2.3.2 Polyurethane**

Polyurethane (PU) is a copolymer consisting of urethane linkages, the result of the addition reaction between an isocyanate and hydroxyl group. The first PUs were discovered by the group headed by Otto Bayer in 1937.<sup>14</sup> Through variation of the monomers different materials are possible: plastics, elastomers, flexible foams, and rigid foams. Producing more elastic PUs is achieved by increasing the length of the polyol, these longer chains allow for increased movement on the molecular scale.

The wide spread use of polyurethanes is due to the flexibility in formulation. This versatility has led to PU synthesised using

sugar<sup>75,76</sup> and oil-based polyols.<sup>77,78</sup> The applications for PU are large, with rubbers, foams, and sealants being researched in detail. Interesting applications such as shape-memory polymers,<sup>79</sup> and porous highly biodegradable scaffolds for soft tissues<sup>80</sup> have also been developed.

Polyurethane is described as having hard and soft segments, which are typically the isocyanate and polyol respectively. The soft nature of the polyol is due to the flexibility of the carbon oxygen bond. PU formulations require at least one isocyanate and one hydroxyl monomer, but they can also include fillers. A common filler is a chain extender, typically a short hydroxyl based monomer. Due to the lack of carbon oxygen bonds in the chain extender, it along with the isocyanate form hard segments. Depending on the mass distribution and the chemical composition the hard and soft segments can segregate or mix, when segregation occurs the hard segment may also crystallise. The crystallisation and the separation are diagrammatically shown in Figure 2-14, which occur due to the ability of the PU linkage to form hydrogen bonds.<sup>81</sup>

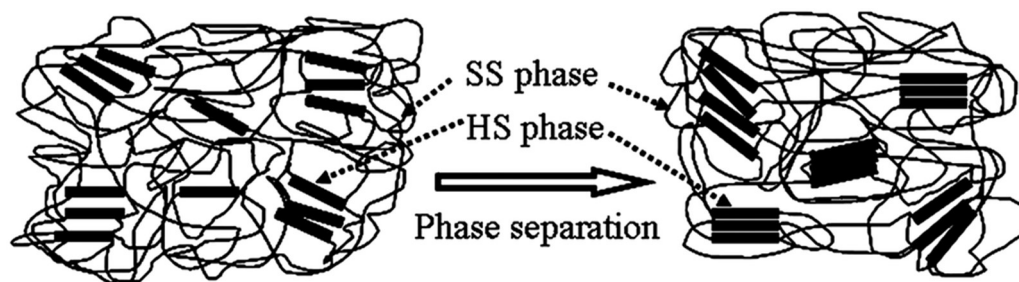


Figure 2-14 - Phase mixed to phase separated polyurethane. Showing the soft segments and hard segments in the polyurethane network. Figure reproduced with permission from the rights holder.<sup>82</sup>

### *Polymerisation of Polyurethane*<sup>14,83,84</sup>

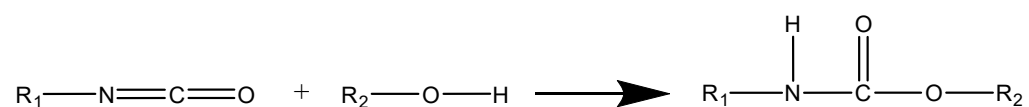


Figure 2-15 - Addition reaction between an isocyanate and hydroxyl end groups. The urethane linkage is typically formed in the presence of a suitable catalyst.

Polyurethane undergoes step growth polyaddition, where any two unlike functional groups can react. As any single monomer has equal reactivity there is no preference for single chain formations, in this way the average chain length grows constantly during the reaction. To achieve high average chain lengths it is required that a high degree of monomer to polymer conversion occurs. The final state of converted monomer is typically a distribution of chain lengths, at various stages of reaction, in a predictable distribution.

The Carothers equation<sup>14</sup> predicts the degree of polymerisation for a given percent conversion. To understand the equation it is first best to understand the different measures of polymer molecular weight. The number and weight average molecular weights are calculated as;

$$\overline{M}_n = \frac{\text{total sample weight } W}{\text{number of molecules } N_i} = \frac{W}{\sum N_i} = \frac{\sum N_i M_i}{\sum N_i} \quad (2-8)$$

$$\overline{M}_w = \frac{\sum M_i^2 N_i}{\sum M_i N_i} \quad (2-9)$$

where  $\overline{M}_n$ , and  $\overline{M}_w$ , are the number average, and weight average molecular weights respectively. The weight average takes into account the fact that larger molecules have a greater contribution to the total mass. The number average molecular weight is useful in predicting the polymers thermodynamic properties. Whereas the weight average is closely related to the melt viscosity, and polymer toughness. The final value related to polymer molecular weights that is important is the polydispersity (PDI), this is a measure of how broad the weight distribution is. For a monodisperse distribution the PDI is 1, where the number and weight average weights are the same.

$$PDI = \frac{\overline{M}_w}{\overline{M}_n} \quad (2-10)$$

Carothers equation is based on the relationship between the number of molecules at the beginning, compared to any time during the reaction.

$$\bar{x}_n = \frac{\text{number of moles at beginning}}{\text{number of moles remaining}} = \frac{N_0}{N} \quad (2-11)$$

where  $\bar{x}_n$ , is the number of repeated units, related to the  $\bar{M}_n$  through the average weight of the repeating unit  $\bar{M}_0$ . Knowing this you can model the percent conversion  $p$  as;

$$p = \frac{N_0 - N}{N_0} \quad (2-12)$$

$$\bar{x}_n = \frac{1}{1 - p} \quad (2-13)$$

$$\bar{M}_n = \bar{M}_0 \bar{x}_n \quad (2-14)$$

$$\bar{M}_w = \bar{M}_0 \frac{(1 + p)}{(1 - p)} \quad (2-15)$$

$$\frac{\bar{M}_w}{\bar{M}_n} = PDI = \frac{\bar{M}_0 (1 + p)(1 - p)}{\bar{M}_0 (1 - p)} = 1 + p \quad (2-16)$$

This equation shows that to produce high molecular weight polymers the reaction needs to reach a high conversion, which is only achieved when the reactants are at the stoichiometric ratio. If the conditions are not ideal the predicted molecular weight is greatly reduced, as shown in Figure 2-16. Finally, the polydispersity can be predicted for step-growth polymerisation from the Carothers equation, where the most probable distribution is two.

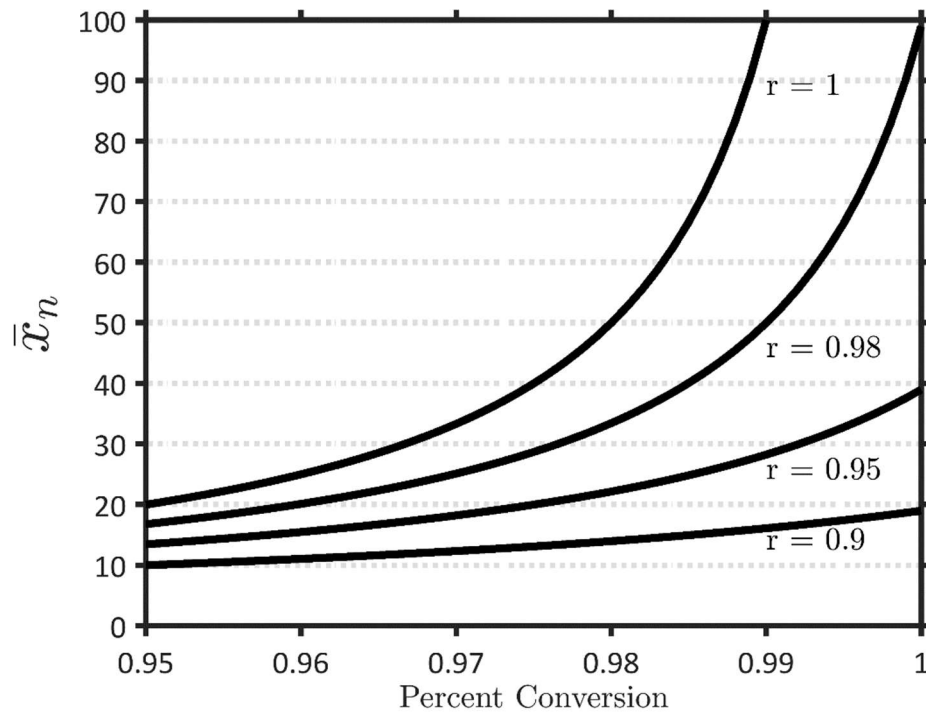


**Figure 2-16 - The result of varying the percent conversion, or the monomer ratio, on the final polymer average molecular number.  $r$  is the actual mixing ratio, where  $r=1$  is the ideal stoichiometric case.**

Producing very high molecular weight polymers is possible with monomer purification and large scale processing, but it is not always desirable. The material properties of polyurethanes are dependent on the molecular weight up to a point, but as it increases the polymers become increasingly difficult to process. The relationship between desired material properties and molecular weight is also not linear, and there is a cut-off at 20,000  $\bar{M}_n$  after which the properties increase slowly. The range after which the properties are desirable and before processing becomes too expensive, is known as the commercial polymer range. This range represents a trade-off between economic viability and material properties. On the industrial scale the molecular weight is intentionally limited, this is achieved through the addition of monofunctional groups which end chain growth.

There are three groups of catalysts used in PU production; organometallic, amine-based, and organic acid. Metallic catalysts provide the fastest reaction rates for PU reaction but are the most

toxic. Amine catalyst, typically tertiary, are primarily used in the production of PU foams. The final catalyst, organic acids, offer the least toxic, but slowest catalyst.

To produce pure polyurethane polymers the reaction must be conducted in a dry atmosphere, this is due to the reaction between isocyanate and water. The reaction between water and isocyanate first produces an amine and carbon dioxide, then further reaction occurs between the isocyanate and amine creating polyurea (PUR) this process is shown in Figure 2-17. The production of carbon dioxide in this process is not always unwanted, in the production of foam additional water is added as a blowing agent. The production of PUR contamination in polyurethane can reduce desirable mechanical properties, limiting the segregation and crystallisation of the PU.

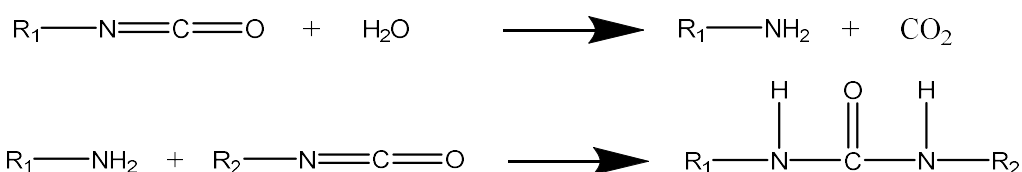


**Figure 2-17 - Reaction of isocyanate with water, forming an amine, which can then react with isocyanate and form a urea linkage. This reaction produces CO<sub>2</sub> gas, and is key in the production of rigid and flexible PU foam.**

### *Polyurethane Morphology*<sup>85</sup>

As discussed, PUs can phase segregate into amorphous and crystalline regions, this segregation is dependent on the monomers used in the reaction. When segregation does occur it is due to the favourable ordered nature of stacked hard segments in which hydrogen bonding can occur.

The chance for segregation is reduced by lower mass fractions of soft segments, and reduced hydrogen bonding between the hard segments. To achieve PU elastomers soft segments with high flexibility and hard segments with a large degree of crosslinking are required. These crosslinks can be physical (hydrogen bonding) or chemical (tri-functional monomers/polymers). Physical crosslinks

allow for the production of melt processable elastomers, which are dissolvable. While chemical crosslinking creates a permanent network, resulting in thermosets and polymers which cannot be immediately dissolved.

### *Experimental Methods for Polymerising Polyurethane*<sup>85,86</sup>

In industry the formation of polyurethane is either through a one-shot process or conducted over multiple stages including pre-polymers.

The one-shot process is one where all the reactants are combined at the same time, these are typically fed into the reactor in two components. Component A is a mixture of catalyst, chain-extender, diol, and other additives, whereas component B is typically just the isocyanate. The one-shot process requires exact chemistry to achieve the correct ratios, as such it is weighed and corrected before processing. Reactive extrusion or reactive injection moulding, is a continual process utilising the one-shot method. These processes involve the use of a screw driven stirrer, where monomers are fed in at elevated temperatures (~60 °C).<sup>87</sup> The exothermic reaction of PU can heat the extrusion reactor to temperatures in excess of 120 °C towards the end of the screw. The polymer produced can either be in pellet form (reactive extrusion) or direct parts (reactive injection moulding).

The pre-polymer technique is a two stage process whereby an initial stoichiometric excess of isocyanate is used in a stirred reactor. The produced polymer with end functional CNO bonds is called a pre-polymer. This can then be used with the remaining polyol, typically the chain extender, to produce polyurethane. Through the two-stage process of polymerisation the processing of more challenging monomers (solids) can be conducted and a higher molecular weight achieved.

### Reaction Kinetics

Typical polyurethane reactions proceed by interfacial polymerisation (Reported by P W Morgan<sup>88</sup> in the paper by Pearson,<sup>89</sup> where the reaction is limited to a zone between the two phases. As the process proceeds the reaction zone moves inwards or outwards depending on the miscibility of the monomer-polymer system. This reaction scheme is shown schematically for the case of emulsion polymerisation (suspension of droplets using a surfactant) in Figure 2-18. In the work of Pearson<sup>89</sup> it was found that the polyurethane produced at this interface was only swollen by the diol. In this case the reaction occurred at the polymer-isocyanate interface and proceeded through the isocyanate medium. The reaction rate of this formulation is then a function of the reaction between the monomers, the molecular diffusion rate of the diol, and the thickness of the interface.

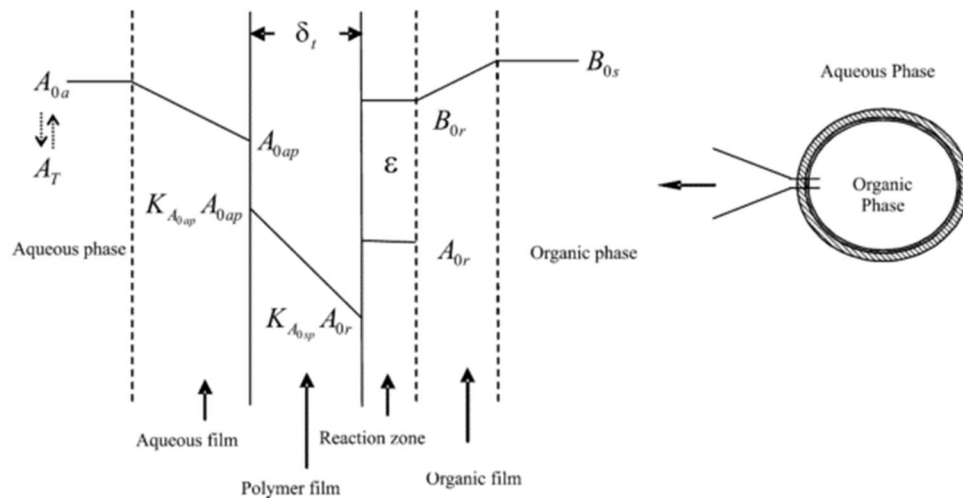
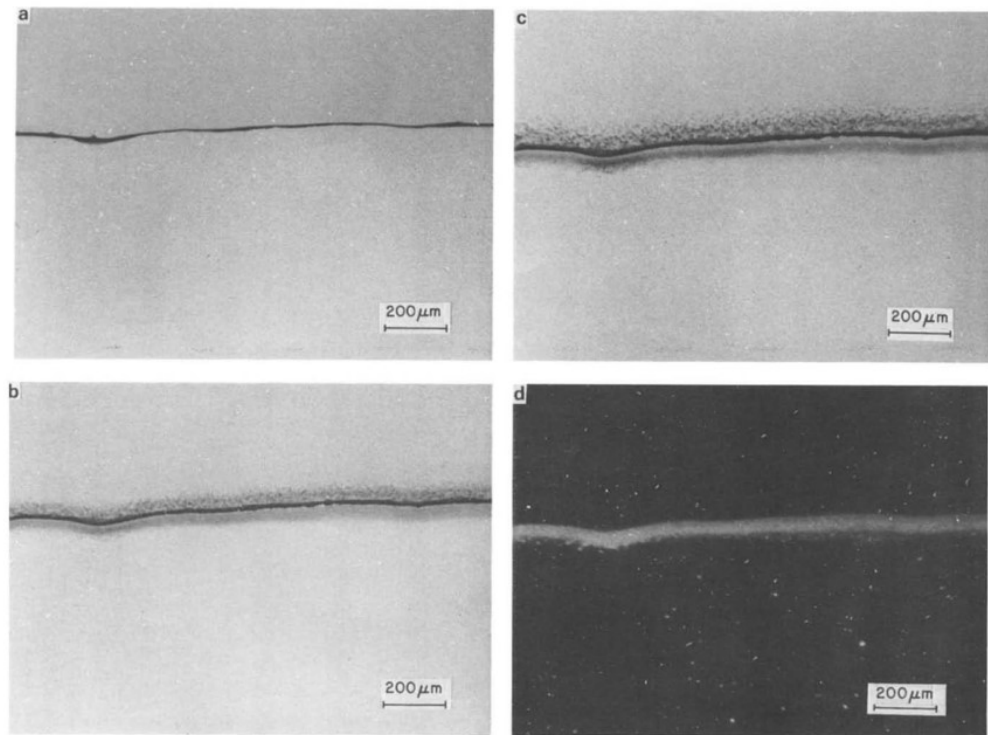


Figure 2-18 “Schematic diagram showing the different regions and physicochemical processes considered in the modelling of interfacial polycondensation. Note the regions in which external mass transfer, molecular diffusion, and reaction kinetics operate and the use of the partition coefficients to treat phase equilibria for HMDA at the interfaces”. HMDA is an amine (instead of a diol in a urethane), organic phase is isocyanate subscript O, aqueous phase is amine (diol in urethane) subscript A. Figure reproduced from Dhumal<sup>90</sup> with permission from the right holder.

Experimental analysis of the interface formed in the polyurethane reaction has been conducted by numerous authors.<sup>91–93</sup> In Fields<sup>91</sup> a 35 mm camera was used to capture multiple frames of the reactions.

Figure 2-19 is one of the results from the paper, it can be seen that initially a stable interface is formed, over time the reaction proceeds and this interface grows. The author reports that this interface reaches a thickness of 100  $\mu\text{m}$ , which is consistent with the diffusion coefficients of the system. Other solutions were analysed and it was found that there were different mixing lengths and interface stabilities depending on formulation. Machuga<sup>93</sup> found that to obtain good mixing it was necessary for initial products to be of low molecular weight and highly flexible. It was also found that to achieve good mixing an initially slow reaction rate was preferred.



**Figure 2-19 - "Interfacial polymerization at 25°C: top phase, BDO + 0.1 %wt catalyst; bottom phase, diisocyanate. Time (a) 0s; (b) 10 min;(c) 20 min; (d) 20 min (crossed polarizers)"** Figure reproduced with permission from Fields 1986.<sup>91</sup> BDO = Butanediol, Catalyst = Dibutyltindilaurate

The interface is counterproductive when desiring a high degree of cure, as it slows or even stops the reaction process. To mitigate this separation the stirring inherent in vat and extrusion methods acts to distribute the monomers. When stirring conditions are correct the isocyanate phase is dispersed in small micron size droplets, it has been reported that these droplets remove the diffusion limiting step.<sup>87</sup>

As well as distributing the components, the fluid flow also acts to break-up interfaces already formed, ensuring a well-mixed product.

### *Additive Manufacture of PU*

In section “2.4 Fully Reactive Inkjet”, a paper that attempts FRIJP of PU is discussed. In this section all other relevant cases of AM PU are reviewed.

### *Inkjet Printing with Solvent PU Ink*

Through the solvent method an aqueous suspension of polyurethane was printed, the formulation contained 40 %wt solid.<sup>94</sup> The polyurethane used had  $M_w = 1600 \text{ g.mol}^{-1}$  with particle sizes of 100-200 nm. To print multiple layers a drying time of 5 minutes was required, which would limit the maximum layer printing rate. The printer used a research focused low frequency print head ( $< 500 \text{ Hz}$ ), and only a single nozzle was employed. The nozzle was  $100 \mu\text{m}$ , larger than typical industrial jetting printers. If this were to be repeated on an industrial scale, the solution viscosity would likely need to be decreased for processing on high nozzle print heads. The nozzles would likely be smaller, resulting in decreased droplet volumes and therefore the layer thickness would decrease. Overall the work is very limited by the low molecular weight of the polymer.

A UV-based aqueous polyurethane ink has been developed from two Polyethylene Glycols ( $M_n = 1000, 2000 \text{ g.mol}^{-1}$ ), isophrone diisocyanate and hydroxyl ethyl acrylate.<sup>23</sup> Formulations of 5, 10 and 20 %wt in aqueous solution were printed. As this research was focused on printing dyes for 2D textiles there were no reports of multiple layers.

### *Material Extrusion of PU*

Material extrusion is an additive manufacturing method whereby material is passed through a nozzle positioned using a two axis stage.

The material is usually in the form of a filament which is solid and can be heated to achieve flow ability, or a gel which dries to become a solid. The process, also known as Fused Deposition Modelling (FDM) is used on the commercial 3D printers such as Stratasys Fortus, Makerbot, Ultimaker, etc. The process is limited in scalability and resolution, but can be a low cost AM method with routine material development.

Through material extrusion an aqueous polyurethane solution was used to create biodegradable cartilage.<sup>95</sup> PU s in solution with Polyethylene Oxide (high Mw PEG) were deposited in a range of viscosities between 1 – 7 Pa s. The author reports that cells are seeded efficiently, and that the main advantage of this method is that there are no toxic components (residual monomers, cross-linkers, solvents, or initiators).

### *Secondary AM PU Printing*

In the paper by Hernández-Cordóva,<sup>96</sup> a PU synthesised with polycaprolactone, urethane, and urea was indirectly 3D printed. The paper does not attempt to directly print the PU, but create forms that can be used to cast an elastomeric PU-PUR for cardiac tissue. Suggesting there are desires for complex geometry for biomedical research with PU.

### *Summary of PU Chemistry*

The reaction chemistry of polyurethane relies on the precise metering of monomers to produce high molecular weight polymers. If there is an imbalance in this ratio the final polymer can be a lower weight, causing a large reduction in the mechanical and thermodynamic properties. As most chemical systems used have components which are immiscible the reaction can only occur at the interface, which has been directly observed through optical microscopy. To achieve a mixed state in PU production stirring is required to distribute the

monomers. The distribution is coupled with monomers with increased compatibility, or the pre-polymer method of producing miscible viscous liquids.

Although material jetting cannot include mechanical mixing on the substrate, there are qualities of jetting that could prove useful to PU production. The dispensing of fluid from inkjet print heads is very repeatable, leading to a high degree of control of the mass of monomers. Inkjet droplets are relatively small, on the order of 20-100  $\mu\text{m}$  in diameter (in-flight), and 1-12  $\mu\text{m}$  in thickness (when printed), this means that mixing lengths between monomers are controlled. The combination of these short mixing lengths and controlled volumes should lead to successful FRIJP of PU without solvent.

The research shows that there is interest in a variety of fields for increasing the materials processable through inkjet printing. Polyurethane is a chemistry which offers a large degree of flexibility, in both the selected chemistry and material properties. This makes it a good candidate for further material development. Finally, it has been shown that there is a desire for complex PU geometries.

## 2.4 Fully Reactive Inkjet Printing

There have been only two authors that attempt to use FRIJP to produce solid polymers on the substrate. From these authors the two key papers are the reactive jetting of polyurethane by Kröber<sup>9</sup> and nylon by Fathi,<sup>97</sup> of these two, only Kröber achieved a solid.

### *Reactive Inkjet Printing of Polyurethane<sup>9</sup>*

Kröber presents and discusses the fully reactive jetting of polyurethane, achieved through the jetting of two inks. The two inks are: an isocyanate and catalyst solution in DMF (47 %wt solvent), and a polyol with cross-linker solution also in DMF (25 %wt solvent). The work sets out to use four different monomers, two isocyanates and two polyols, but reports that one combination (2-4-toluene diisocyanate and PEG 400) produced severe bubbling. This bubbling was likely caused by the water isocyanate reaction, but this was not confirmed. The majority of the work concerns the jetting of isophrone diisocyanate and polypropylene glycol 400. It was reported that a solid product was formed using a catalyst and a cross-linker solution in three minutes. The paper also reports the use of a fluorescent dye introduced to the polyol ink to determine the mixing, shown in Figure 2-20. The work detailed in the paper neglected key polymer chemistry considerations, but it is the only FRIJP work reporting a solid.

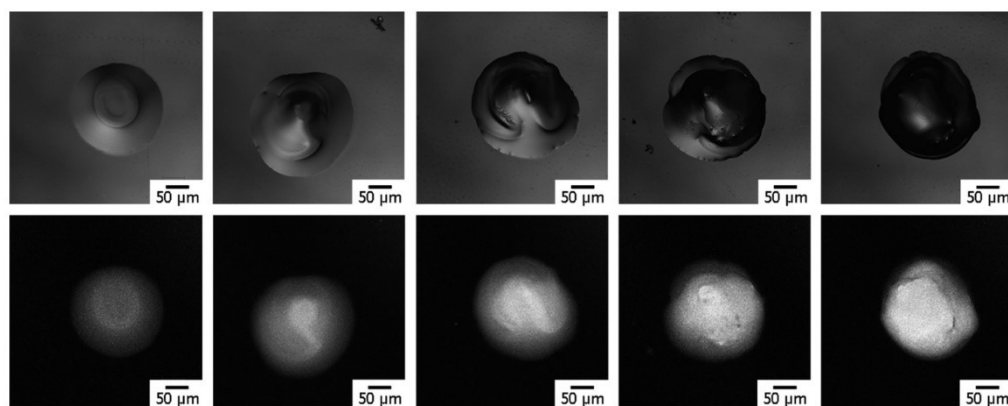


Figure 2-20 - Confocal laser scanning microscopy tracking a fluorescent dye included into the polyol components. Images represent an unknown time series,

top is reflectance, bottom is fluorescence. Reproduced from Kröber<sup>9</sup> with permission from rights holder.

The paper does not conduct any chemical analysis on the printed samples, instead the reported conversion is from direct pipetting experiments. The printed polyurethane is chemically cross-linked, due to the introduction of a tri-functional hydroxyl group. The cross-linking concentration in the diol ink was 52 % (molar), this would result in a highly cross-linked polymer likely to be extremely brittle.

There is no mention of achieving the correct mixing ratio between the two inks, instead it is suggested that they are printed in volumes determined by line stability. This means that the mixing ratio between the two monomers is not stoichiometric. The paper is written in a manner that suggests solid polyurethane was unobtainable without the use of cross-linker, implying the degree of mixing and conversion is low. This is in agreement with the predicted  $\overline{M}_n$  of  $\sim 850$  from the Carothers equation (based on 70% CNO curing).

To achieve solid samples three minutes of heating to 90 °C was required, at this temperature and for this duration it is possible that all unreacted chemicals evaporated or reacted with the moisture in the air (slower as to release the carbon dioxide).

The use of 2D microscopy with fluorescent imaging (Figure 2-20) only determines the initial spreading across the top of the droplet, not the depth dependent distribution. From literature it is now expected that molecular diffusion is the only mechanism for mixing. The use of a dye that is independent from the monomers is only useful for tracking convective flow, for the case of FRIJP dye tracking is therefore unsuitable.

*Challenges in drop-on-drop deposition of reactive molten nylon materials for additive manufacturing<sup>97</sup>*

Fathi<sup>97</sup> describes an attempt at fully reactive printing of nylon by the co-deposition of two solutions. These solutions were initiator and activator, in a caprolactam medium. The caprolactam was jetted as a phase change ink, where head heating melted and reduced viscosity into the printable range. The work reports that the fully reactive printing was unsuccessful due to the failure of the catalyst ink, as no mixing occurred there is little to gain from this PhD.

This paper also makes use of fluorescent dye to colour an ink, this has the same issues as previously discussed.<sup>8,64,98</sup> A second, specific, issue with the method of Fathi is that the reaction isn't just a single droplet, but a large puddle (>5 mm across) created by the multiple deposition of droplets.

## **2.5 Gaps In Research**

From reviewing the literature it is clear that the research area of fully reactive printing is still unexplored. A possible cause for this may be due to the difficulty of running the printers. Despite how advanced home inkjet printers are, the tools for research inkjet printing of 3D objects are still only recently developed<sup>8</sup>. This is then worsened by the requirement of at least two inks. Not only do these inks need to be developed, they also need to be deposited at the same time with a high accuracy. To conduct analysis on these samples they also need to be printed quickly to achieve moderate sample sizes. Despite the speed and scalability of industrial printers, the step from research to high throughput requires an expensive outlay.

The area of fully reactive jetting is very interesting for producing new polymers for material jetting. Material jetting is currently dominated by photo-curable inks, with issues related to mechanical properties, part life, thermal degradation, and industrial relevance.

### **2.5.1 Statement Of Novelty**

The literature related to material jetting has been reviewed, specifically research of fully reactive jetting. The novelty of this PhD can now be re-assessed by comparing it to the currently available literature.

There is no area in the literature that discusses the requirements of a multiple component reactive inkjet ink. In the development of a printer this PhD encountered a number of challenges overcome in novel ways.

PDMS is an interesting material in its own right, but it is also seeing use in conductive track printing. There are currently no methods for additively printing it, this PhD developed and analysed the printing of PDMS from a two component ink. Previous works that have printed using multiple materials have not been able to sufficiently

characterise or control the output. This PhD has conducted dimensional and chemical analysis of all printed samples. In the case of PDMS this involves FTIR and Raman techniques to determine degree of cure. For the polyurethane work the molecular weight achieved on the substrate has been the focus, while also using NMR to determine if the process was successful in producing polyurethane. In the literature, single droplet cases have been analysed but there has been no analysis of larger samples to determine homogeneity. For the printing of PDMS in this work spatial Raman was conducted which could determine if the printing process produced homogenous samples, or if concentration gradients were present.

### **2.5.2 Intention of Research**

The intention of this work was to demonstrate successful FRIJP, whereby one or more ink combinations are shown to produce a viable mechanical polymer in an AM process. To demonstrate a working process the research needs to challenge the assumptions that mixing without stirring is an issue,<sup>8</sup> that there is a lack of usable materials for AM,<sup>5</sup> and that there has not been any quantifiable evidence for successful FRIJP.<sup>9</sup>

The research then not only considers the chemistry, but also the process. With a large focus on developing and refining a research printer designed for the FRIJP process. In tandem the research investigates and refines three different ink systems (from two ink chemistries) to produce three multi-component inks that result in three distinct materials.

The research was not focused on improving the performance of the materials created, as this is a study of itself. However, it aimed to show that there was merit in further investment into inks for the FRIJP process. It proves this capability by showing that high degrees of mixing and reacting were possible, whilst obtaining shape and form as desired.



## CHAPTER THREE

### ***3 Materials and Methods***

The following section details the materials used in this study, the methods used for analysis, and the developed printing method.

#### **3.1 Materials**

The solvents used as viscosity modifiers for the printing of PDMS and PU were Octyl Acetate (112-14-1) and Anhydrous Dimethylformamide (68-12-2). For the NMR and SEC analysis Dimethylsulfoxide (DMSO-d<sub>6</sub> : 2206-27-1) and Dimethylformamide (68-12-2) were used as solvents. The solvents were supplied by Sigma Aldrich, and they were used without modification. For the PU reaction n-Butylamine (109-73-9) was used as a quenching agent.

##### **3.1.1 PDMS**

A commercially available two-part silicone (Polytek PlatSil 71-Siliglass) was used as the basis of the reactive ink. The viscosities of the reactants (155 mPa.s and 200 mPa.s) are close to the operating range of industrial print heads (~30 mPa.s), this allows for a high polymer loaded ink. The two parts of the PDMS ink are referred to as A (hydride containing) and B (catalyst containing), the crosslinking reaction is shown in Figure 3-1. The formulation is designed to react in a 1:1 (weight) ratio. The mixing of the two components allows for the platinum catalysed cross-linking reaction to occur. The reaction is not inhibited by oxygen or moisture, and consequently, the reaction proceeds as normal without a controlled atmosphere.

Cure analysis has been conducted on PDMS samples using Raman and FTIR techniques. Research conducted by Cai<sup>99</sup> identified the peaks of interest for both techniques. The two bonds used in the Raman and FTIR analysis to determine residual cross link component were: silicone hydride 2152 cm<sup>-1</sup> (Si-H stretch), silicone hydride 913

$\text{cm}^{-1}$  (Si-H bend), and siloxane at  $488.6 \text{ cm}^{-1}$  (Si-O-Si vibration). The last bond, siloxane, was used to calibrate the intensity of the captured waveform, allowing the comparison of multiple samples.

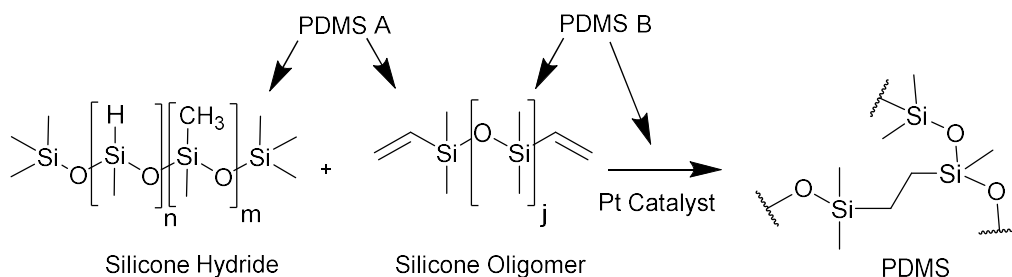


**Figure 3-1** – The components of the PDMS purchased as Polytek Platsil 71-Siliglass, the formula are estimated and the molecular weight unknown.

### 3.1.2 Polyurethane

Solid polyurethane samples were produced from monomers and pre-polymers that are already used in commercial production. These monomers and pre-polymers were selected so that no chemical modification was required for reaction. Chemicals were also selected based on the available data regarding viscosity and surface tension, choosing only those chemicals which required minimal viscosity modification.

#### *H<sub>12</sub>MDI*

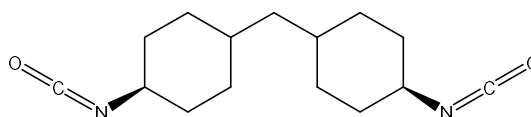


**Figure 3-2** - *H<sub>12</sub>MDI* chemical structure, *cis-cis*, isomer.

*H<sub>12</sub>MDI* is an isocyanate and is the hydrogenated version of Methylenebisphenyl Diisocyanate (MDI). The lack of phenyl groups, due to hydrogenation, increases its light stability over MDI.<sup>100</sup> It was selected due to the expected printable viscosity (based on 30 mPa.s at 25 °C<sup>101</sup>), allowing for a 100% loaded ink. It is sold under the trade name Desmodur W, but it is also known as HMDI, 4,4'-Methylenebis(cyclohexyl isocyanate), and Diisocyanato Dicyclohexylmethane.

H<sub>12</sub>MDI has been used in research to create Thermoplastic Polyurethane (TPU) through reactive extrusion.<sup>102,103</sup> It is typically available in a mix of isomers, *trans-trans*, *cis-trans*, and *cis-cis*, with different polymer properties for varying isomer concentration.<sup>100,104–106</sup> H<sub>12</sub>MDI can be purified through fractional crystallisation to modify the isomer content. This purification was not conducted for this work as increasing the trans content would make H<sub>12</sub>MDI a solid at room temperature.

### *Hexamethylene Diisocyanate (HDI)*

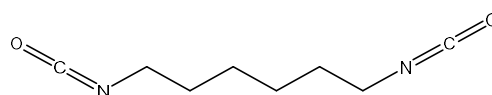


**Figure 3-3 - Chemical structure of Hexamethylene Diisocyanate.**

The second isocyanate, Hexamethylene Diisocyanate, is a linear isocyanate. It was selected as a potential viscosity modifier for the isocyanate ink. It has been used in biomedical polyurethanes<sup>107</sup> and exhibits the same light stability characteristics as H<sub>12</sub>MDI.

### *1,4 – Butanediol (BDO)*



**Figure 3-4 - Chemical structure of 1,4 Butanediol.**

Butanediol, known as BDO, is a common chain extender used in polyurethane production. It is used to increase the hard segment ratio in the final product. Due to its short chain length it was expected to be printable using print head heating, requiring no further viscosity modification.

### *Tripropylene Glycol (TPG)*

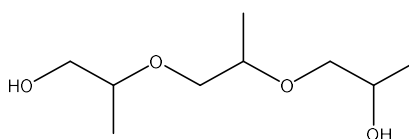


**Figure 3-5 - Chemical structure of Tripropylene Glycol.**

Tripropylene glycol is a longer chain diol, chosen as it was estimated to be miscible with the isocyanate. The estimation of miscibility was performed using the partition coefficient, a value which is an indirect measure of chemical polarity. TPG has a partition coefficient of 0.5-0.6 which,<sup>108</sup> unlike butanediol's -0.23,<sup>109</sup> is the same sign as the estimated value of H<sub>12</sub>MDI  $5.48 \pm 0.69$  (ACD Labs LogP Database).

### *Polyethylene Glycol (PEG)*

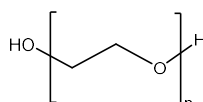


**Figure 3-6 - The chemical structure of Polyethylene Glycol. The molecular weight used in this study was  $M_n = 1000$ .**

Polyethylene glycol was used as a soft segment in the polyurethane polymerisation, the use of PEG as a soft segment allows for a more flexible and elastic PU polymer.<sup>23,85,86,110,81</sup> The molecular weight of the PEG was  $M_n = 1000$ , it was selected as the estimated highest weight PEG that could be printed without viscosity modification. It was a solid at room temperature so an external cartridge heater was required to print this ink, it is also the only ink used which changed phases during printing.

### *Dibutyltin Dilaurate (DBDT)*

DBDT was used as the catalyst in all PU printing, it is an organotin system which has been shown to be an effective catalyst.<sup>111</sup> DBDT has been found to have no great effect on the side production of the urea,<sup>112</sup> an unwanted by-product in this study. There is data available in the literature regarding the kinetic constants of TPU using DBDT, the PU was reactively extruded using DBDT, H<sub>12</sub>MDI, BDO and PEG.<sup>102</sup>

### *Polyurethane Material Summary*

The H<sub>12</sub>MDI (5124-30-1), HDI (822-06-0), BDO (110-63-4), TPG (24800-44-0), and DBDT (77-58-7) were used as received from Sigma-

Aldrich (UK). The PEG (25322-68-3), also received from Sigma-Aldrich, was freeze-dried before use.

For NMR analysis of the PU samples the works of Shih<sup>113</sup> and Saralegi<sup>105</sup> were useful in resolving the spectra.

### 3.2 Methods

In the following sections the methods are discussed. These are as follows: preparing the inks, printing the inks, and analysing the samples.

The experimental method used in this study for developing and characterising a fully reactive ink was as follows;

1. The selection of monomers and pre-polymers which were either printable or through heating and viscosity modification, became printable.
2. Complete characterisation of ink viscosity and surface tension for printability prediction, followed by trial printing on the Dimatix printer.
  - a. Measuring the viscosity and surface tension on the rheometer and drop shape analyser.
  - b. Carrying out any viscosity modification if required.
  - c. Determination of printing parameters; waveform, printing frequency, temperature, and vacuum pressure.
3. FRIJP to assess liquid to solid curing mechanism, using optical time base microscopy on the Dimatix-LP50.
4. FRIJP printing of samples for profile and chemical analysis.
5. Analysis and characterisation of the printed samples.

**Stage 1** was based on reviewing literature and material data sheets for monomers that have suitable properties for inkjet printing. As data pertaining to the viscosity of monomers in the temperature range of 20-70°C (print head range) was not normally accessible,

assumptions were made based on the viscosity data available (typically at 20 or 25 °C).

**Stage 2ab** was carried out using a Kinexus Pro rheometer (Malvern, UK), and a drop shape analyser DSA100 (KRÜSS, Germany). The rheometer was used to determine the temperature and shear rate dependent viscosity of the monomer or pre-polymer, and to decide whether any viscosity modifier was required. The drop shape analyser was used to determine the surface tension of the prepared ink.

**Stage 2c** was conducted when a printable viscosity was achieved. The printing parameters of the ink were developed on the Dimatix (Fujifilm, USA) printer. The use of a drop watcher imaged droplets so that ink ejection, separation, and stability could be determined.

**Stages 3-4** were conducted on the developed FRIJP printer, based on the LP50 printer (Roth&Rau, Netherlands), and Dimatix material cartridges (Fujifilm, USA).

Depending on the ink printed, **stage 5** took two different forms. The PDMS ink was cross-linked and therefore not soluble and could only be analysed using solid state methods. The PUs were all soluble, and bulk solution analytical chemistry methods were employed. The PDMS chemistry was analysed with Raman and Infrared (IR) spectroscopy on a Horiba–Jobin–Yvon LabRAM Raman microscope (HORIBA, Japan), and a Fourier Transform (FT)-Infra Red (IR) spectrometer (PerkinElmer, USA). The PU chemistry was analysed using Size Exclusion Chromatography (SEC) and Nuclear Magnetic Resonance (NMR); on the PL-GPC50 (Varian, USA), and the AV(III)500, DPX 300 (Bruker, USA).

**Stage 5** also included measuring the profiles of the printed samples. The InfiniteFocus (Alicona, UK) was used to capture profile scans of an area.

### 3.2.1 Material Rheology

The print head used in this study was the Dimatix Material Cartridge, DMC-11610 (10 pL). The manufacturer has specific guidelines for this cartridge in terms of the printability range<sup>114</sup>, also known as the Ohnesorge number in the literature review. The recommended range for printing is stated as  $0.54 < Oh < 0.70$ . An extended range is also mentioned, where printing can be achieved in the range of  $0.37 < Oh < 1.75$ . To aid in achieving these printable ranges an in-built heater can increase the nozzle plate temperature thereby reducing ink viscosity. The range of the heater is between 20 – 70 °C, but in practice values below 30 °C were unreliable (due to ambient thermal fluctuations).

#### *Viscosity Background*

The Dimatix guidance material states a viscosity range of 10-12 mPa.s, and a maximum of 30 mPa.s. Once measured, an ink that was inside this viscosity range was determined printable, inks outside were further modified with the use of a compatible solvent.

The Kinexus Pro rheometer, can be used to measure shear viscosity, and dynamic material properties. In this process, the torque required is proportional to the viscous losses of the loaded material. In this way, the rheometer can determine fluid viscosities over a range of shear rates.

The rheometer can reach a range of shear rates from  $0.1 \text{ s}^{-1}$  to  $2000 \text{ s}^{-1}$ , it is however, limited to the maximum torque it can apply. When using highly viscous fluids the maximum attainable shear rate is reduced. The rheometer is also capable of heating the measured fluid to temperatures of up to 180 °C. Finally, because it can analyse over a range of shear rates it is possible to determine if the measured fluid is Newtonian.

Two different geometries are available for the rheometer: the cone and plate, and the concentric cylinder, Figure 3-7. The cone and plate geometry required less fluid for measurement (< 1 mL), but splashing can occur when measuring low viscosity fluid. The concentric cylinder geometry used more fluid (~ 3mL), but splashing could not occur. As ink costs were low, the geometry chosen to use for all viscosity measurements was the concentric cylinder.

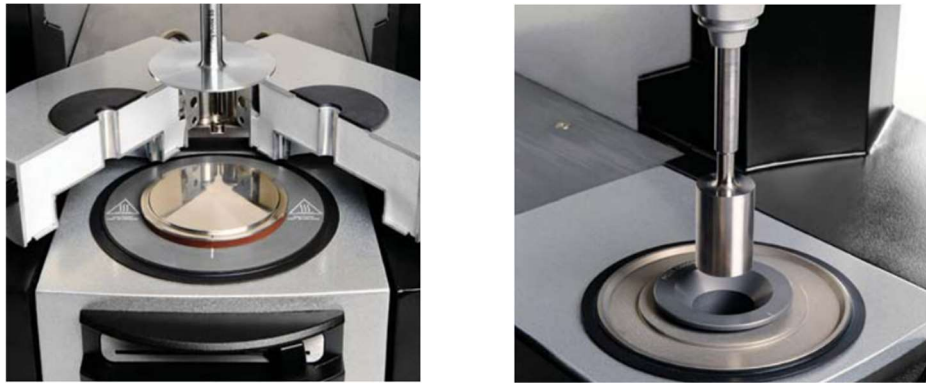


**Figure 3-7 - Geometries used in rheological measurements. First the cone and plate, secondly the concentric cylinder.**

It was discussed in the literature review that although the shear rate of material jetting is much higher than typically measured, issues only arise if non-Newtonian behaviour is observed. When conducting the viscosity measurements a shear rate table was used, measurements were taken between 10-1000  $\text{s}^{-1}$ . It was found that with low viscosity inks at low shear rates the Kinexus was not able to achieve a steady state value. This was likely related to the very low torque required. It was also found that above 100  $\text{s}^{-1}$ , and especially above 500  $\text{s}^{-1}$ , the apparent viscosity would increase. This apparent viscosity increase was not found to relate to any issues in printability and was not present when the alternative geometry was used. It was then hypothesised that this error was found to be due to the concentric cylinder geometry and not a result of the ink. Therefore, the data represented in this study for sample viscosity is taken between 10 and 100  $\text{s}^{-1}$ . These effects can be observed in Figure 3-8.

An exponential model was used when presenting the data of viscosity versus temperature;

$$\mu(T) = ae^{-bT} \quad (3-1)$$

where  $\mu$ ,  $a$ ,  $b$ , and  $T$  are the dynamic viscosity, constants, and temperature respectively.

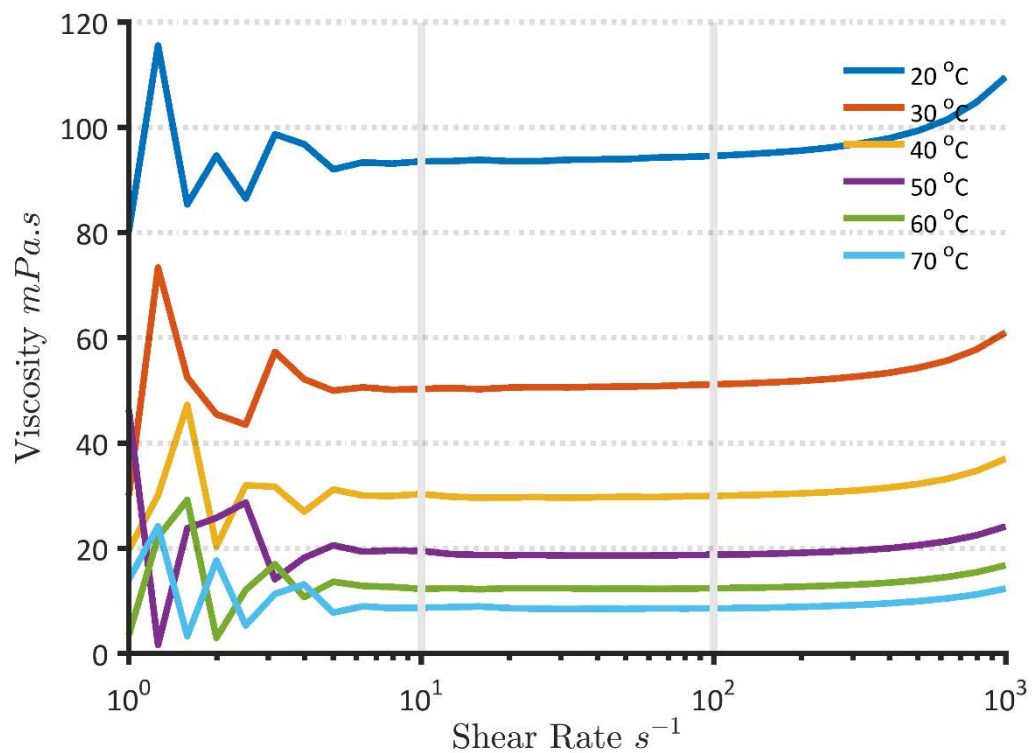


Figure 3-8 - Example of data when the scan is conducted over a shear rate of 1 – 1000 s<sup>-1</sup>. Sample is Tripropylene glycol

### Viscosity Process

To measure the viscosities of the inks a script was created. The script swept through the temperature range 20-70 °C in increments of 10 °C. Once set to a temperature the machine waited for thermal equilibrium; which was defined by a deviation of less than 0.1 °C over 3 minutes. Once thermal equilibrium was reached a shear rate table

scanning between 10-1000 s<sup>-1</sup> taking 5 samples a decade was conducted.

### *Surface Tension Background*

Once a printable value for viscosity was achieved the surface tension of the ink was measured. Surface tension was determined using the pendant-drop method. The equipment used was a DSA100 (KRÜSS Germany), consisting of a fluid deposition module and image capturing device. The calculation of surface tension is through image analysis and processing.<sup>115,116</sup> Samples loaded into a syringe are slowly dispensed until the maximum volume hanging droplet is achieved. At this point, after some rest time (5 seconds) the image can be captured. Hanging liquid in the absence of gravity will form a spherical droplet, but the effect of gravity will disturb this, producing a pendant shown Figure 3-9. The curvature at the bottom of the droplet is then a function of the material surface tension and the force of gravity. This technique requires a value for the density of the liquid; all density information was taken from the supplier material data sheet.

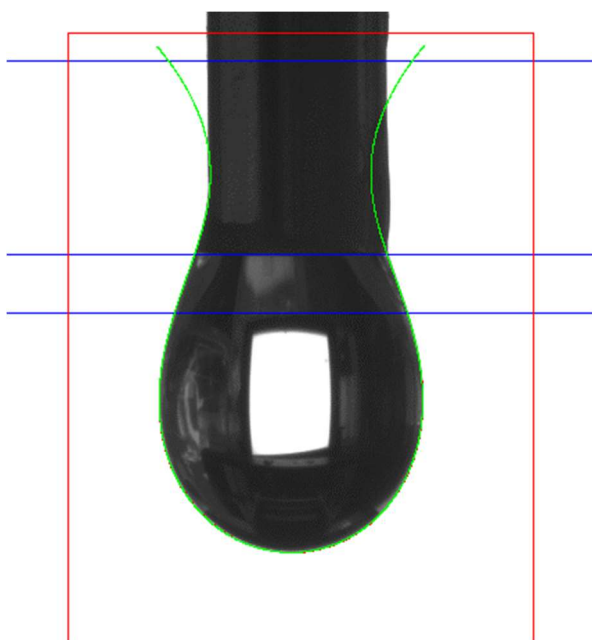


**Figure 3-9 - KRUSS DSA100, pendant drop of H<sub>12</sub>MDI (diisocyanate). Red region defines the analysis zone, blue lines are user specified limits, and the green line is calculated profile fit.**

The error of this analysis is reduced as the drop size increases, so measurements were taken up to the point of the droplet falling. All measurements were taken in ambient temperature. The relationship between temperature and surface tension typically has a negative coefficient. As the printing ranges are typically concerned with surface tension that is too high, lower surface tensions are not an issue.

### *Surface Tension Process*

Samples for surface tension measurement were loaded into a 1 mL syringe and placed inside the DSA. The software, KRUSS DSA, was then used to auto dose ink and capture images using the pendant drop mode. The automated software repeated this process until a maxima of fluid was hanging. At this point the data was captured and a result produced. The measurement was conducted in a lab environment at 25 °C.

### **3.2.2 Printability Assessment**

To assess the printability of the inks they are first loaded into the Dimatix Material Cartridge (DMC). The DMC has two parts that clip together once ready, the top part contains a fluid bag and a fill port; the bottom half contains, the nozzle plate, heater, and connector. The ink was dispensed into the fill port with a syringe, fitted with a 5 µm filter - a total of 4 mL of ink was used.

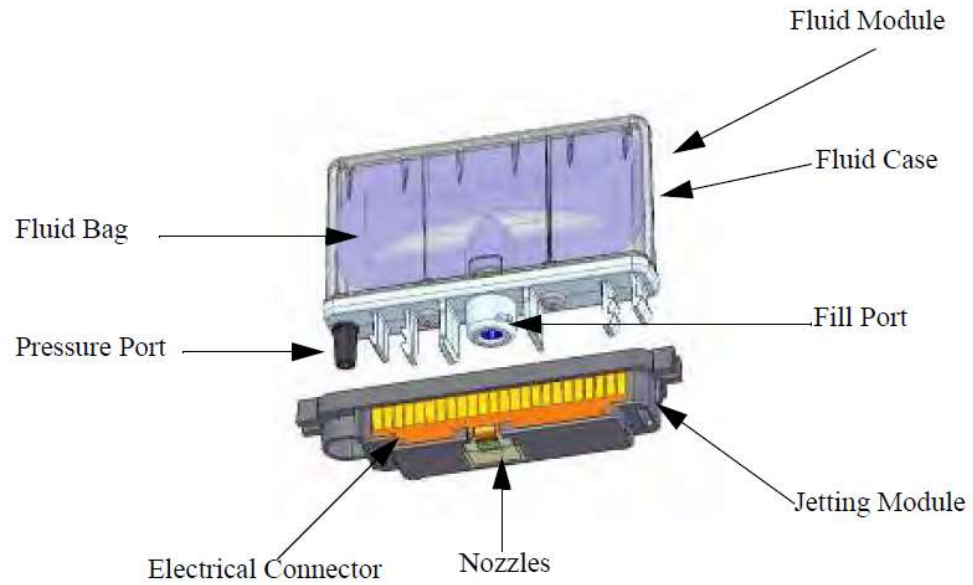


**Figure 3-10 - Dimatix Material Cartridge, the cartridge is shown in the two pieces, on the top the fluid bladder and pressure chamber, on the bottom the nozzle plate and connector. From the DMP 2800 User Guide.<sup>117</sup>**

The Dimatix material printer was used in this study for the initial determination of printability. The printer includes a dropwatcher stroboscopic imaging camera. The stroboscopic method, as described in the literature review, can capture a detailed series of images. Each frame is a composite of multiple events (1000s), where videos are created by varying the delay between print signal and image illumination. The Dimatix software which is used to control the printing parameters and waveform are shown in Figure 3-11.

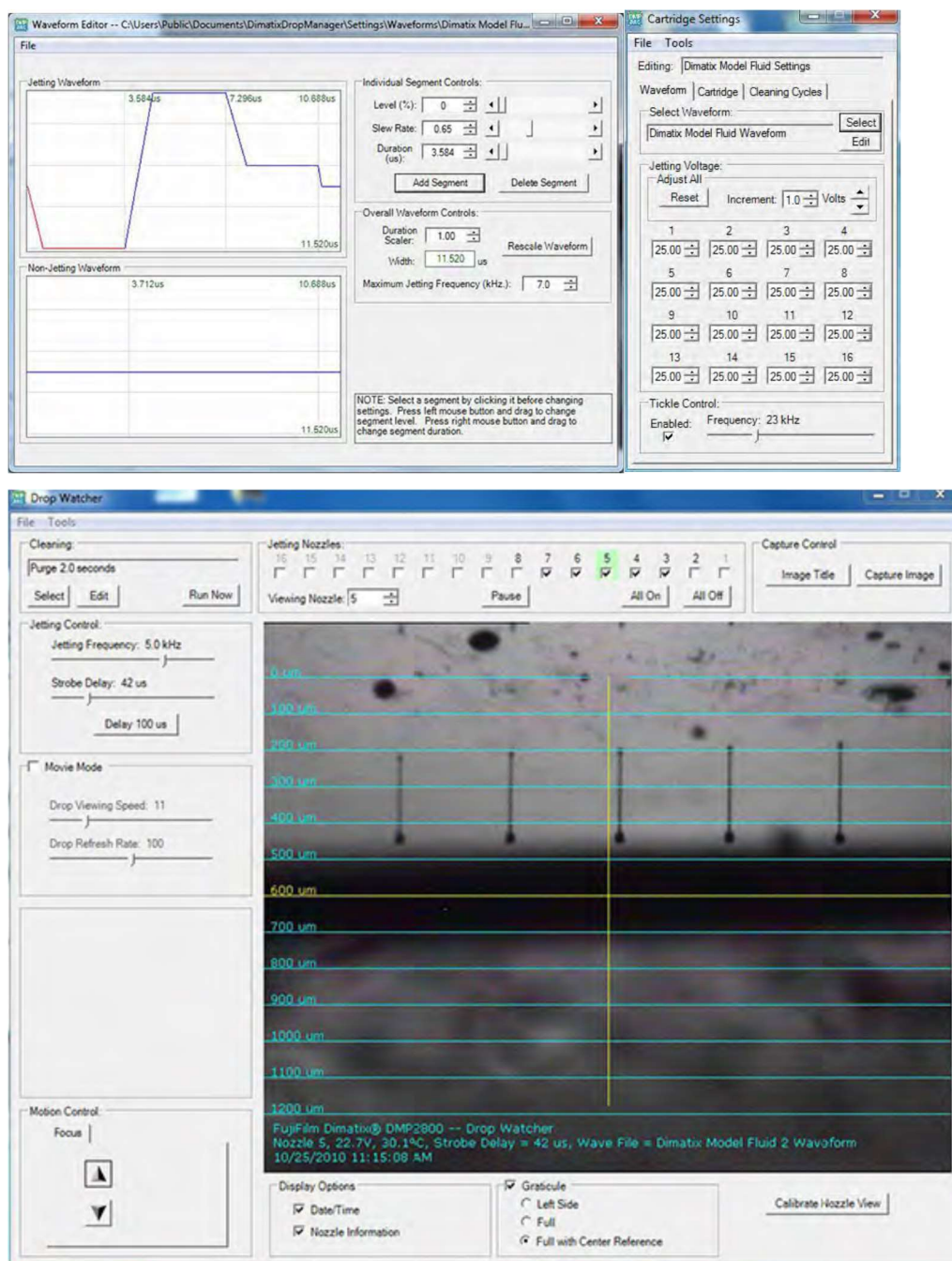


**Figure 3-11 - The Dimatix software, the three windows used when developing a new ink. Top-left, the waveform editor where the voltage controlling the PZT can be changed. Top-right, the voltage for each nozzle, to balance velocity of droplets each nozzle can have its own voltage. This page has multiple tabs to also control the pressure and temperature. Bottom, the dropwatcher view, in this menu you can toggle the nozzles, change the jetting frequency, switch from still to video, and run cleaning cycles.**

The printing parameters were determined in the following sequence: temperature set point, waveform, maximum frequency, and then the voltage. Stability was assessed by running the dropwatcher for over 5 minutes continuously. The temperature set point was based on the data from the rheometer, using a value that produced a viscosity of

less than 20 mPa.s. Further refinement of the temperature was conducted when the waveform was selected, it was changed to produce droplets with velocities around 6 ms<sup>-1</sup>. The Dimatix printer has a catalogue of waveforms, these examples were used as starting points in waveform development. The maximum printing frequency determines at what rates inks can be printed. In industrial inks development time is spent on developing an ink which is capable of the high frequencies for DoD process. It was decided that further development of inks for higher frequency jetting was not an effective use of research time, so ink frequencies above 3 kHz were accepted. Although the process was conducted in stages there was an element of iteration.

### 3.2.3 FRIJP Printing

The FRIJP printer will be described in the developed jetting methods section; however, techniques relating to general printing are described here.

#### *Environment Control*

The moisture sensitivity of the PU reaction, coupled with the toxicity of diisocyanate, required a controlled and sealed atmosphere. The printer used was equipped with a glove box designed to achieve low O<sub>2</sub> and H<sub>2</sub>O (Figure 3-12); however, it required large volumes of N<sub>2</sub> gas to achieve this and it was found that the H<sub>2</sub>O level increased over time.

An air drying and recirculation apparatus was added which pumped air out of the box through a drying column and back into the far side of the chamber. The pump (6025SE : THOMAS, Germany) was capable of quickly recycling the chamber air through the column (Drierite 26800 : W A Hammond, USA) and readings (Moisture Meter 635-1 : Testo, UK) below 5% Relative Humidity (RH) were achieved and maintained for the duration of all PU printing. To increase the

duration between desiccant reconditioning the  $N_2$  gas purge was first used to decrease the RH to less than 15%. Environment control was not used for the PDMS printing.

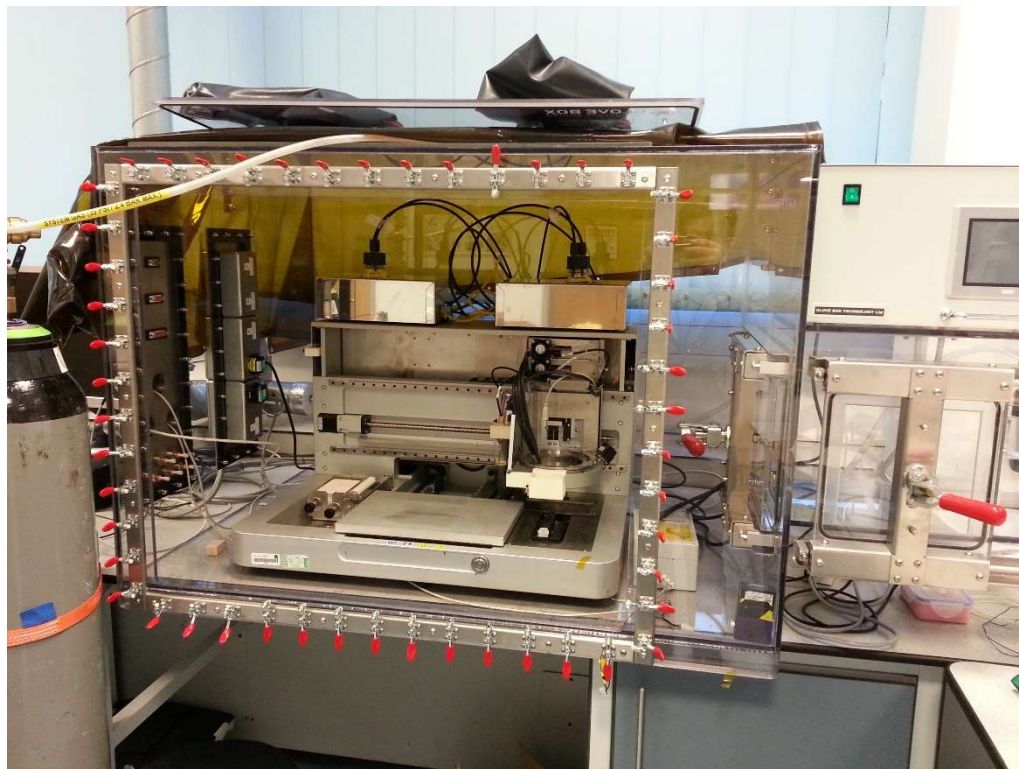


**Figure 3-12 - LP50 Printer inside the glove box. The front panel is currently off but when in place access is through the side chamber.**

### *Drop volume determination*

To determine whether an ink would work in the FRIJP process it was first necessary to determine the ejected ink volume. For this the printer was setup to repeatedly print 500 000 - 1 000 000 drops onto a low weight metal pan (15.6 mg). The sample masses typically weighed around 5 - 13 mg, corresponding to droplet masses around 5 - 13 ng. The print head was positioned over the pan using the substrate view camera of the printer, and the pan was weighed with a balance. The measurement was repeated until a steady result was obtained with a minimum of 5 readings. It was found that occasionally the print head would stop printing, these cases were easily identifiable by the considerable decreased mass and were removed from the mean result.

### *Substrate Preparation*

There were three material substrates used in PDMS printing: glass slides, Polytetrafluoroethylene (PTFE), and coated glass. The pre-cleaned glass slides (48500-00: Cole-Parmer, UK), were used as received. The PTFE substrate (282-0575 : RS-Components, UK) was machined into 5 x 5 mm squares and then the surface was prepared down to P200 grit with abrasive paper.

The final substrate used was a chemically coated glass slide. The process, using 1H,1H,2H,2H-perfluorooctyltriethoxysilane (PFOTS), produced glass slides that maintained their optical transparency, and surface roughness – whilst drastically reducing surface energy. The coating process was as follows;

1. Sonicate substrates in Decon90 (detergent: Decon, UK) for 10 minutes.
2. Rinse in de-ionised water, then dry using nitrogen gas.
3. Rinse in acetone, then air dry.
4. Rinse in isopropanol, then air dry.
5. Submerge in nitric acid overnight.
6. Rinse in toluene.
7. Submerge in 1% PFOTS toluene solution for one hour.
8. Rinse in toluene, then rinse with isopropanol, drying with nitrogen gas.
9. Finally place the substrates in the oven at 100 °C for one hour.

Once the glass slides were coated they were suitable for re-use or cleaning. It was found that cleaning with isopropanol, acetone, or Decon90 did not affect the surface energy determined through contact angle analysis.

#### **3.2.4 Chemical Analysis**

Once samples were printed, chemical analysis was conducted to determine the degree of mixing. All the printed PDMS samples were

chemically cross linked polymers, so were insoluble. The chemical analysis on these samples consisted of FTIR-ATR and confocal Raman. The PU samples were soluble in DMSO and DMF, and were analysed through SEC and NMR.

### *FTIR-ATR Background*

Fourier Transform Infrared spectroscopy is a technique by which an excitation beam can be passed through a sample; the attenuated energy at each wavelength can then be measured. The specific wavelength of attenuation is related to the bonds that the beam has passed through, and in this way it is possible to understand what chemical bonds are present in the sample. Attenuated Total Reflectance (ATR) is a standard accessory that makes it possible to analyse solid and liquid samples without preparation. ATR conditions the beam path so that despite it not leaving the crystal it can analyse samples in contact with it.

FTIR-ATR has limitations: the technique is not inherently quantitative as the degree of attenuation is dependent on sample concentration, and beam length. However, it is possible to use calibration peaks to quantitatively compare samples. Due to the mechanism by which the ATR controls the beam path, only limited sample penetration is achieved. The resulting spectra from an ATR scan is an average concentration of bonds in a depth of 0.5 – 5  $\mu\text{m}$ , in an area related to crystal size. Therefore, when this method has been used to analyse printed samples multiple locations have been analysed.

### *FTIR-ATR Process*

The FTIR-ATR was conducted on a Frontier (Perkin Elmer, USA) machine. The ATR accessory was exclusively used for all sample analysis. Scans were initially conducted from 4000 to 650  $\text{cm}^{-1}$ , at a resolution of 4  $\text{cm}^{-1}$ . Later scans reduced the range to 2500  $\text{cm}^{-1}$ ,

increasing scan speed without losing information. The resulting spectra were taken from the average of four scans corrected by a baseline.

The analysis was conducted in both Perkin Elmer's Spectrum software and using MATLAB. Curve fitting was used to determine peak area. For the quantitative analysis of the PDMS the hydride and siloxane peak areas were obtained.

### *Raman Background*

Raman spectroscopy is similar to FTIR in the results it produces, but measures scattering, not absorption. For this reason, it is possible to have bonds which are active in one measurement and not the other. For the case of PDMS samples the bond of interest were active in both machines. The Raman technique was used for PDMS sample analysis to determine the spatial dependency of curing. The Raman apparatus used was fitted with a confocal microscope to facilitate measurement in highly refined X, Y and Z volumes.

### *Raman Process*

Raman spectra were recorded on a Horiba–Jobin–Yvon LabRAM Raman microscope, with an excitation laser wavelength of 532 nm and a 600 lines.mm<sup>-1</sup> grating. The detector was a Synapse CCD detector. The Raman shift was calibrated using an Si(100) reference sample. Scans were conducted in the print direction (Y), transverse to the print direction (X) and through the printed depth (Z). The complete scan dimensions were 750 μm x 750 μm x 100 μm (X, Y, and Z).

Samples were removed from the printing substrate and placed onto Calcium Fluoride glass. The CaF<sub>2</sub> slides are transparent to the excitation wavelengths, and removed fluorescent effects otherwise observed. Raman data was processed with MATLAB and a curve

fitting scheme was used to determine peak area. Analysis of the cure degree was carried out through monitoring the silicone hydride and siloxane absorption.

### *SEC Process*

For the determination of molecular mass distributions, a size exclusion chromatography (SEC) apparatus (Varian PL-GPC50) comprising an auto-injector and a guard column followed by two linear columns and a differential refractive index detector was employed. DMF (0.1 %wt LiBr) as the eluent was used with a flow rate of 1 mL min<sup>-1</sup> and at a temperature of 50 °C. The SEC was calibrated using narrow poly(methyl methacrylate) (PMMA) standards ranging from 1,010 to 2,136,000 g mol<sup>-1</sup> (EasyVial-Agilent). Data acquisition and calculations were performed using Cirrus Multi GPC/SEC software.

SEC samples were prepared by first transferring the printed solid to a 1.5 ml vial, then the eluent was added. The vials were warmed and agitated until complete dissolution occurred; the solution was then filtered and transferred to the SEC vial fitted with a septa lid. These vials were then placed on the auto sampler and run on schedule.

### *NMR Process*

Proton and carbon scans were run on printed PU, and constituent monomers for confirmation and characterisation of curing. Quantitative proton scans were run with a recycle delay of 30 s to assure adequate relaxation of all responses. Two dimensional scans were not conducted as information regarding PU structure was obtained from literature.<sup>113,118</sup>

Dimethyl sulfoxide-d<sub>6</sub> (DMSO) was used as the solvent, samples were dissolved in the same manner as those prepared for SEC. The

solutions were loaded into 5 mm NMR tubes and placed on the auto sampler.

NMR data was processed with the software package MestReNova and used to obtain information regarding residual isocyanate concentration. As the isocyanate reactive group contains no protons it was reacted with n-Butylamine prior to analysis.

### 3.2.5 Profile Analysis

The printed samples were measured using profilometer techniques to determine the resolution and print fidelity achievable using FRIJP methods. Profile analysis was used to determine the volume of the sample when evaporative effects were expected, this method was preferred over weighing as the samples were difficult to remove from the substrate in one piece.

#### *Focus Variation Process*

The focus variation technique uses a high resolution camera with a precise translation stage. The process revolves around software that is used to determine which area is in focus for each image taken. In this manner large areas can be scanned and resolved to a high resolution – if there is surface variation. The machine used was the Alicona Infinite Focus G5.

Typical samples prepared were smooth and transparent, so could not be directly measured. Instead a physical replica of the sample was created using AccuTrans replica PDMS. The PDMS works well because it has a colour variation that aids the software in resolving features. The Alicona was able to capture the whole profile of the printed samples, however it does have issue with high angles. In these cases scans were conducted with the replica at an angle, and this substrate angle meant the edge could be captured. The substrate angle resulted in loss of the data on the other side of the printed

sample. PU printed samples were typically thinner than the PDMS so no substrate angle was required.

### **3.3 Summary**

The materials in this investigation were selected to represent two different types of reactive jetting. Firstly, a simple reaction scheme was selected that could be carried out without environment control (PDMS). Secondly a reaction scheme was selected that required high degrees of control and mixing to produce desirable materials (PU). When using the first ink, the PDMS, it was found that chemical analysis was difficult due to the cross-linked nature, therefore, when choosing the PU monomers no cross-linker was included.

The analytical methods applied to the printed samples were concerned with the chemistry and shape of the printed samples. Through understanding the chemistry in terms of FTIR, Raman, SEC, and NMR, the degree of mixing and curing could be established. The profile analysis was conducted as a means to determine the suitability of the reaction for self-supported structures and to predict the reaction speeds. Profilometry was particularly challenging due to the small size, smoothness, and transparency of the printed samples.

## ***4 Developed Jetting Methods***

There were two research inkjet printers available at the start of this PhD. As detailed in the methods they were the Dimatix Material Printer, and the PiXDRO LP50. These two printers both had advantages and disadvantages in relation to the work conducted. Therefore a hybrid FRIJP printer was developed during this PhD to fulfil the process needs encountered. As such printing work was conducted on the setup in multiple stages;

1. Dual Dimatix print head, positioned on an Aerotech three axis stage - the printing strategy was layer based.
2. Replaced the Aerotech stage with a PixDRO LP50 unit to reduce setup size. Environment control was then added.
3. The LP50 was modified to use a line based printing strategy, instead of the previous layer based approach.

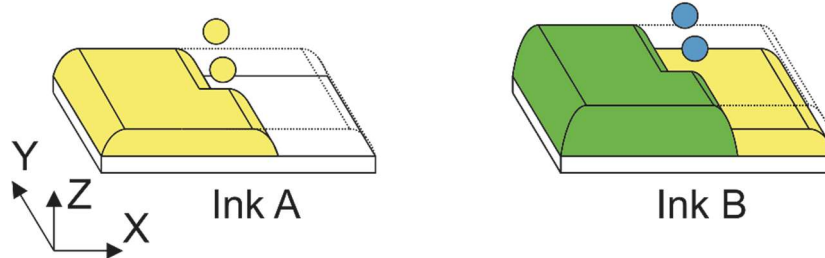
The movement from setup stage one, to two, was due to the new focus of printing PU during the PhD. The toxicity and moisture sensitivity of the PU was such that a secure environmental chamber was required. Once on the new setup an extra ability to rotate the print head assembly facilitated the transition from stage two to three.

### **4.1 Developed Jetting Machine**

Already discussed in the literature review was the limitation of research based printers in relation to multiple inks.<sup>8</sup> In this PhD it was observed that the profile and mixing results were dependent on the printing process, and to explore this fully, greater control of the printing parameters was required. For example, it was found that using a line printing strategy (verse layer printing) both degree of mixing and printed profile could be improved. Figure 4-1 shows how these two strategies differ, critically, the difference is that for reaction

to occur in the layer method a complete layer of component A is printed first. With the printing of layers typically took 1-2 minutes, whereas, the line based approach printed both materials in a single pass and the time to reaction was typically 0.3 s.

### Layer Strategy



### Line Strategy

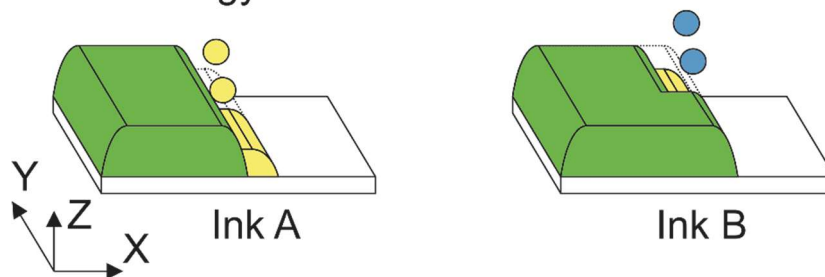


Figure 4-1 - Layer and line printing strategy, yellow = ink A, blue = ink B, green = product.

#### 4.1.1 Print Head

The primary component in an inkjet printer is the print head. Industrially, there are a large range available. For research purposes a low cost, simple print head would afford the most flexibility. Dimatix DMC Cartridges (Fujifilm, Dimatix) were selected. These print heads operate in a similar range (viscosity, surface tension) to industrial print heads with a similar resolution (21  $\mu\text{m}$  nozzle), however they are much less complex (due to only 16 nozzles) and are available at lower cost (~£100 : industrial ~£700+).

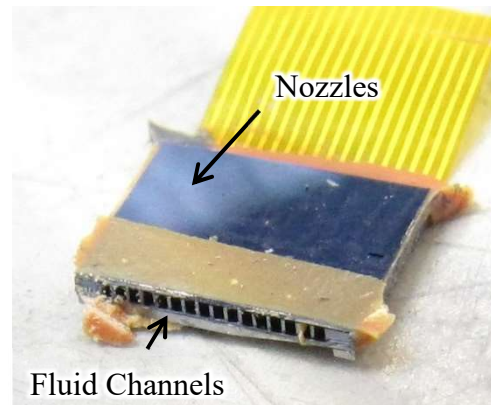
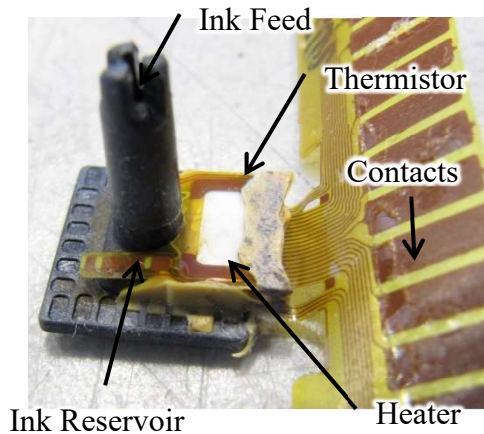
The Dimatix printer interfaces to the print cartridge with a spring contact onto a copper pad. The numbering for the pins was determined through disassembly and investigation, they are listed in Figure 4-2.



Open	1
	2
Heater	3
Nozzle GND	4
Nozzle n	n+4
Nozzle 16	20
Nozzle GND	21
Heater	22
Sensor	23
	24

(a)

(c)



(c)

(d)

**Figure 4-2 - Dimatix DMP Cartridge. (a) Image of an actual cartridge showing the assembly of fluid bladder and nozzle plate. (b) Function of each contact on the print head. (c) Disassembled cartridge where all structural components are removed. (d) Destroyed nozzle plate exposing the fluid channels, these pass over the PZT and to the nozzles.**

### *Driving the Dimatix Head*

Through investigation of the Dimatix printing software, and the corresponding hardware on the driving board, it was discovered that the print head is driven by a field programmable gate array (FPGA). The FPGA generates a print waveform through a digital to analogue converter, which is amplified up to 40 V (Figure 4-3). Each of the 16 nozzles needs individual timing to correctly recreate the jetting pattern. To individually fire nozzles with analogue waveforms each

nozzle needs a dedicated digital to analogue conversion (DAC) channel. The resolution of the waveform is dependent on the resolution of the DAC, the Dimatix printer uses a 256 bit DAC, which requires 8 digital pins. This means the Dimatix printer has 128 digital pins solely designated to nozzle control. To replicate this design for two print heads 256 digital pins would be required. To reduce the design complexity in the circuitry and pattern generation, it was decided that single nozzle control of each print head would be sufficient. This meant for complete pattern control only one nozzle from each print head could be activated at once. This then reduces the complexity of the print pattern generation, as only one nozzle is controlled, only a single trigger signal for each print head is required. This meant that the software for pattern conversion was simplified.

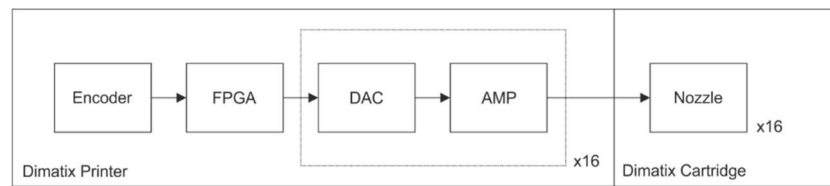


**Figure 4-3 - Schematic of the control of Dimatix nozzles with the Dimatix printer.**

The required circuit was triggered by a 5 V logic signal produced by the positioning stage (after some basic logic operations), the Arbitrary Function Generator (AFG 3252C: Tektronix, UK) was preprogrammed with the waveform. Once triggered, the AFG would output a signal of 0-2.5 V, which was amplified by the operational amplifier (OP-AMP) up to 30 V (limitation of chosen Op-Amp). This setup facilitated the printing of any nozzle on a single Dimatix cartridge (Figure 4-3).

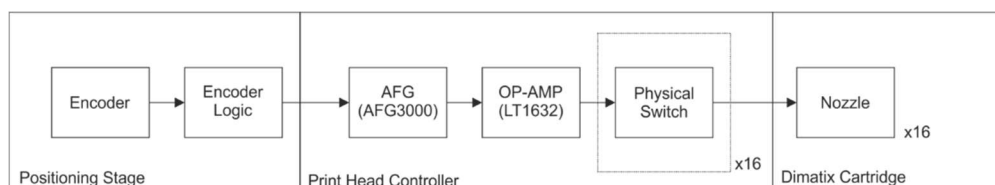


**Figure 4-4 - Schematic of the Print Head Controller designed to take a single trigger input and output a complex waveform.**

For FRIJP, two print heads are required that can be independently controlled in both triggering time, and waveform. Using a two

channel AFG each print head was driven by a single channel. Channel 1 stored the waveform for head A, and was only activated when head A was printing, Channel 2 drove head B. In this way the independent firing of each head with custom arbitrary analogue waveforms was possible.

### *Thermal Control*

The Dimatix material print heads have the ability to heat the ink chamber, this is used to achieve decreased ink viscosities. A PID controller (Arduino Uno), was used to maintain the head heating. The controller read the thermistor, and switched a 30 V power supply through PWM and a power MOSFET (HA210NO6).

In this study phase change reactive monomers were also used. The Dimatix print head requires inks to be a liquid for the purging and filling of the nozzle, therefore heating to the ink bladder was required. This was achieved through the use of a secondary thermistor and heating element, which was attached to the exterior of the cartridge.

### *Control Box*

The signal amplification, switching, and thermal control systems were all housed in a single “PRINT HEAD CONTROLLER”. Two of these controllers were used in conjunction with a dual channel AFG. The exterior of the box has a display and control knob for the nozzle heating, and sixteen switches to enable nozzles individually.



**Figure 4-5 - Dimatix Print Head Controller, a device which accepts a 0-2.5 V waveform, amplifies it to 30V (Gain 15) and control the internal heater.**

### 4.1.2 Aerotech Printer

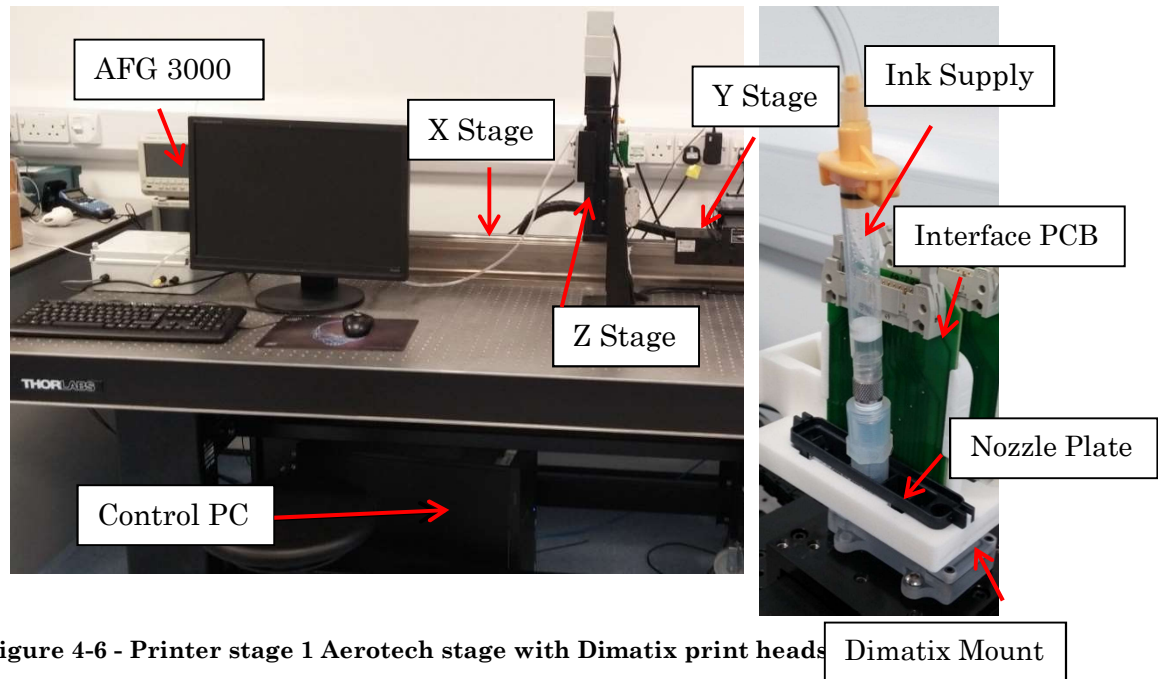
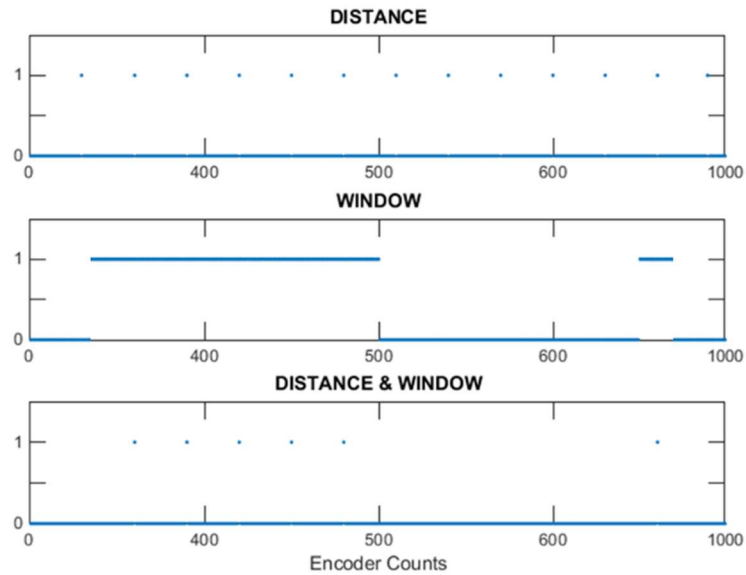


Figure 4-6 - Printer stage 1 Aerotech stage with Dimatix print heads

The first translational stage used to position the dual head Dimatix mount was an Aerotech stage (Aerotech, UK). There were three stages, X Y and Z. The X stage used a linear drive motor with a maximum speed of  $1.5 \text{ ms}^{-1}$ , and a  $1 \mu\text{m}$  positional encoder. The other two drives, Y and Z were ball screws, they had a lower maximum speed of  $100 \text{ mms}^{-1}$ . The stages were controlled with Labview software, through the Aerobasic command (G code) language. The trigger signal was produced by the Ndrive HP control board via the Position Synchronised Output (PSO).<sup>119</sup> This PSO option is capable of a resolution up to  $1 \mu\text{m}$  and at a rate of 32 MHz. A circuit was created to translate the optical relay control to a 5V TTL signal which fed into the AFG.

*PSO Manipulation*

**Figure 4-7 - Result of using the WINDOW and DISTANCE command to control droplet placement. Where  $C = 30$ ,  $A1 B1 A2 B2 = 300,500,650,800$  respectively. A value of 1 reflect a print signal.**

The Aerotech stage has multiple commands related to programming the PSO. The two that are required to reproduce any complex pattern are “PSODISTANCE” and “PSOWINDOW”. These two commands were used to convert bitmap based images to printing Gcode. The function of “PSODISTANCE” was to define the droplet spacing, for example 30 encoder counts would result in a trigger every 30  $\mu\text{m}$ . The second function “PSOWINDOW” would transisiton from disable (low) to enable (high) when crossing the white-black boundary of an image. The printer would then use Boolean logical to combine these two signals to the one trigger signal. With these two commands the print head firing can be controlled (Figure 4-7).

*Labview Pattern Generation*

To generate a file for printing the Labview program needs a BMP file as well as information about the desired printing speed, drop spacing and offsets. With this information it follows an algorithm detailed in Figure 4-8. The code scans line-by-line the BMP file. Where ink is

required it collects the start and stop locations, and this information provides the window start and stop. The output of the Labview generation is shown in Figure 4-9.

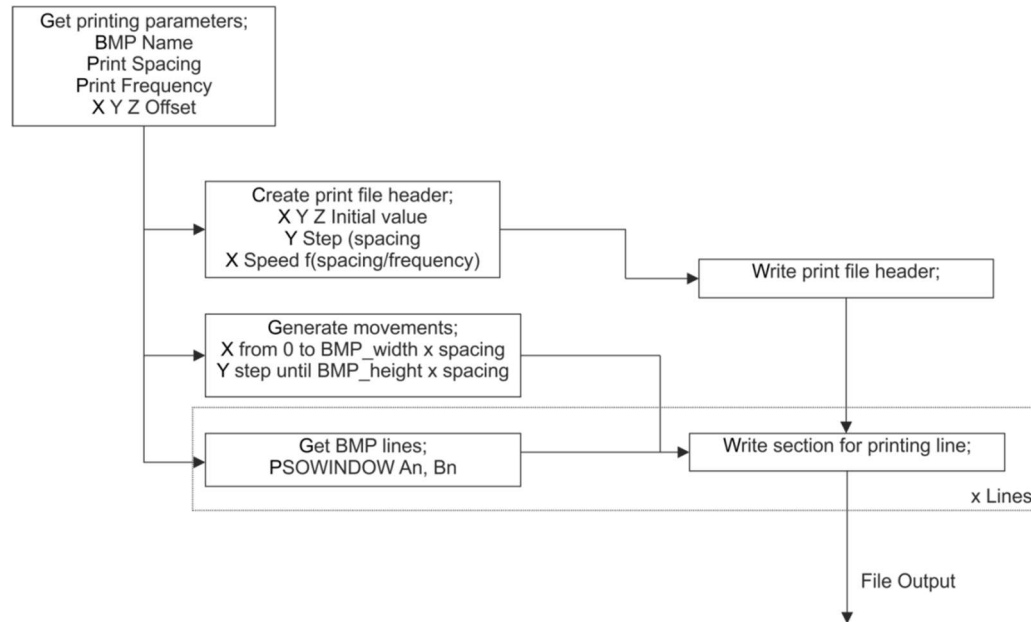


**Figure 4-8 - Process for creating Aerobasic PGM file from a BMP.**

To generate patterns for multiple print heads this process was carried out twice. For the second head the X and Y offsets were shifted by an amount equal to the print nozzle spacing.

Despite the X stage having a high acceleration a set distance of 10 mm was added to printing passes and encoder locations. This distance allowed for the acceleration and stabilisation of the linear stage before jetting commenced.

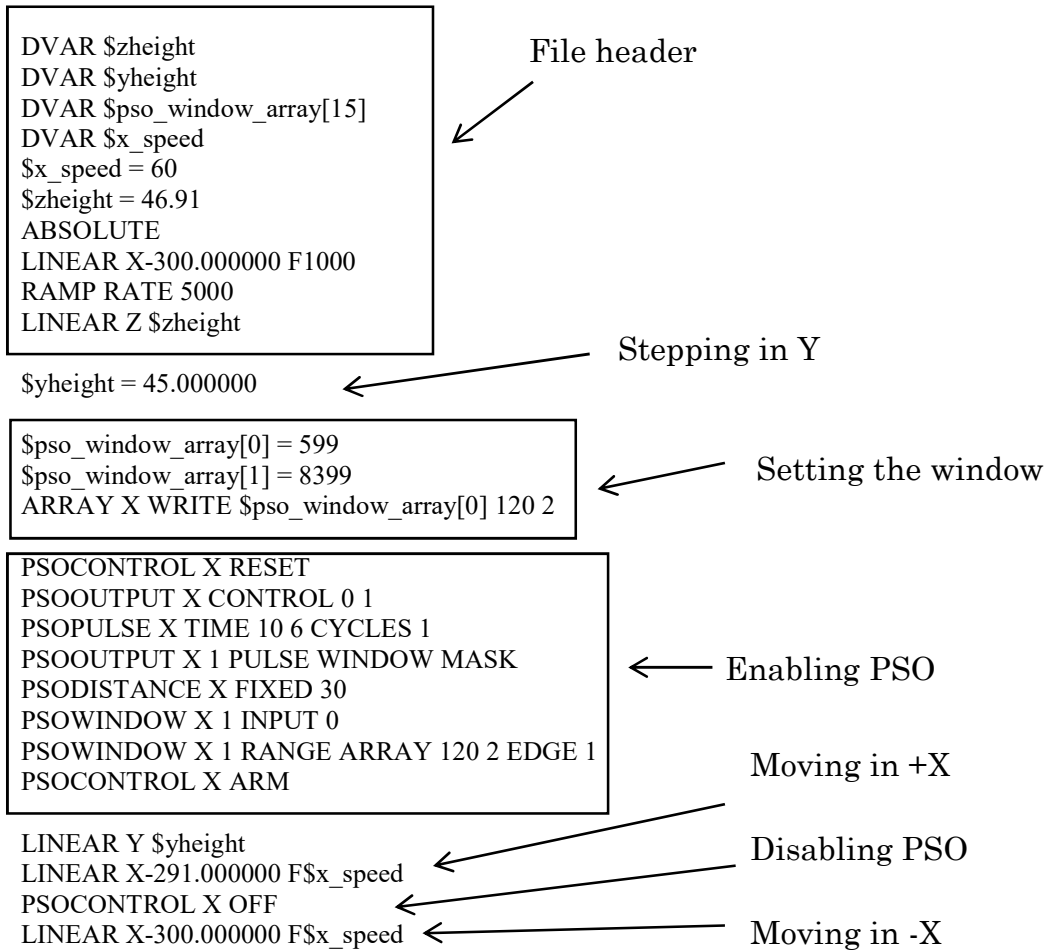


**Figure 4-9 - Generated code snippet from the Labview software for driving the print head.**

### 4.1.3 LP50 Printer

#### *LP50 Printer (unmodified)*

The next stage was conducted on the hybrid setup created during the PhD. The setup combined Dimatix cartridges with the LP50 printing stage, this printer was driven to allow multiple ink deposition in a single print pass.

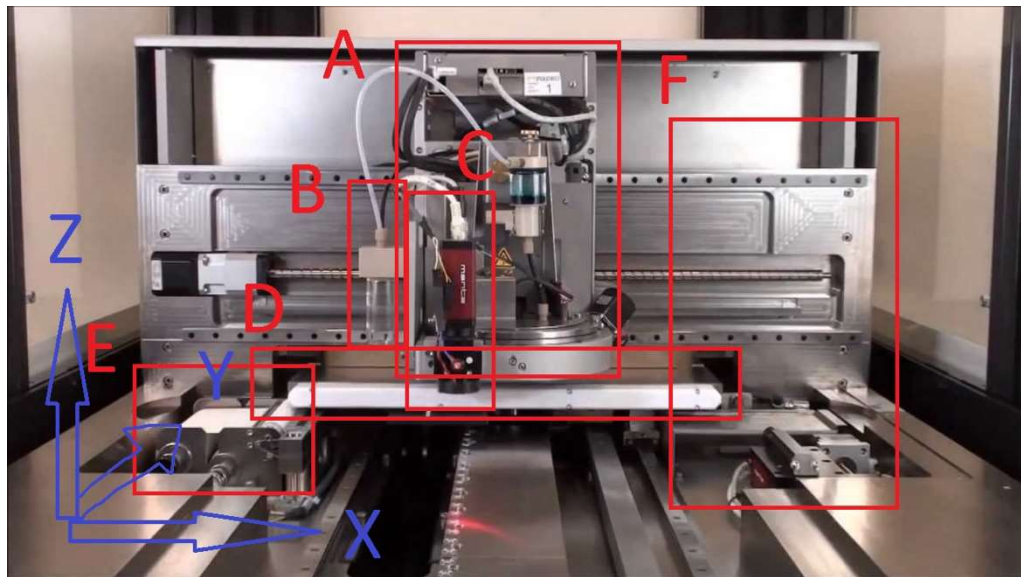


**Figure 4-10 - Un-modified LP50 printer.** a) Print head carriage, translation in X and Z. b) Pressure feed and overflow reservoir. c) Substrate camera. d) Print substrate, heated and vacuum chuck, translation in Y. e) Cleaning station. f) Dropview area.

The unmodified LP50 printer is shown in Figure 4-10. Printing is typically carried out by placing the print head and drive board in the printer carriage (Figure 4-10a), then the dropwatcher (Figure 4-10f) is used to confirm correct ink ejection. When printing a pattern the machine contains an offset between the substrate camera (Figure 4-10c), and the substrate (Figure 4-10d), so positioning the camera above the desired location also positions the bottom left of the desired pattern.

When using multiple print heads the heads need to be aligned by entering the X and Y offset into the software. The substrate camera is calibrated when the LP50 is manufactured so it can be used for this

task. Once aligned the printer can use both print heads, with full control over the printing pattern.

### *LP50 Printer (Modified)*

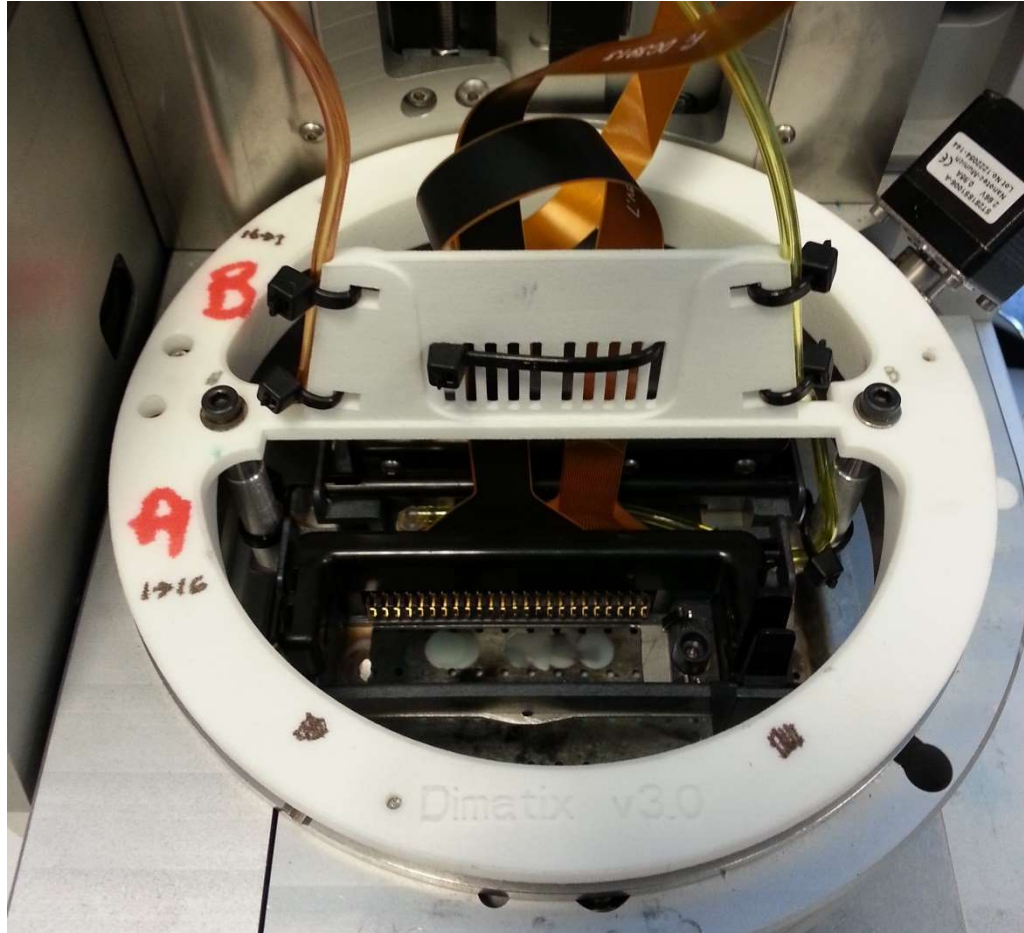


**Figure 4-11 - Dual Dimatix assembly for the LP50 printer. Heads A and B are interfaced through the actual Dimatix interface device (sourced as spares). These are mounted on a metal plate, connected to a laser sintered hub. The whole assembly can rotate up to 90° counter clockwise.**

Printer stage 1 was effective in positioning and printing with Dimatix cartridges. However, when producing large parts, other features, such as head cleaning, substrate heating, substrate camera, and more complex pattern control, were required. To achieve this the LP50 printer was used, this was configured using the auxillary output to produce a trigger signal identical to printer stage 1. The print head drive electronics were transferred without modification.

Once the electrical interface was setup the software of the LP50 could be used in an unmodified state. The LP50 is setup with a “Single

Nozzle Assembly” which uses the inbuilt print generator (Bitmap to print file converter). The only software change required was to add into the printing recipe (C# programmed file), the serial communication required to directly switch the AFG from channel 1, to channel 2.

Dimatix cartridges are a low cost PZT jetting solution, as such they have a lower build quality than other print heads. The location of the print head in the holder was not repeatable; therefore, whenever the head was removed or replaced a recalibration was conducted. Calibration involved printing a pattern with each head, measuring the offset from the origin, and updating the head assembly files.

It was found, that due to the size of the Dimatix holders, the nozzle positioning was towards the edge of the head assembly. This meant that the dropwatcher on the LP50 could not be used. Therefore, all drop watching was conducted on the Dimatix printer, and nozzle stability was gauged using printed grids.

#### **4.1.4 Line Printing**

It was necessary to align the print heads specifically for line based printing. The print head mount was fixed onto the head assembly, and to maintain the alignment it was necessary to allow for adjustment. The alignment was then achieved by rotating the print head carriage. This rotation aligned the two printing nozzles parallel to the print head movement, shown in Figure 4-12.

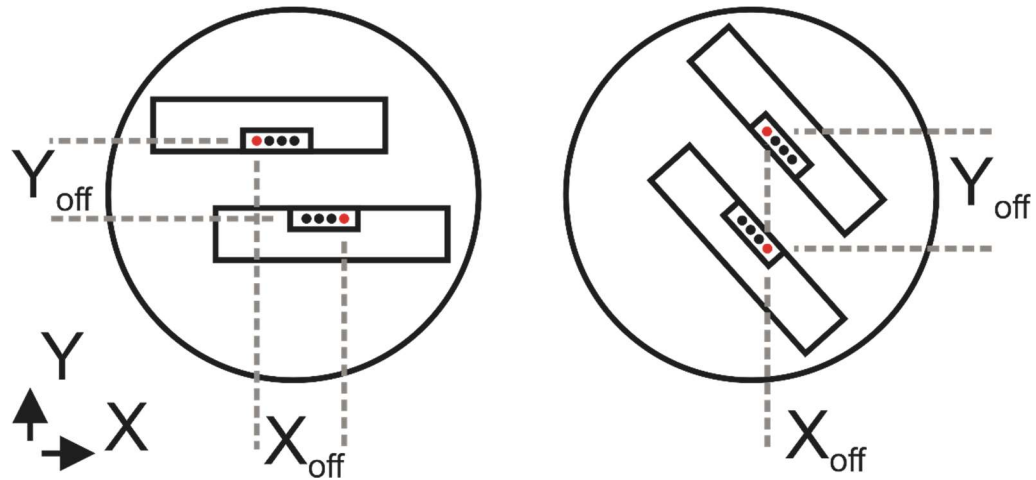


Figure 4-12 - Aligning the print head nozzles through rotation of the print assembly. With a zero  $X_{offset}$  in a single pass both materials can be printed.

### *Mechanism of Alignment*

As the printer developed could only print with one nozzle it allowed for head alignment to be carried out by rotating the whole print head assembly (Figure 4-12). In this manner the X and Y offsets were translated into a Y offset and an angle. The values were calculated through the following relationships;

$$Y_{line\ off} = \sqrt{\Delta X_{off}^2 + \Delta Y_{off}^2} \quad (4-1)$$

$$\theta_{line\ off} = \text{atan}\left(\frac{\Delta X_{off}}{\Delta Y_{off}}\right) \quad (4-2)$$

### *Design of a Printing Pattern*

This operation aligns the print head in the X direction, but creates a large Y offset of around 45 mm. The LP50 printer only has one external trigger signal. Previously, when layer printing it was possible to use serial communication to switch print heads at the AFG, however this process took around 30 s so was too slow for line based printing. Therefore driving each print head independently, in one pass, was not possible.

Instead driving both heads with one trigger signal was used, in this way the printing could be a continuous pass. To drive both print heads with one signal a complex pattern was required, the pattern involved

both printing patterns for the A and B inks and also the Y nozzle offset. Through the use of a MATLAB script a generation of a specifically offset overlapping pattern was developed. This pattern allowed for single pass printing of both materials, shown Figure 4-13.

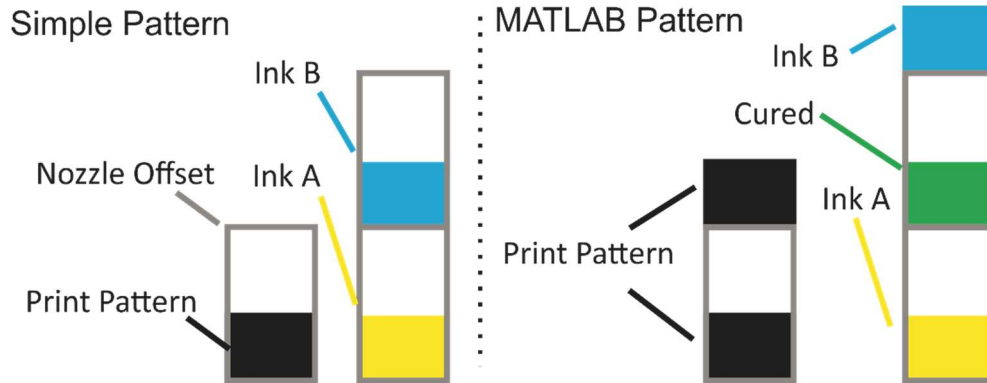


**Figure 4-13 - Creating a line printed sample through the manipulation of the printing pattern. The printing pattern has two duplicate patterns with an offset equal to that of the nozzle spacing.**

In this pattern the two squares are for each print head, the drop spacing is not identical. This method also results in two additional patterns, printed with only a single material. This effect was unavoidable with the current printing process. The time taken for mixing to occur in the line based strategy was fixed, unlike the layer based strategy that was dependent on pattern size. Typical times were 0.3 s, with an offset of 45 mm and a head speed of 120  $\text{mms}^{-1}$ .

### *Drop Ratio*

The mixing ratio required for printing is a function of the specific formulations used and the printed droplet mass. It is also necessary to take into account any unreactive mass, either solvent or catalyst. Inkjet printers produce discrete volumes, as such only a finite ratio can be achieved. As patterns become larger, many thousands of droplets are used, increasing the accuracy of the attainable ratio. To control the droplet ratio the drop spacing was changed. The equation to determine the secondary drop spacing based on the first is;

$$DropSpace_b = \frac{DropSpace_a * DropMass_b}{DropMass_a * MassRatio} \quad (4-3)$$

In this study droplet ratios were controlled in a line by line case, changing the drop spacing in only the Y direction. The primary reason for changing drop spacing in only the Y direction was to decrease the number of passes required, decreasing total print time.

Achieving the correct mixing ratio whilst limited to integer values for drop spacing was achieved through supersampling - creating a pattern at a higher resolution than required to print. The patterns were generated with each pixel corresponding to 1  $\mu\text{m}$ . To achieve a drop spacing of 10  $\mu\text{m}$  a single black pixel followed by 9 white pixels was required (black is printed). Through supersampling, the print spacing for each head can be changed during a single pass. Through careful selection of discrete spacing, average fractional spacing can be achieved. An example generated file for the printing of H<sub>12</sub>MDI and butanediol is shown in Figure 4-14. The pattern includes both the fractional drop spacing, and the nozzle offset to achieve line by line printing of multiple materials.

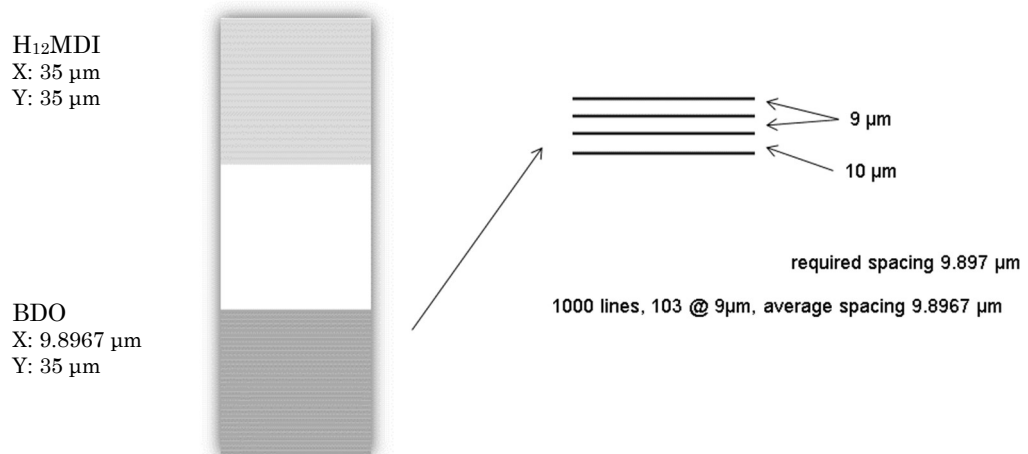


**Figure 4-14 - Creating fractional droplet spacing through supersampling printing pattern. Achieving a droplet ratio of 1:3.5364. Without this method only 1:3.5 could be achieved, an error of over 1%. In this image the space between the two patterns has been reduced.**

*Issues*

Two issues arose using the line based strategy for printing. The first was that both print heads were printing the pattern twice, one to overlap, the other to be wasted. When printing large patterns the waste area could spread, contaminating the overlap region. To solve this, raised substrates (glass slides) were used to isolate the desired area. The second issue is related to driving both heads with the same trigger signal. To maintain printing in the stable frequency range it was necessary to account for both patterns with either head. This meant that printing at too high frequency could cause nozzle blockage, so the head speed was set to limit the maximum frequency of the head accounting for both printing patterns.

## 4.2 Discussion

Until now there has been no consideration of the total printing process related to FRIJP. The works described in the literature review still consider FRIJP as a method of single drop reactions with research printers. Through minimisation of solvent, understanding the dispensed drop volume, and printing multiple materials in a single pass, the printing scheme designed in this study was able to produce complex printing patterns to fully utilise FRIJP.

The developed printer combined low cost print heads, high degree of printing control, and facilitates the line based printing process. The major advantage of the line based approach was that it removed the connection between pattern size and time to mixing. When printing with the layer based approach doubling the pattern size doubled the time to mixing, with the line based approach the time to mixing was fixed based on the print head scan speed, and the physical print head spacing.

The method to achieve the line by line approach was created to work around existing hardware. It revolved around the fact that the LP50 printer only supported a single external trigger output. If there were two outputs the pattern would not need to have the nozzle offsets, as they would have been independently driven. If there were more than two outputs, or if there were ways of driving all the nozzles, the method of rotation to align the print heads would not work. The strategies outlined here are not for adoption in industrial systems, they are a method for replicating the capabilities of industrial systems on a research level.

## 5 FRIJP of Polydimethylsiloxane

The FRIJP of PDMS was conducted with three different setups which were discussed in 4 Developed Jetting Methods. In all cases, the ink formulation is maintained but the strategy and ratio of the inkjet depositions are changed.

### 5.1 Results

#### *Ink Formulation and Printing*

The PDMS based FRIJP ink was designed around the principle of separating the cross-linker and the catalyst. The chemical used was a commercially available two-part silicone (Polytek PlatSil 71 Siliglass) where the viscosities of the reactants (155 mPa.s and 200 mPa.s) are sufficiently close to the operating range of industrial print heads (2 – 30 mPa.s) to be processable. The two parts will hereafter be referred to as PDMS A and PDMS B, Figure 5-1. This specific chemistry was also used because it is designed to be mixed in a 1:1 wt:wt, resulting in almost 1:1 droplet ratio, and the production of no by-products and it represents option 2 in Figure 2-13.

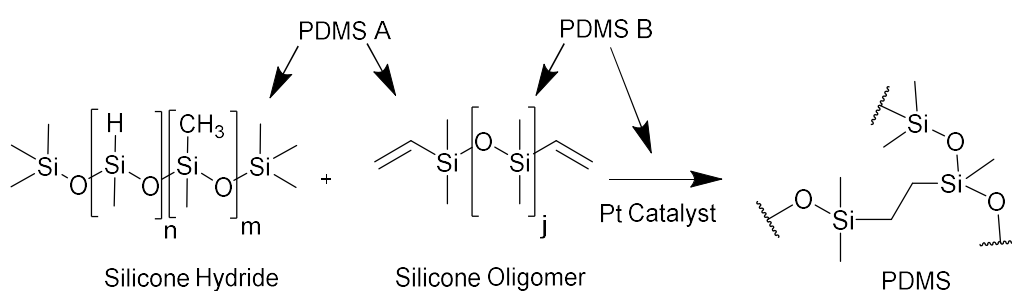


**Figure 5-1 - Crosslink reaction of PDMS in the presence of a platinum catalyst, the silicone hydride bond Si-H is replaced with a Si-C bond when the C=C bond opens, and the hydrogen relocates to the new carbon. The compounds in each component of the PDMS formulation are labelled, as specified in the MSDS.**

The viscosity of the PDMS A and B was too high for printing at the maximum temperature of the print head (80-60 mPa.s @ 70 °C). Therefore, a compatible solvent was required. Solvent compatibility was determined through miscibility tests, and it was found that Octyl

Acetate was miscible with both of the PDMS parts and was not found to damage the print head. The production of a solution containing the pure PDMS and a solvent will hereafter be referred to as an ink, PDMS A will be Ink A, and PDMS B will be Ink B.

A range of dilution ratios were trialled using, 80, 70 and 60 wt% PDMS loadings. These were analysed with the rheometer, and it was found that, with combined head heating and 60% loading, a printable ink could be formulated. The viscosity at 60 °C was  $19.71 \pm 0.24$  mPa.s, and  $17.68 \pm 0.12$  mPa.s, for Ink A and Ink B respectively. The values for the temperature dependent viscosity for both the pure PDMS, and solvent ink are shown in Figure 5-2.

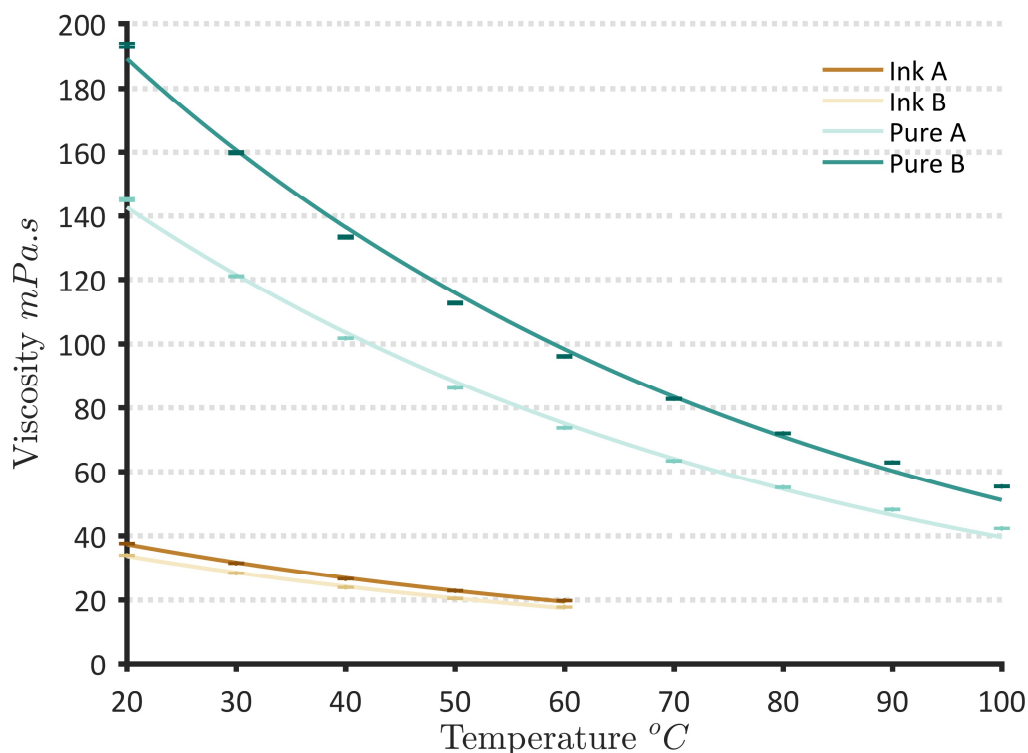


**Figure 5-2 - PDMS, and PDMS ink viscosity versus temperature. A printable viscosity was achieved when using 40% Octyl Acetate as a solvent.**

Once a printable viscosity was achieved, the surface tension was determined. The surface tension for the inks was found to be  $23.6 \pm 0.2$  mN.m, and  $23.3 \pm 0.1$  mN.m, for Ink A and B respectively. These values led to an Ohnesorge number of 0.89, and 0.80, a value within the printable range of the Dimatix cartridge. The printing fluid

parameters, Ohnesorge number, and droplet mass are summarised in Table 5-1.

**Table 5-1 - The fluid properties of the printable ink formulation. Droplet mass was conducted only after printing setup 3 was used.**

Ink	Tem p. (°C)	Viscosity (mPa.s)	Surface Tension (mNm <sup>-1</sup> )	Ohnesorge	Droplet Mass (ng)
<b>Ink A</b>	60.00	19.71 ±0.24	23.60 ±0.20	0.89	10.4 ±0.24
<b>Ink B</b>	60.00	17.68 ±0.12	23.30 ±0.10	0.80	11.92 ±0.18

‡ - Printing conducted before mass was considered

† - Value found in literature

It was found that both inks could reliably jet up to a rate of 5 KHz. The ink properties led to no stable satellite formation, and only simple waveforms were used. An image series showing the process of the jetting for ink A is shown in Figure 5-3: formation of a satellite can be observed which then combines with the primary droplet.

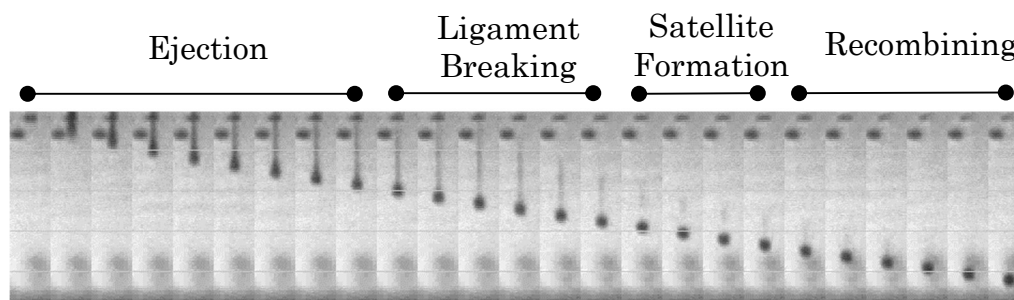


**Figure 5-3 - Jetting process of Ink A. Duration of the capture is 100 μs, droplet diameter is 20 μm. Image series captured using the Dimatix drop watcher camera.**

Despite prolonged periods of inactivity the nozzles did not become blocked; after a purge cycle, the nozzles worked as new. Due to the nature of this FRIJP ink there is no reaction until the two materials are combined. The lack of reaction until combination meant that the PDMS ink was not susceptible to light initiated and did not require special storage conditions, unlike UV based inks. Also because the physical form of the ink was a liquid and solvent was added to further reduce the viscosity it was possible to purge the ink despite solvent evaporation.

It was found that the PDMS ink was affected by the fluid bag on the standard Dimatix cartridge. This meant that after contact with the bag the ink would no longer cure, alternative fluid bags from Dimatix were sourced which solved this issue. The manufacturer states that the alternative bags are fabricated from a more chemically resistant material, and only provides the list shown in Table 5-2. The only two differences between the two cartridges was the replacement of the peroxide treated EPDM by Kalrez, and removal of polypropylene. There are no reported issues with PDMS curing in the presence of polypropylene, therefore, it is likely that the Peroxide treated EPDM was the cause for the lack of curing.

**Table 5-2 - Showing the manufacturer reported materials used in the manufacture of the cartridges.**

Standard Cartridge	Chemically Resistant Cartridge
Chemically resistant epoxy	Chemically resistant epoxy
Peroxide Treated EPDM	Kalrez
Polypropylene	LCP (Liquid Crystal Polymer)
Silicon	Silicon
Silicon Dioxide	Silicon Dioxide

It was observed that the PDMS crosslinking reaction occurred slower when in the presence of the solvent. At ambient temperatures the reaction took longer than one hour, whereas it was complete in around five minutes without solvent. Through observation of the reaction in glass phial it was determined that heating to around 60 °C was found to increase the rate of curing from > 1 hour to roughly 5 minutes. It was also expected that when printing the ink the evaporation of the solvent would lead to faster curing times on the substrate.

### 5.1.1 Printing on Setup 1

#### *Print Resolution*

The ability of PDMS to spread on most material surfaces is desirable when using moulding techniques, but for inkjet printing it directly reduces the feature resolution. Three material substrates: glass, PTFE, and PFOTS-glass were used in this study as they had reducing surface energies, this reduced surface energy leads to reduced liquid. Contact angle measurements were conducted, but the most robust way of gauging substrate suitability was by printing a grid. Table 5-3 shows the results from contact angle measurements, and Figure 5-4 shows the results of printing a disconnected grid.

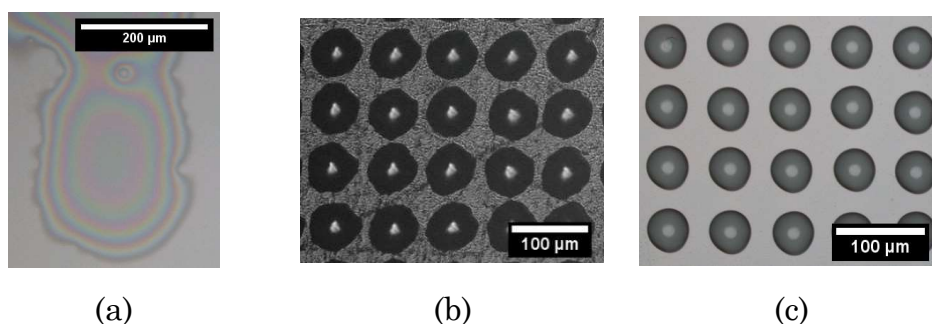
It should be noted that the contact angles measured are not the expected contact angles for large patterns. The reason for this is that pinning and material curing can increase the range of stable contact angle. This variation, between receding and advancing contact angles, is discussed in the literature view and called contact angle hysteresis.

**Table 5-3 - Contact angle of Ink A on different substrates using the sessile drop technique (KRUS DSA100).**

SUBSTRATE	CONTACT ANGLE PDMS A INK
GLASS	<2°
PDMS <sup>1</sup>	20-15°
PTFE	25°
PFOTS <sup>2</sup>	55°

1. Two component PDMS spin coated onto a clean glass slide.

2. A Fluorosilane (Perfluorooctyltriethoxysilane) coated glass slide (PFOTS).



(a)

(b)

(c)

**Figure 5-4 – A printed droplet grid comprising both Ink A and Ink B, resulting in cured PDMS spherical caps. The three substrates are a) cleaned glass slide b) on a pre-prepared PTFE coated slide and c) PFOTS-glass. It was found that the most circular and smallest droplet size was produced on the PFOTS glass.**

The printed grids showed that cleaned glass produced the largest droplet size which was greater than 150  $\mu\text{m}$ . The PFOTS-glass and PTFE had similar spot sizes, at  $48 \pm 2 \mu\text{m}$ , and  $64 \pm 2 \mu\text{m}$  respectively. The smaller and more circular drops of the PFOTS-glass were likely due to the decreased surface roughness. The preparation of the PTFE using 400 grit paper removed casting defects, but did not produce a smooth surface for printing. The PTFE was found to be relatively soft and easy to scratch. The ability to clean the PFOTS-glass, and the increased hardness over the PTFE meant that it was the selected substrate for continued work. However, preliminary work was conducted on the PTFE due to the substrate size limitation of setup 1 (4.1.2 Aerotech Printer).

### *Maintaining Pattern Shape*

Initially when printing layers it was found that the reaction would proceed slowly, likely due to the low rate of solvent evaporation at ambient temperatures. Substrate heating was employed to increase the evaporation and reaction rates. Figure 5-5 shows the results of trying to print a square using the PDMS inks. The result is solid PDMS, but without any controlled shape.

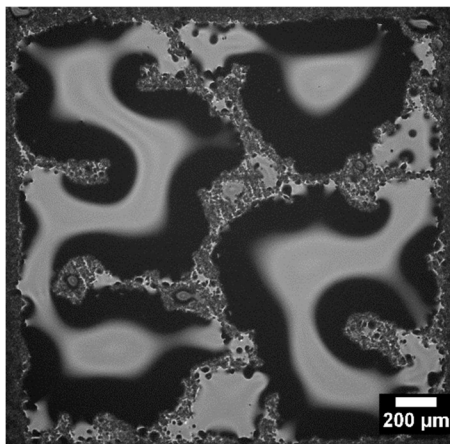


**Figure 5-5 - Image of printed film. The substrate temperature was 80 °C, the solid material was observed immediately.**

This uncontrolled distribution of material was suspected to be caused by the long cure time, related to the layer based FRIJP approach. This effect was not present when printing disconnected grids, so a method of printing grids that could spread in a controlled manner was attempted; this is shown in Figure 5-6. This process was termed microstructuring as it created small micron size pinning sites for the printing pattern.

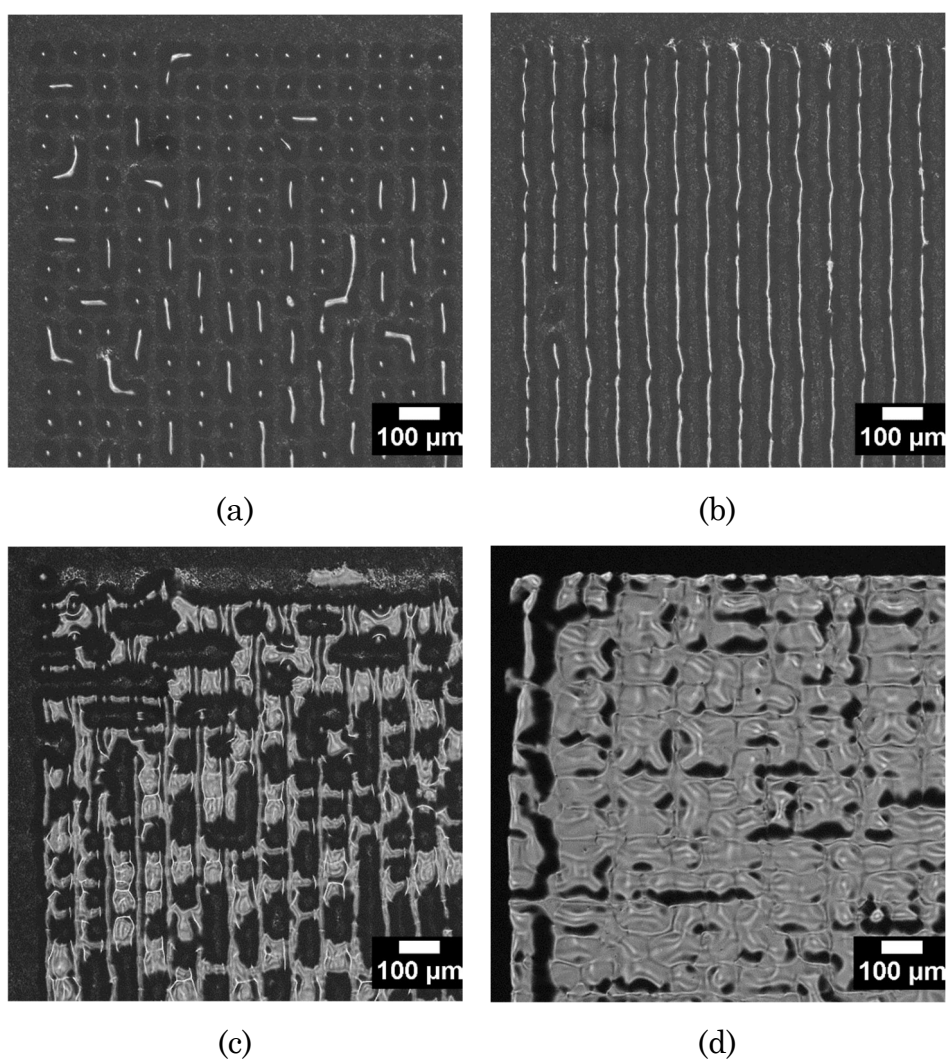


**Figure 5-6 – Substrate microstructuring, disconnected droplet printing to maximise the effect of pinning on a substrate where single PDMS ink does not pin. (a) a single layer of each component, Ink A and B is deposited, the initial spacing of the ink is such that the Ink A does not coalesce. (b-d) additional layers printed onto the grid, controlled spreading occurs and finally a continuous film is produced.**

This method produced a thin film directly on the substrate which had the desired 2D profile. However, an irregular surface was formed that was observed through SEM and optical microscopy of the resulting

printed film (a corner was torn to confirm curing), as shown in Figure 5-7

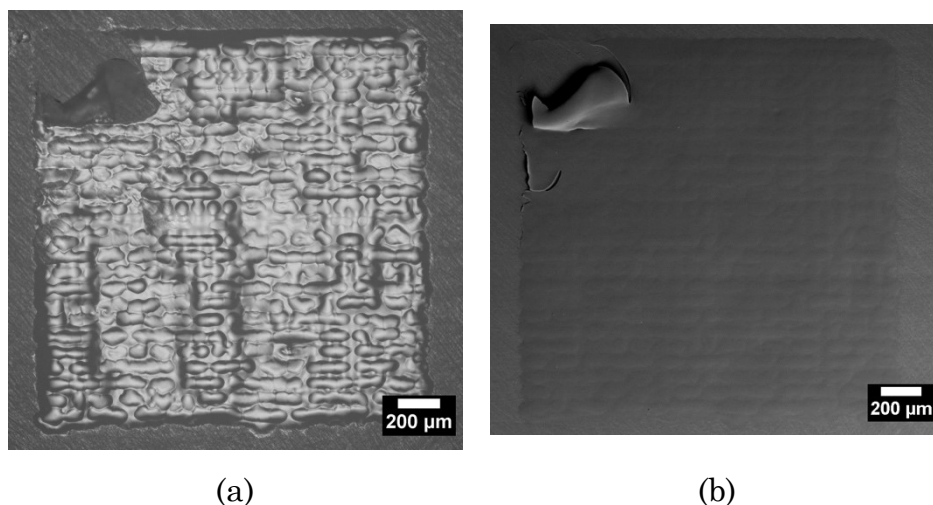


**Figure 5-7 – (a) Microscope (Nikon ECLIPSE LV100ND) image of a printed film, and (b) SEM (Hitachi Analytical Benchtop SEM TM3030) image of a printed film, sample platinum coated for 90 s, printed on a polished PTFE substrate heated to 80 °C. High sample wavyness was caused by the initial microstructured film process, visible in the microscope image, the SEM image however. To confirm that the sample was a continuous film the top left corner was peeled.**

### 5.1.2 Printing on Setup 2

The printing was continued with setup 2 which afforded increased control over the substrate temperature, positioning in relation to a substrate camera, and the ability to print onto glass slides. The following work was conducted on the PFOTS-glass.

#### *Printing Thick Films*

A strategy for printing a thin film was already created in the previous section; the aim of this PhD was to produce thick films using this method. The printing of thick films was accomplished by printing in two stages: the first stage involved printing the microstructure pattern with a drop spacing of 75 μm; the second stage printed successive layers with a reduced drop spacing of 35 μm. This strategy attempted to achieve the desired feature definition with the microstructuring method, and the increased speed of the reduced drop spacing. In this way, the continuous liquid film reduces the

surface irregularity whilst increasing the printing rate by around 4.5 fold.

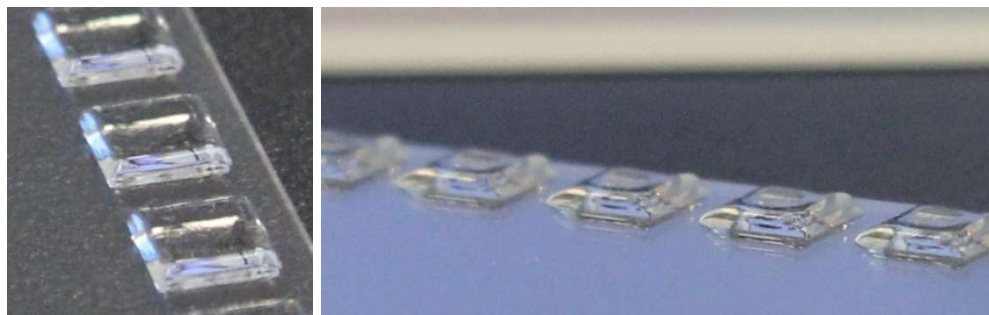
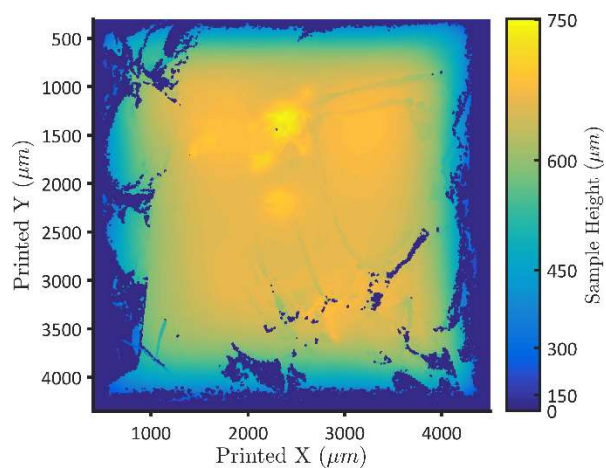


**Figure 5-8** – 4 mm<sup>2</sup> PDMS samples consisting of 50 reacted layers printed on a PDMS microstructured, PFOTS coated glass slide. The images show that the printed films are still very transparent despite being produced in discrete layers and lines.

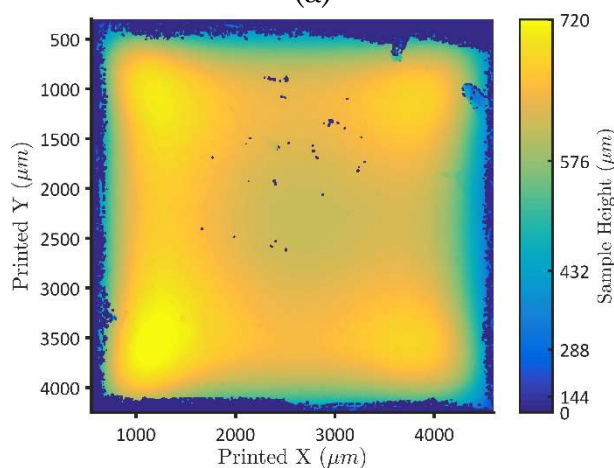
Figure 5-8 shows the appearance of printed thick films, demonstrating their transparency and smoothness. With the increased control of the LP50 substrate heater a series of temperatures; 40 °C, 60 °C, and 80 °C was used to print samples. Through variation of the substrate temperature the effect of evaporation and reaction rate could be measured. In this image there is an apparent lip on the printed samples, this is artefact is clearer in Figure 5-9c.

#### *Thick Films Profile Measurement*

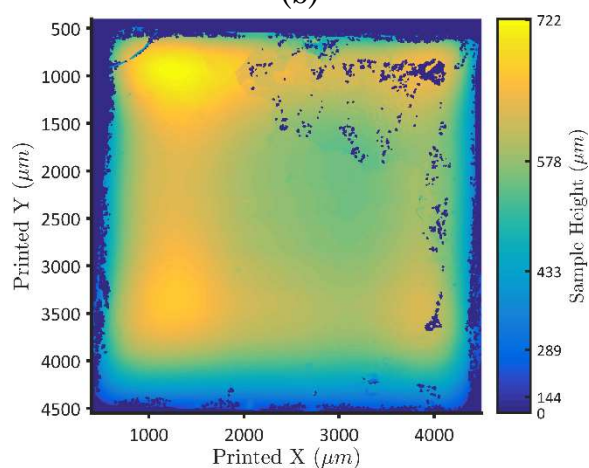
The results of the profile analysis are shown in Figure 5-9. The difference in profiles is most pronounced in the 40 °C to 60 °C substrate temperature prints, where instead of a domed like profile in the low temperature case a more uniform distribution occurs. However, this uniformity is still subject to edge effects where material recedes from the outer edges. This movement is known to be caused by the surface tension of the liquid as discussed by Thompson.<sup>50</sup> Further heating appears to maintain the same profile but increase the variation of material height throughout.



(a)



(b)



(c)

**Figure 5-9 - Profiles of the printed PDMS using the layer method. (a) printed at substrate temperature of 40 °C, (b) 60 °C, (c) 80 °C. Missing data is due to either high angles that are unscannable or the replication process causing incorrect replication.**

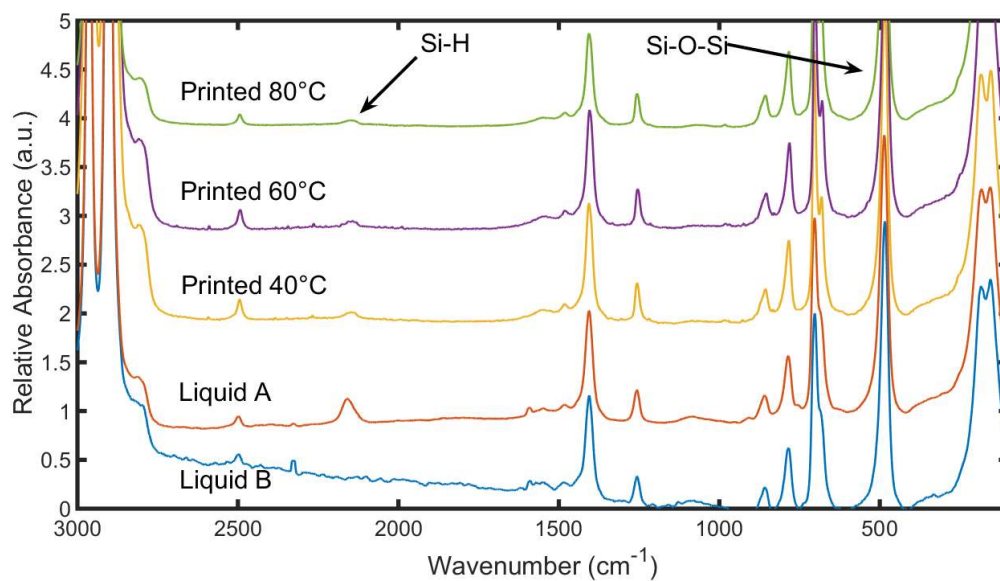
The increased rate of curing from the increased substrate temperatures appears to work to resist the fluid transport. Despite

the increased curing rate flat profiles were still not observed, likely caused by the time to print both reactive materials.

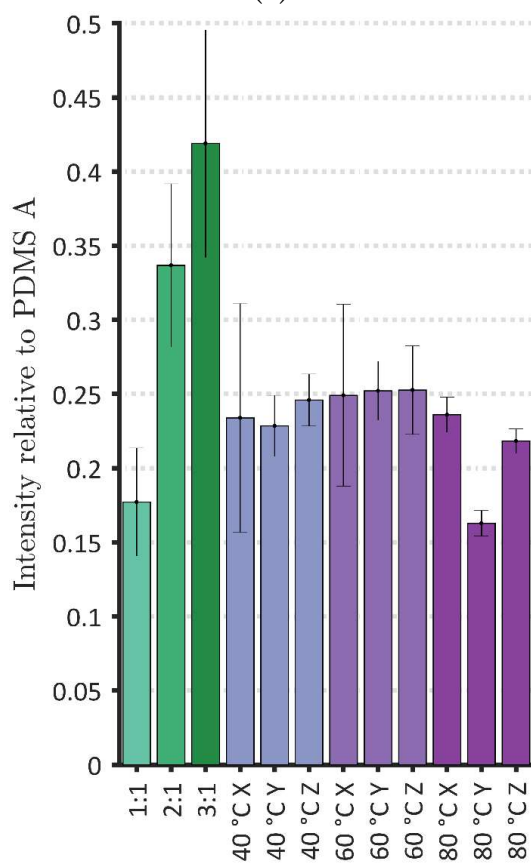
### *Thick Films Cure Analysis*

The increased cure rate of the printed PDMS due to the substrate heating leads to potential issues with the mixing of the inks. Methods to determine the mixing in single printed drops were used, but the results were inconclusive. Instead an alternative method involving spatial analysis using Raman spectroscopy was conducted. Through the use of Raman spectroscopy the residual silicone hydride component was measured across the printed samples.

It was found that there was no spatial dependency of the hydride component in all samples, excluding the X direction scan of the printed 40 °C. In the case of the 40 °C scan there was only a small amount of evidence for spatial dependency. This result suggests complete mixing in all other temperature cases. Figure 5-10a shows the resulting spectra in Raman for the printed samples and the liquid components. Figure 5-10b shows the results of the line scans where the error bars represent the error in measurement and are not from any spatial dependency. Figure 5-10b also includes the results from calibration samples, which were produced in different ratios, including 1:1, 2:1, and 3:1 (ratio PDMS A to PDMS B), representing a controlled hydride excess.



(a)



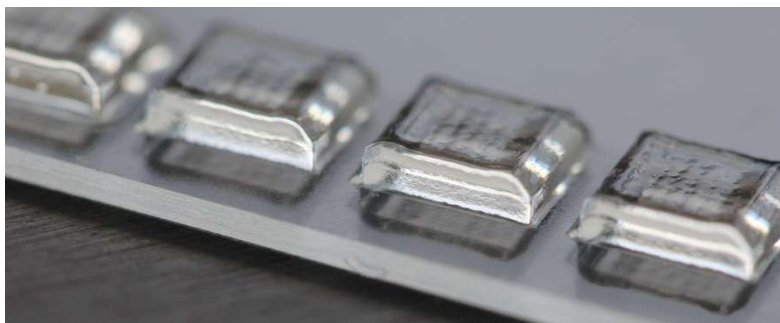
(b)

Figure 5-10 – (a) total spectra for printed samples and the liquid inks (b) quantified residual crosslink component in each printed sample in relation to uncured part A also included are cast samples created at 1:1 2:1 3:1 A:B ratio, data is shown as mean  $\pm$  standard deviation (XY: n = 75, Z: n = 50).

### 5.1.3 Printing on Setup 3

The benefit of Setup 3 was the reduction in time to material combination on the substrate, which also reduces the time to cure.

Setup 2 had a mixing time of around 2 minutes, whereas, Setup 3 was around 0.3 s. With this increased printing speed it was possible that the first lines of a single layer cure while the last line is still printing. This affords increased printing control over the previous method. As such the microstructuring method was no longer employed in the PDMS printing.



**Figure 5-11 - Samples printed using setup 3 with PDMS.**

After the work on Setup 2 was completed it was determined that from the results of the cure analysis that the printed volume varied between Ink A and Ink B. Compensation for this variation would be required to achieve the correct 1:1 mixing ratio. Ink A and ink B were printed into metal pans and weighed. Ink A weighed  $10.40 \pm 0.24$  ng, Ink B weighed  $11.92 \pm 0.18$  ng, and these masses suggest that in the previous work the Ink A was printed with a lower concentration than desired. Finally, the work already conducted determined that a substrate temperature of 80 °C was most suitable for inkjet printing of PDMS: with decreased height variation, reduced edge length, and no spatial cure dependency.

### *Print Spacing*

With the removal of the microstructuring to achieve the desired geometry, it was possible to determine the lowest drop spacing that produced a stable line through experimentation. Print spacings of 30  $\mu\text{m}$ , 35  $\mu\text{m}$ , 40  $\mu\text{m}$ , and 45  $\mu\text{m}$  were used. When printing with a set spacing this controlled only the droplet spacing of Ink A, Ink B was controlled through the mixing ratio. The corresponding spacings were

determined to result in a 1:1 wt:wt mixing ratio using Eq 4-3, the drop spacings for Ink B were 34.4  $\mu\text{m}$ , 40.1  $\mu\text{m}$ , 45.8  $\mu\text{m}$ , and 52.6  $\mu\text{m}$ . The results of the drop spacing test are shown in Figure 5-12.

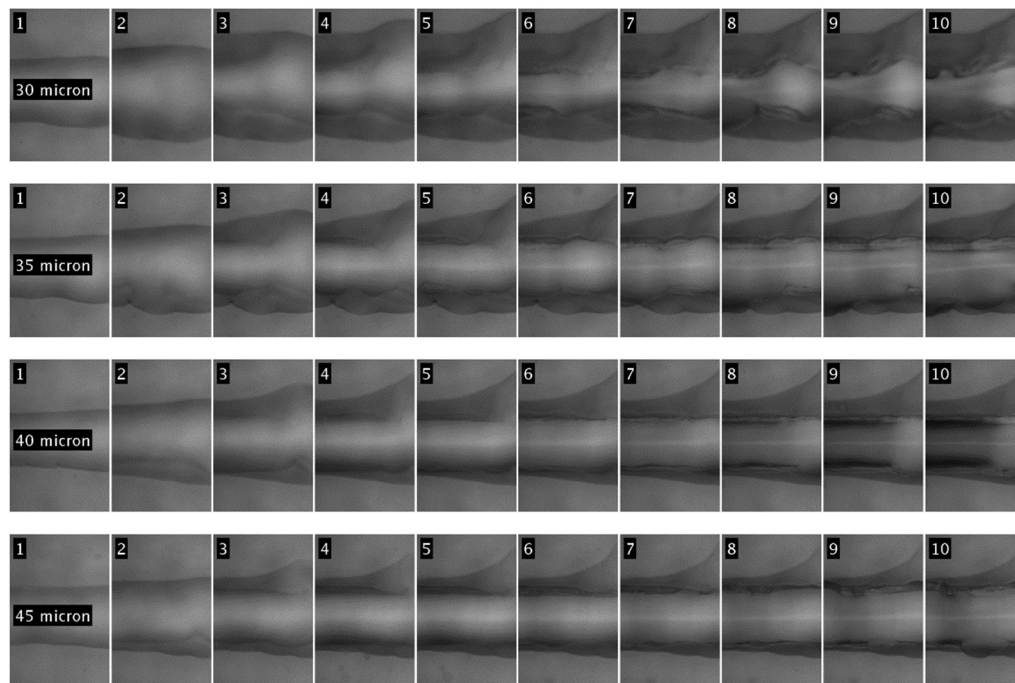


**Figure 5-12 - Determination of the minimum drop spacing for stable line formation of printed PDMS. Ten layers of five lines were printed at different drop spacings. Number of layers increasing from left to right.**

The decision was made to conduct the stability tests on multiple layers, with multiple lines, as this was closer to the case of AM. The selection of the drop spacing was based on which series of images had the most uniform appearance over a series of layers. From the results of the line stability tests a primary drop spacing of 40  $\mu\text{m}$  was selected for future printing.

### *FRIJP without Microstructuring*

Images were captured of the bottom right corner of prints at the end of every layer. These images can be used to determine both heads are work correctly, but also as a means of analysis. Figure 5-13 shows the first five layers of a printed sample. The first layer is directly printed onto the PFOTS-glass, and due to the fast curing rate it does not

recede. Successive layers print onto the PDMS film and create the 3D object.

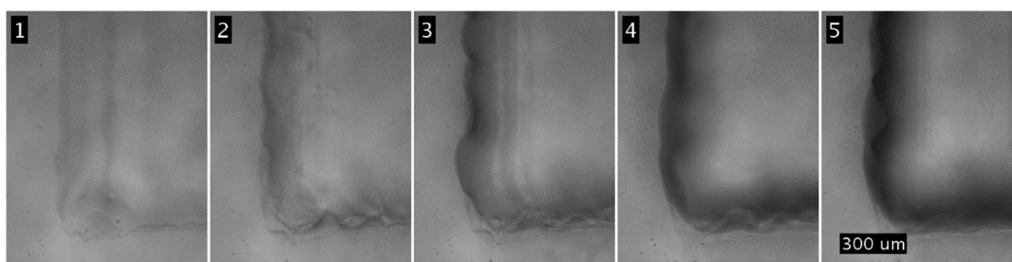


**Figure 5-13 - FRIJP Line strategy printing directly onto the PFOTS-glass. The substrate temperature is 80 °C.**

When using material jetting to construct three dimensional objects, only the first ink layer is printed onto the substrate; after this all successive layers are printed onto the jetted material. To determine how the PDMS behaves printed onto the jetted PDMS, a stepped ziggurat design was employed (Figure 5-14).

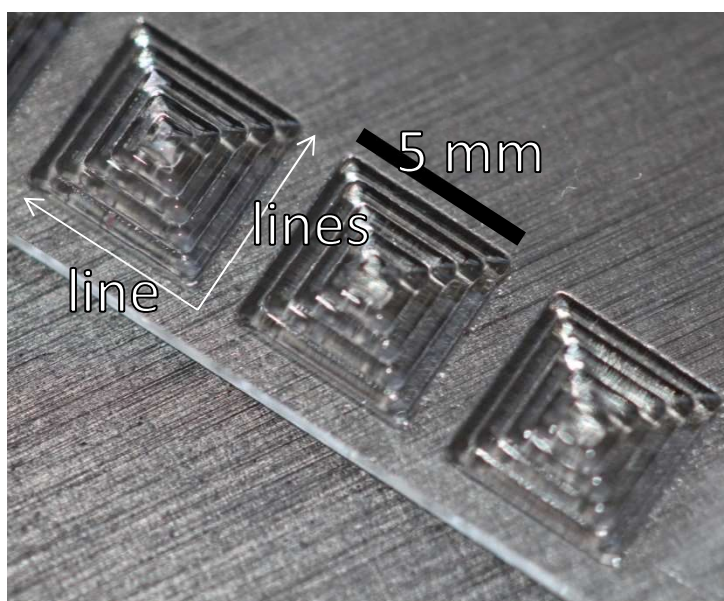


**Figure 5-14 - Stepped ziggurat, 4x4 mm PDMS consisting of 5 steps, each printed with 30 reactive layers.**

The stepped ziggurat design was chosen as it meant that the step was printed on a continuous PDMS substrate. There were then no edge effects related to the PDMS contact angle on glass. The image series shown in Figure 5-15 displays the effect of printing onto the PDMS substrate. Despite the apparent receding, in only five layers this receding has been removed and a uniform layer is built, the reason

for this phenomenon is not currently understood but is under further investigation.

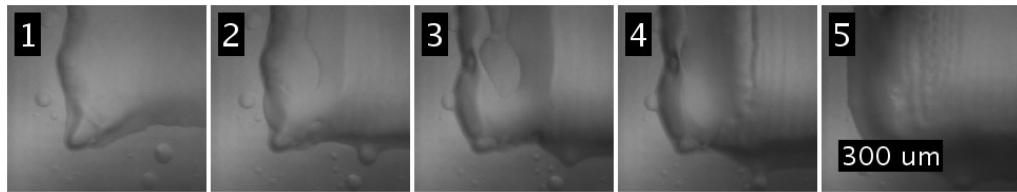


**Figure 5-15 - Printing PDMS directly onto PDMS substrate. First step in the ziggurat design. Substrate heated to 80 °C.**

### *Profile Analysis*

The line based printing of the stepped ziggurat design was used to determine if the length of the printed line effected the profile. It can be seen in Figure 5-16 in the Y direction (along the print direction) that increased scan length resulted in a more uniform layer height. As the scan lengths shortened, the height variation increased. The variation in this single sample is 17  $\mu\text{m}$  for the first layer, and increasing to 34  $\mu\text{m}$  for the penultimate layer. The variation is lower than samples printed on setup 2. The variation is also seen to reduce further when scanning the profile at the centre (green line), therefore, this variation is likely due to the two edge effects at the corner.

The profile of the stepped ziggurat in the X direction shows a highly uniform and level line for the first two steps. However, further layers are seen to show an increased variation with a constant decline to the final line. Despite the constant variation there is no evidence for edge height as seen before on the samples produced using setup 2. It can also be seen that the profile does not replicate the contact angle measured previously, this is likely caused by preferential wetting on PDMS over the build substrate, in effect, increasing the advancing contact angle.

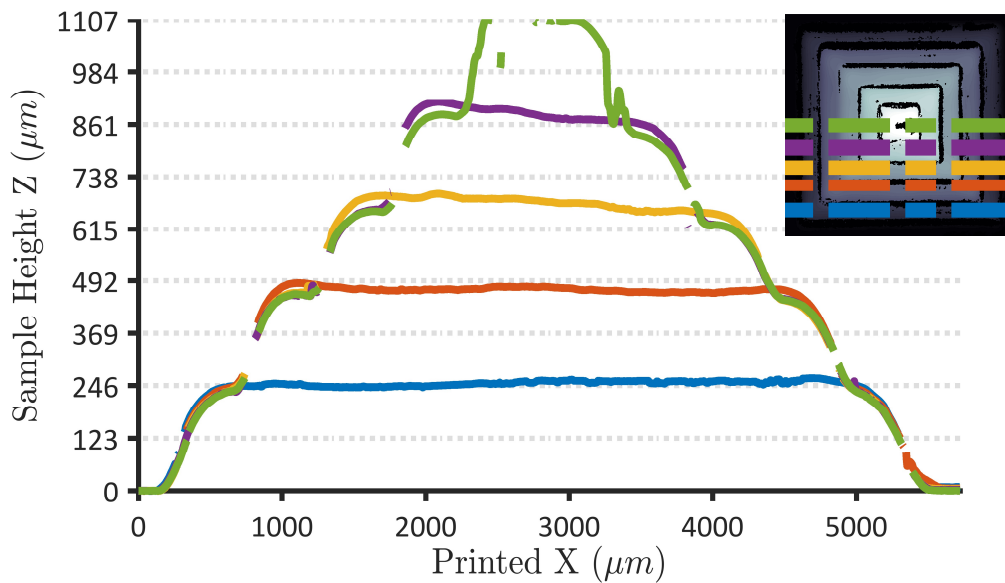


(Figure 5-16a)

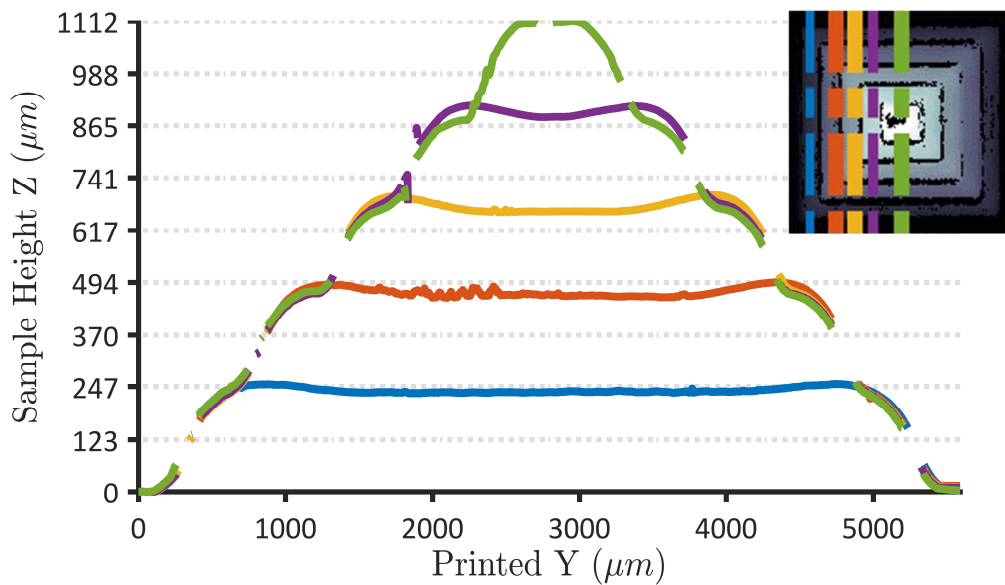
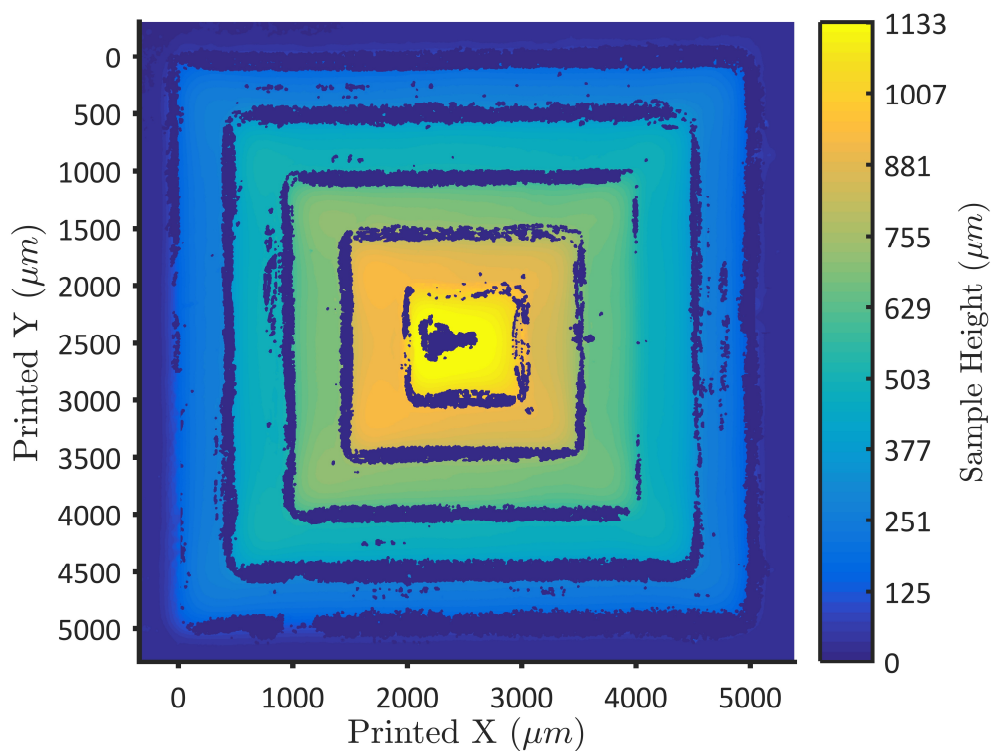


(Figure 5-16b)



(c)

**Figure 5-16 - Profile analysis of the stepped ziggurat printed design conducted on the Alicona. (a) line scans immediately before a step in X, (b) line scans in Y, (c) area profile, with highlights where line scans were taken from.**

### *Curing in Line Based Printing*

Due to the previous scans using spatial Raman microscopy, it was known that there were no imbalances across printed samples, and therefore, cure analysis in this stage was conducted in bulk. Bulk analysis was conducted using the FTIR-ATR apparatus; the samples were cut and scanned in three places. The large square samples were scanned, and compared to the calibration pieces. To carry out the comparison the spectra were normalised to the peaks at  $1020\text{ cm}^{-1}$  (Si-O-Si asymmetric stretch) and  $1090\text{ cm}^{-1}$  (Si-O-Si symmetric stretch), and the concentration of residual cross-linker determined from the peak at  $912\text{ cm}^{-1}$  (Si-H, SiH<sub>2</sub> wagging).<sup>99</sup> The peak at  $2152\text{ cm}^{-1}$  (Si-H stretch) was also considered, but results showed that the intensity was too low which resulted in a large error. Gaussian curve fitting was found suitable for all analysed peaks; an example fitting for the calibration 1:1 scan 1 is shown in Figure 5-17.

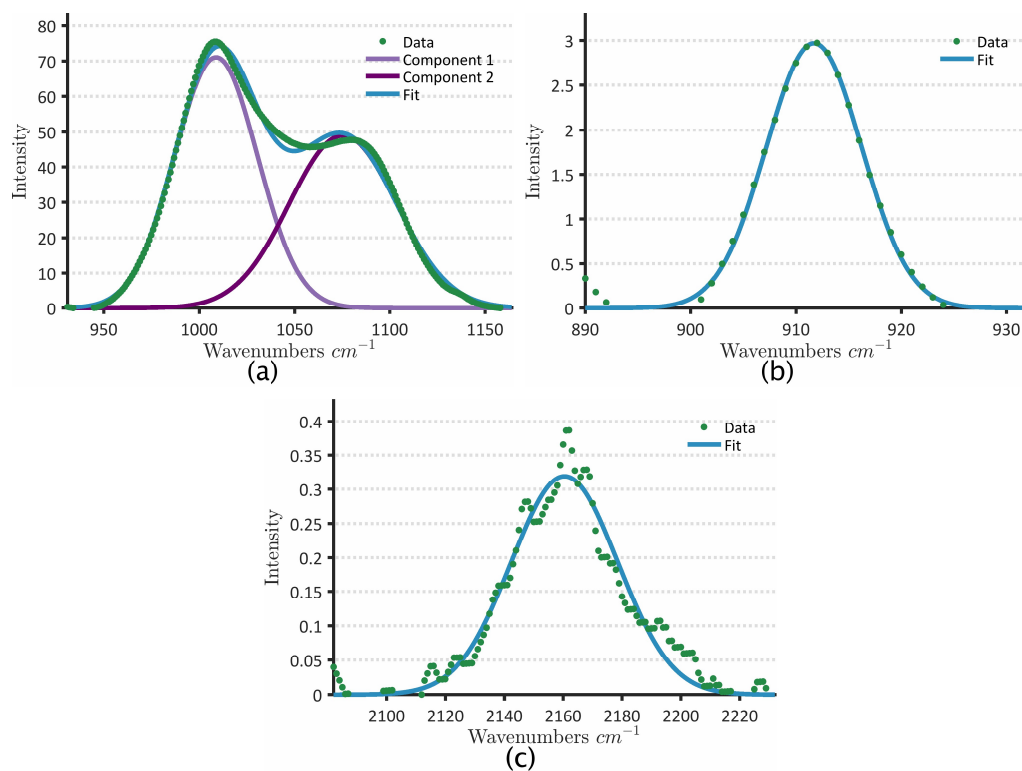


**Figure 5-17 - Gaussian curve fitting to the FTIR spectra. The sample was the 1:1 calibration, scan 1. a) the calibration peak fitting b) the fit at  $912\text{ cm}^{-1}$ , used for determination c) alternative low intensity peak at  $2150\text{ cm}^{-1}$  not used due to increasing noise.**

The results from the cure analysis are shown in Figure 5-18. They show that residual Si-H intensity in the printed samples corresponds to the 1:1 cast calibration. In all cases, the printed samples were the same, or better than the cast ones.

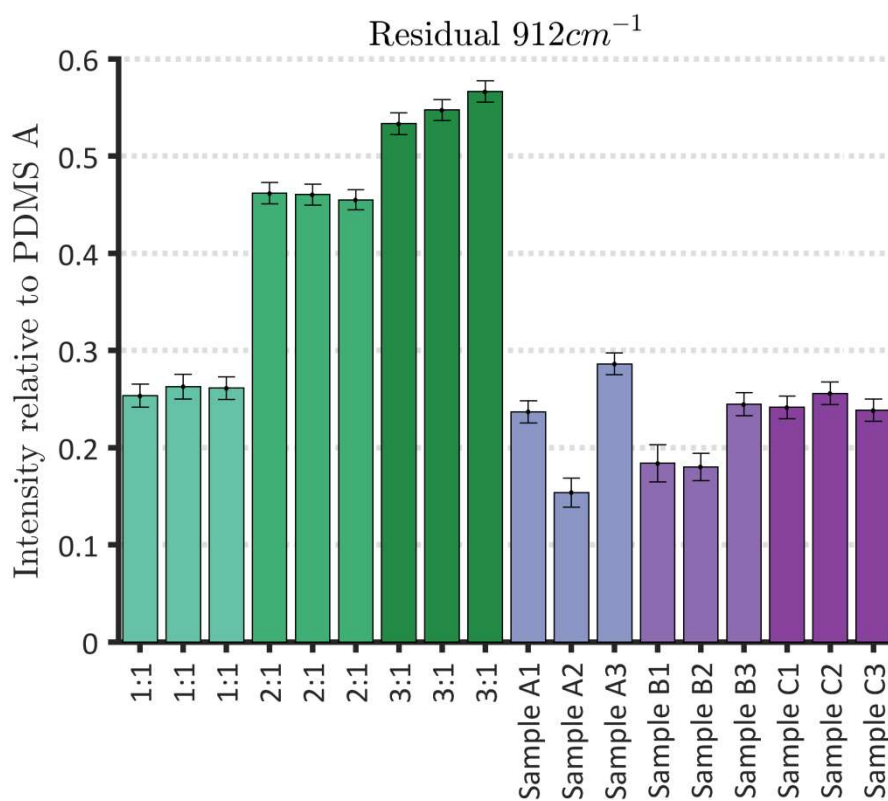


Figure 5-18 - Residual cross link component Si-H in the calibration and printed samples. The bond at  $912\text{ cm}^{-1}$  was used to determine the residual. The errors are from the curve fitting GOF of both the calibration and residual combined.

## 5.2 Discussion

### *Ink*

A stable FRIJP ink was developed from a two-part silicone chemistry. The viscosity of each component was such that a 40 % wt loading of solvent was enough to achieve a printable ink. The material used was chosen directly in relation to the low viscosity, on the understanding that the produced part would have low elongation to break. The focus of printing in the case of the PDMS was not to achieve highly elastic material, but to produce polymer objects using FRIJP whilst providing a vehicle to develop understanding of any issues in the process.

### *Pinning*

The low degree of interaction between the ink components, the glass, and the PTFE substrate, meant that the first layers could not achieve a stable line formation. A microstructuring method was introduced that made use of the increased pinning between liquid component and solid PDMS, and through the creation of isolated droplets ensured that no movement would occur between layers. Once the second layer was printed, and the PDMS mixed, the curing could occur. The cured, isolated PDMS structures then became anchor points for further ink deposition. It was found that using this method the liquid ink would not recede on the PDMS, as with other substrates, allowing for increased pattern control.

### *Profile*

Despite achieving the desired footprint, the distribution of the liquid on top of the printed films was not uniform. In printing with the layer based approach it became apparent that the long time to mixing led to a large degree of reflow which was evident in the profile analysis. This flow is driven by the surface tension forces, as investigated by Thompson<sup>50</sup> in reference to single printed lines. In the PDMS printing

it is apparent that this occurs in a two dimensional film when time to cure is very long.

The investigation involving setup 3 shows how the edge effects can be reduced and the reflow stopped. The ziggurat sample was found to have a near constant height when measured in the Y direction. This constant height was also seen in the X direction for the first steps. The line strategy also shows that the raised edge can be reduced in both the X and Y direction (excluding the corner). These improvements were achieved without the use of the microstructuring technique of setup 1 and 2. Setup 3 demonstrates how high definition profiles can be achieved with a two-part reactive ink if the time between the two inks deposition is reduced.

### *Reaction*

The curing in the FRIJP of PDMS has been investigated in both the line and layer based methods. From the review of the literature it is understood that the mixing mechanism is diffusion driven, therefore, if printing can achieve a short mixing length then the long timescales associated with diffusion should not prevent a mixed product forming. In the layer based printing strategy there is a separation between layers of around 5-6  $\mu\text{m}$  (calculated as half the single layer height). This separation has been shown to be sufficient for mixing to occur and no residual concentration gradients to exist. For the work involving the line method the separation is maintained, or reduced (due to reduced drop spacing). The bulk analysis of the line based samples show a highly cured component.

Characterisation of mixing and reaction in the PDMS chemistry is difficult as silicone hydride is the only identifying peak for component A, and as the reaction progresses this disappears. There are no other unique peaks produced or removed in this reaction process. As the PDMS was cross-linked, methods such as liquid state NMR were also

not possible. Also, due to the nature of crosslinked material the limit of reaction is not always when all components have been consumed, but when the molecular structure of the produce becomes rigid enough to limit further mixing through molecular diffusion. To carry out chemical analysis using FTIR and Raman, calibration samples with specifically prepared concentrations were used. The predicted concentration and results do not match in these calibration samples; however, they show that for both the layer and line based printing the PDMS curing is in the region of the 1:1 calibration.

In developing the PDMS printing the focus was to increase the printed profile definition and the degree of cure. The key challenge for the profile definition was the time it took for the liquid inks to become solid on the substrate. The challenge for the curing of the PDMS was initially thought to be based on incomplete mixing, however, Raman showed no concentration gradients and calibration samples showed similar curing degrees to all printed samples. Therefore, it was determined that the mixing and reaction was not an issue.

In FRIJP the time to cure depends not only on the reaction rate, but also the time for deposition and mixing. To increase the control of the profile each step had to be shortened. The major concern was the time to mixing, which was dependent on geometry and around 2 minutes (for a 4 mm square sample) in setup 2. To reduce this, both inks were printed in a single pass, the time to mixing was then independent of printed geometry and only dependent on head printing speed. The time to deposition was calculated to around 0.3 s. As no external mixing could be added, and the literature indicates that no convective mixing occurs, the PDMS mixing was based on diffusion alone. The only method to increase this was then through substrate heating to elevate the liquid temperature. The rate of the PDMS cross-linking

reaction is also increased by substrate heating, so a temperature of 80 °C was used for all printing from setup 3.

The result of these improvements is a highly cross-linked PDMS network, FRIJP printed onto a glass substrate which was modified to increase contact angle. The thickness of the printed geometry had an increased uniformity over previous samples, and the correct footprint was maintained.

## ***6 FRIJP of Polyurethane: Immiscible Components***

In this chapter the results and subsequent discussion for the printing of three reactive inkjet chemistries are presented: H<sub>12</sub>MDI and butanediol, HDI and butanediol, and H<sub>12</sub>MDI and a mixed ink of PEG-butanediol (further material details are available in 3.1.2 Polyurethane). Printing was conducted using the co-deposition of inks in a single line as discussed in 4.1.4 Line Printing. Once printed, the samples were analysed with: Profilometry, SEC, and NMR, using the methods described in 3.2.5 Profile Analysis and 3.2.4 Chemical Analysis.

The initial aim was to use simple monomer repeating units to carry out the printing. It was observed that the H<sub>12</sub>MDI and butanediol combination showed a large degree of immiscibility, coupled with the volatile butanediol this produced very porous structures with low molecular weights. It is known that the mixing relies on molecular diffusion. It was then decided to use the H<sub>12</sub>MDI and PEG-butanediol. The introduction of the soft segment polyethylene glycol would facilitate increased chain flexibility, leading to increased rates of diffusion and reaction. The samples printed with the H<sub>12</sub>MDI and PEG-butanediol formulation showed greatly increased molecular weights over the H<sub>12</sub>MDI and butanediol.

As previously discussed the reactions were chosen due to the absence of by-products produced in ideal conditions. Where a representative reaction scheme is shown in Figure 2-15. The urethane linkage forms from the catalysed reaction between an isocyanate group and a hydroxyl group. In this work the catalyst used is DBDT.

## 6.1 Results

### 6.1.1 Ink Development

For the FRIJP of polyurethane through immiscible inks five chemicals and one solvent was used: H<sub>12</sub>MDI, HDI, butanediol, PEG, DBDT, and DMF. These inks are discussed in 3.1.2 Polyurethane, they were used in the formulation of two isocyanate inks and two hydroxyl based inks.

**Table 6-1 - Method for viscosity modification if used for producing a printable ink.**

	FUNCTIONAL GROUP	MODIFICATION FOR PRINTING
<b>H<sub>12</sub>MDI</b>	Isocyanate	Temperature
<b>HDI</b>	Isocyanate	Temperature
<b>BDO</b>	Hydroxyl	Temperature
<b>PEG</b>	Hydroxyl	Reactive and Unreactive Diluent Temperature

The method for viscosity modification is described in Table 6-1; where three of the inks were printable through temperature based viscosity modification. The PEG-butanediol ink was formulated to achieve a 30% hard segment ratio, where PEG was the soft segment and butanediol and H<sub>12</sub>MDI were the hard segments. The desired formulation was 1:2 moles of butanediol and Polyethylene Glycol 1000. The butanediol reduced the viscosity of the PEG as a reactive diluent, but the final formulation required a further 15 %wt DMF as an unreactive diluent. The viscosity of the PEG, the PEG + BDO, and the solvent inks are shown in Figure 6-1.

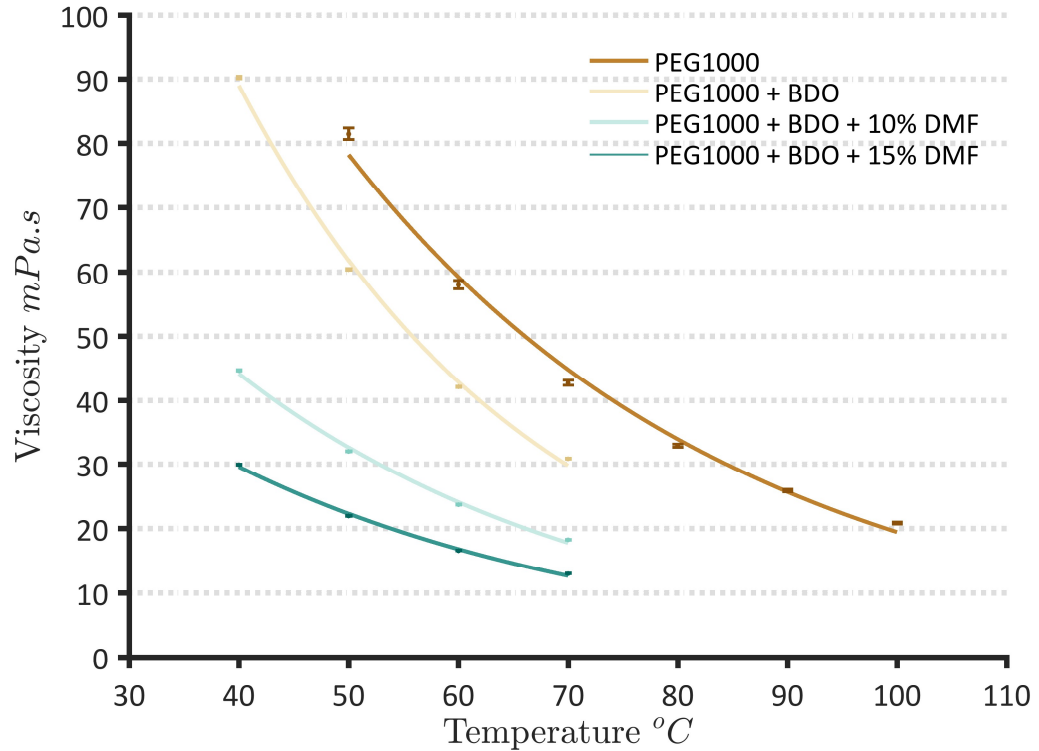


Figure 6-1 - Viscosity modification of the polyethylene based ink. There was a noticeable reduction in viscosity upon adding the butanediol, but further reduction was required. The final formulation contained 15 %wt DMF, achieving a printable viscosity at temperatures above 60°C. The data was selected from the stable shear rate range and the exponential model was used to fit the points (as described in 3.2.1 Material Rheology)

The viscosities of the printable inks are shown in Figure 6-2, except for HDI, all the inks achieve a printable viscosity at temperatures over 55 °C. The isocyanate inks, Hydrogenated-MDI (H<sub>12</sub>MDI) and Hexamethylene Diisocyanate (HDI), both include a 3 wt% concentration of the catalyst Dibutyltin Dilaurate. The printing parameters for all inks are listed in Table 5-1.

Table 6-2 - The material properties used to calculate the printability, and the measured droplet volume (if conducted).

Ink	Temp. (°C)	Viscosity (mPa.s)	Surface Tension (mNm <sup>-1</sup> )	Ohnesorge	Mass (ng)
HMDI	50.00	12.14 ±0.44	37.84 ±0.15	0.43	8.21 ±0.17
HDI	30.00	1.41 ±0.05	35.00 †	0.05	‡
BDO	60.00	16.37 ±0.27	44.00 †	0.55	‡
PEG BDO	70.00	13.00 ±0.09	43.50 †	0.41	14.31 ±0.59

‡ - Printing conducted before mass was considered  
 † - Value found in literature

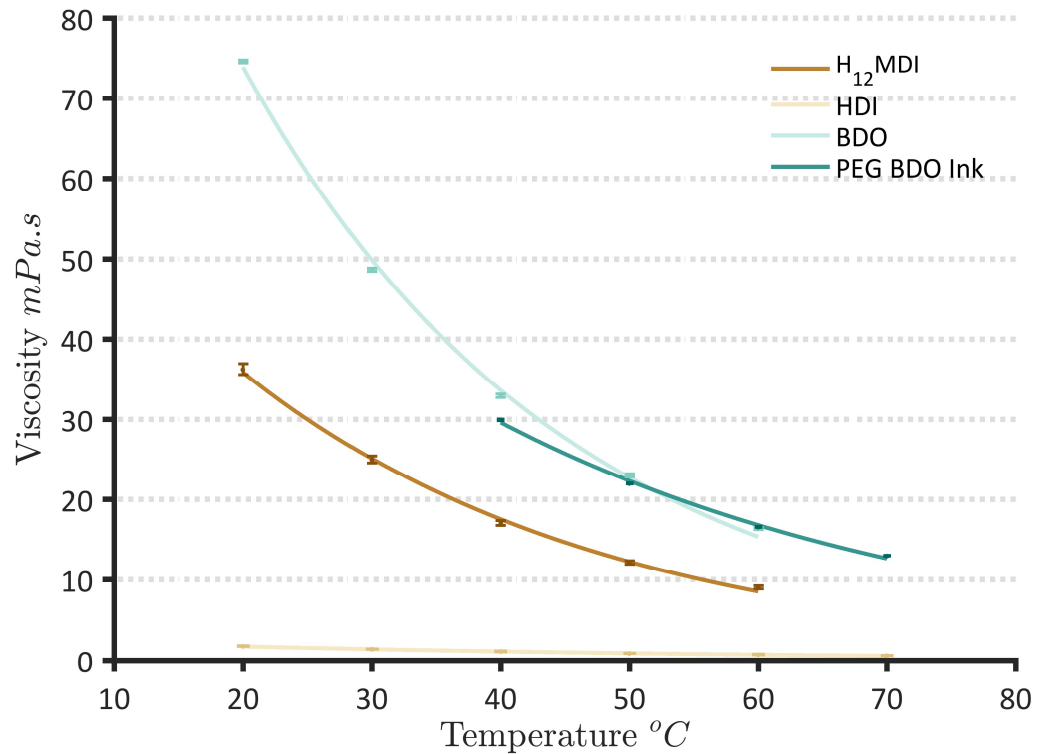


**Figure 6-2 - The viscosity temperature profiles for the inks chosen for immiscible PU printing. HDI ink has a printable viscosity over the total temperature range, the other inks require heating above 50 °C. The data was selected from the stable shear rate range and the exponential model was used to fit the points (as described in 3.2.1 Material Rheology)**

It was found that the catalyst at ambient temperatures was immiscible with the hydroxyl group inks. Therefore, it was added to the isocyanate, which meant that the reaction rate between moisture in the air and the ink was increased. An environmental chamber was used for the printing with the relative humidity controlled to a maximum of 5 %, which was found to reduce the occurrence of the unwanted reaction. When the head was idle for over 4 hours some formation of Polyurea (PUR) was observed, but this was readily dissolved with toluene. Despite the PUR blocking the nozzles, the benefit of the two-part reactive ink was that when the unwanted reaction occurred it was to a low degree. The polurea produced during this unwanted reaction was then easier to dissolve than the desirable polyurethane.

It was found that the DMF solvent was not compatible with the Dimatix cartridge; after prolonged exposure the seal inside the print

head failed. Printing was unaffected for up to one week of use, but it is recommended that any future work using this ink should select an alternative solvent.

### 6.1.2 Line Substrate Microscopy

The LP50 camera was used to capture a time-based series of images immediately after the printing of the second material. This video was used to determine how mixing occurred, in the same way Fields used a microscope to analyse interfacial polymerisation.<sup>91</sup> The line samples were printed lines of 10 passes, of both reactive inks.

#### *H<sub>12</sub>MDI and Butanediol*

This imaging method discovered that despite printing droplets with a diameter around 20  $\mu\text{m}$ , once both materials are printed the two immiscible components segregate. This segregation greatly reduces the component distribution and eventually the butanediol evaporated. Figure 6-3 shows the process over five minutes after printing. The formation of large droplets reduces the interface area and increases the mixing length, both these factors reduce the rate of mixing and reaction. Eventually when the separated butanediol evaporates it leaves behind pores. The presence of these pores has been confirmed using profile analysis which is shown in Figure 6-16.

Although Figure 6-3 shows some individual droplets this formation was not stable, and on repeated analysis total segregation occurred (Figure 6-4). Therefore, the isolated droplets previously encountered are likely due to satellite droplets in printing. Where the true case of printing the material results in an agglomeration of large, and separate drops.

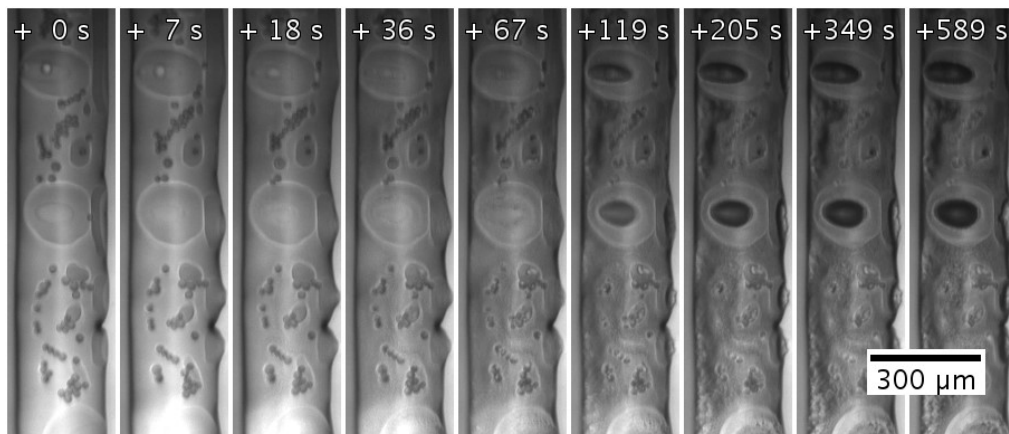


**Figure 6-3 - Post printing reaction of H<sub>12</sub>MDI and butanediol printed at 30 °C. Suspected satellite formation produced single droplets.**

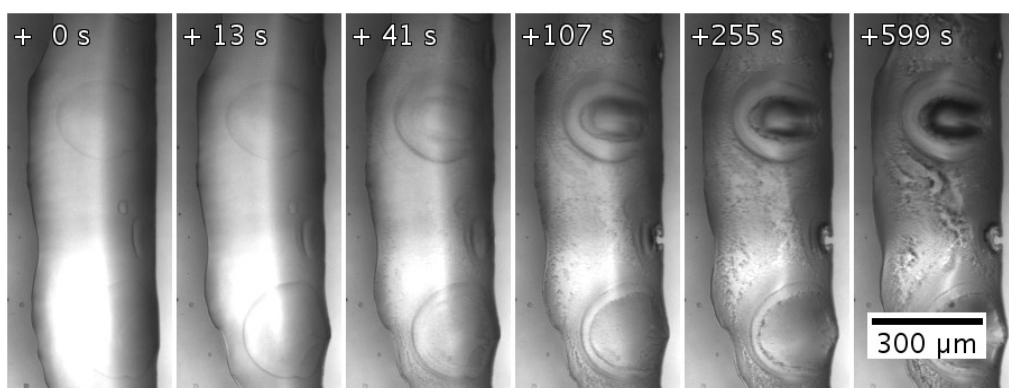


**Figure 6-4 - Post printing reaction of H<sub>12</sub>MDI and butanediol printed at 30 °C. Repeated without the satellite formation.**

The reaction scheme of polyurethane is understood to be interface driven, dominated by the rate of molecular diffusion and reaction.<sup>89</sup> Therefore, this experiment was repeated at two elevated temperatures: 50 °C, and 70 °C. The results of the elevated cases are shown in Figure 6-5. Increasing the substrate temperature caused the formation of smaller droplets likely due to the increased reaction rate during printing. In the 50 °C case shown in Figure 6-5a the printed lines of butanediol no longer completely merge, they instead form two separate rows suggesting transport is reduced. When the substrate temperature was set to 70 °C (Figure 6-5b) the butanediol distribution in the printed line was further increased, which is further evidence for reduced liquid transport. This is likely due to the increased reaction rate leading to polyurethane formation at the interface

between the liquids, which then leads to increased liquid viscosities or the possibility of liquid on liquid *pinning*.

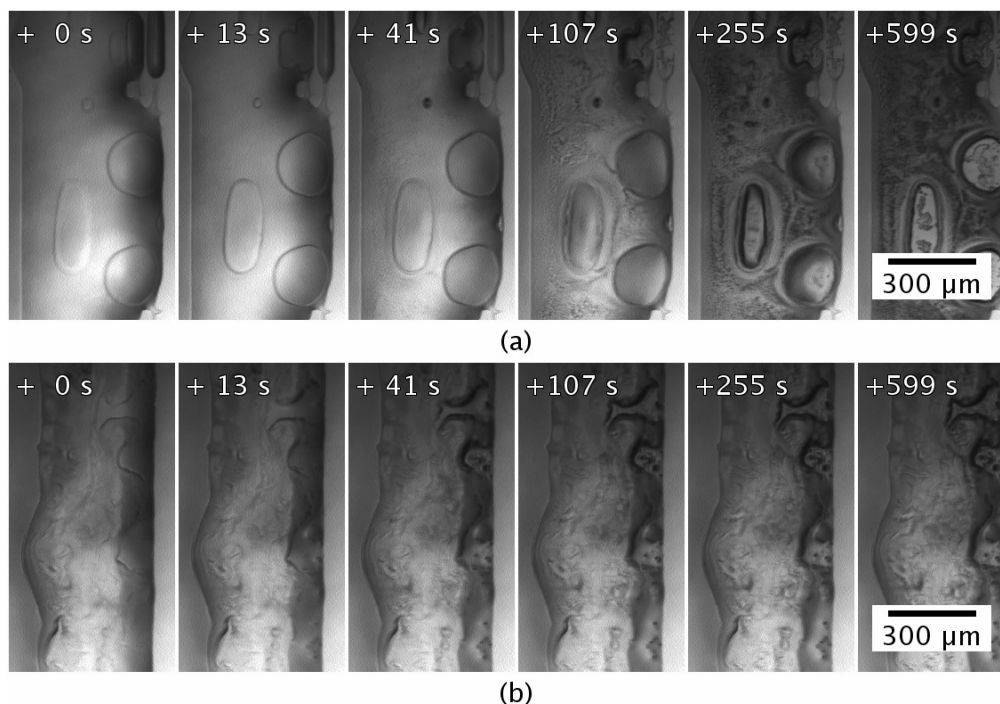


**Figure 6-5 - Post printing of H<sub>12</sub>MDI and butanediol printed at a) 50 °C, b) 70 °C. There is apparent increase in uniformity of the printed lines.**

The time series was repeated with the monomers individually printed. It was found that the H<sub>12</sub>MDI (Figure 6-6a) did not evaporate or react, while the butanediol showed considerable evaporation (Figure 6-6b). This means that despite the observed separation of the monomers there is some transport of the butanediol through the isocyanate, which causes the solidification and discoloration observed. Despite the apparent increase in mixing from increased substrate temperatures the uncontrolled evaporation of the hydroxyl component ink leads to incorrect mixing ratios. Therefore, unless evaporation of components is accounted for in the mixing ratio, high conversion rates cannot be achieved using substrate heating.

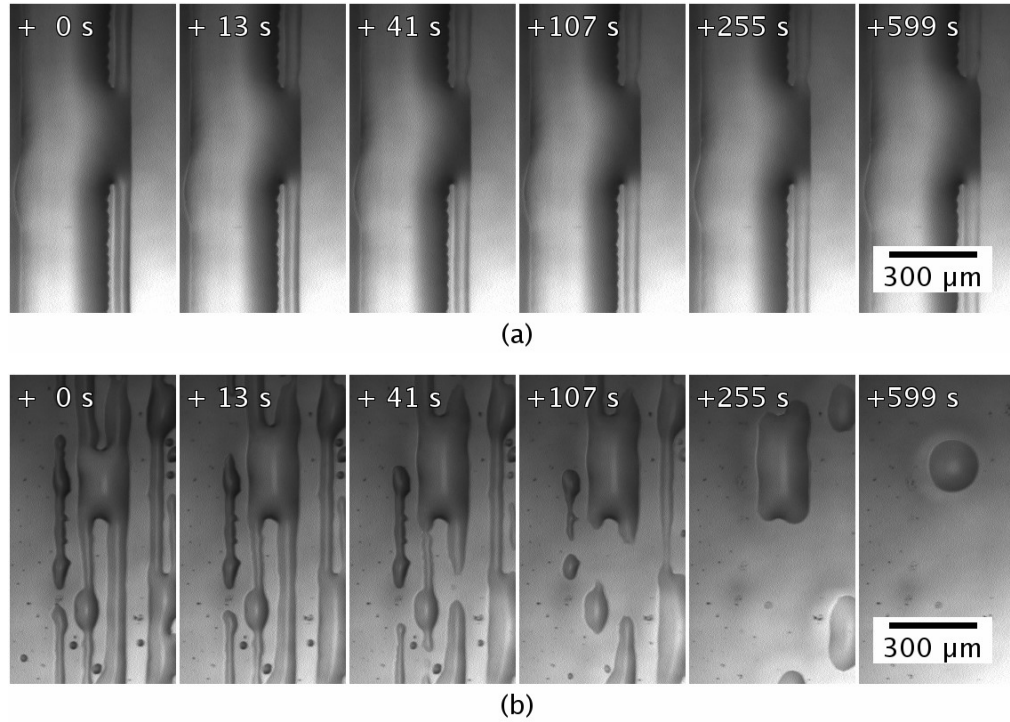


**Figure 6-6 - Post printing of a) H<sub>12</sub>MDI, and b) butanediol, both monomers are printed at 50 °C. It is observed that considerable evaporation of the butanediol occurs, with no visible reaction or evaporation of the H<sub>12</sub>MDI.**

### *HDI and Butanediol*

The effect of low reaction rate leading to perceived separation of monomers has already been observed. HDI is an isocyanate monomer with increased reactivity. It was printed with the butanediol in the same manner as before at a substrate temperature of 30 °C.

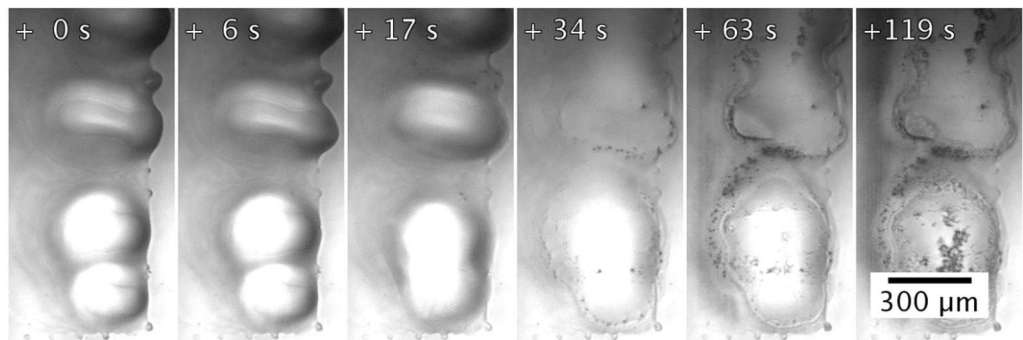


**Figure 6-7 - Post printing reaction of HDI and butanediol. Printed at 30 °C.**

Figure 6-7 shows the result of printing the HDI, a chemical with increased reactivity. There is still a large degree of separation between the monomers with multiple printed lines merging, suggesting no liquid-liquid pinning encountered by the H<sub>12</sub>MDI at 70

°C. However, the final state of the material suggests that more conversion has occurred. Multiple layers were printed and imaged, as shown in Figure 6-8. It appears that printing onto the previous layer reduced the separation of the monomers. A different issue was observed with the HDI ink as it was apparent that the low viscosity led to a significant ink transport.

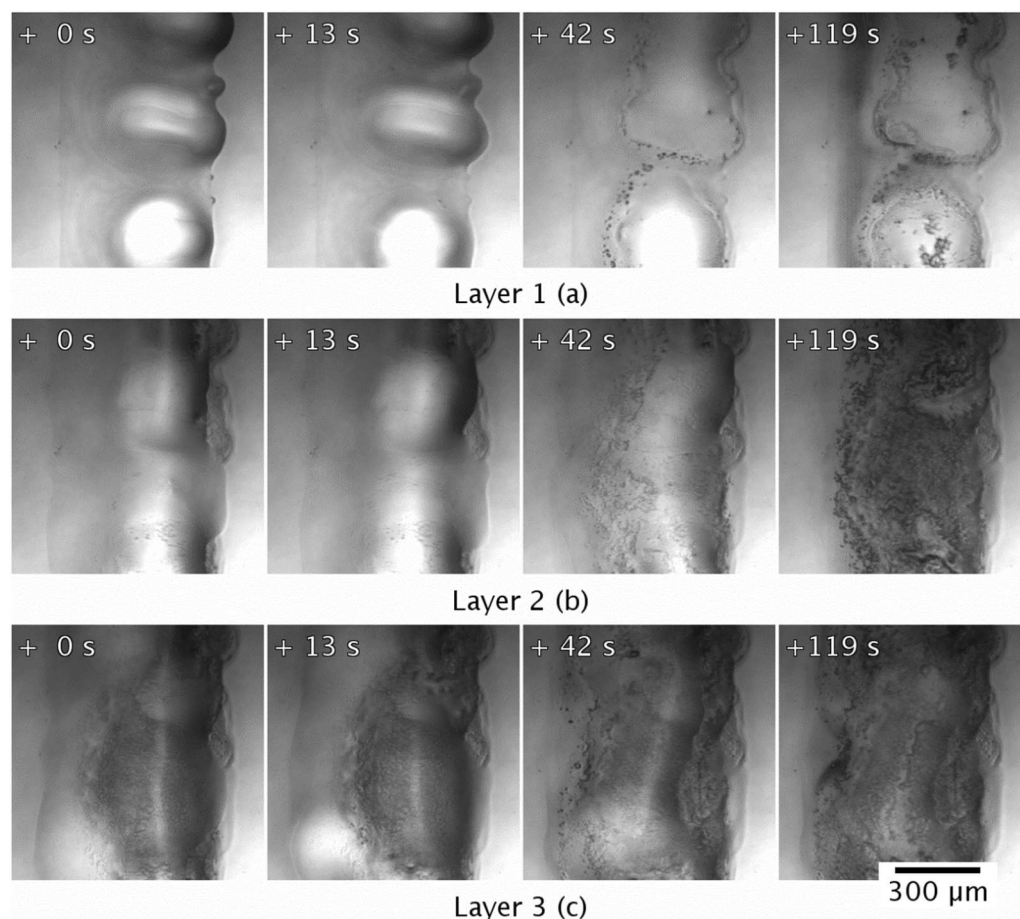


**Figure 6-8 - Multiple layer printing and imaging of HDI and butanediol. Printed at 30 °C. The time units are from the first capture of an image after printing a layer.**

### *H<sub>12</sub>MDI and PEG BDO*

The final formulation of immiscible ink was the combination of H<sub>12</sub>MDI with polyethylene glycol and butanediol. Like the monomers, the two inks are immiscible before reaction. Unlike the monomers, the optical microscopy revealed continual mixing over time. Figure 6-9 shows how the substrate has an effect on separation, where the first layer showed large separation and further layers showed

decreased separation. The separation in the first layers was attributed to the differential wetting of the two ink components on the base glass substrate.

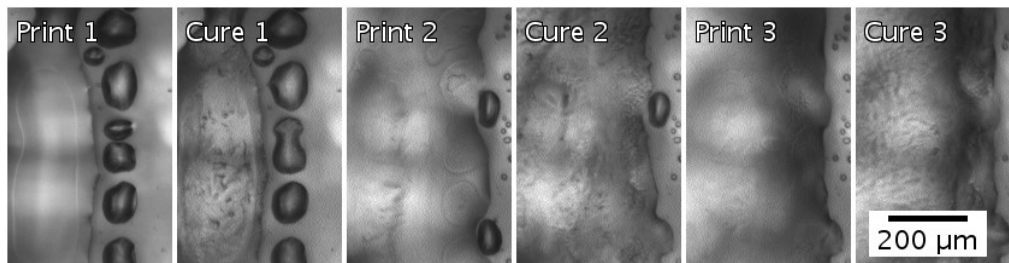


**Figure 6-9** – Three successive layers of printed H<sub>12</sub>MDI and PEG BDO. Printed at 30 °C. Drop spacing set to 45 μm to increase separation. Showing how the initial printed layers segregated and how the later layers did not.

The most uniform curing results were obtained using a drop spacing of 40 μm. The first layers printed separated as seen in Figure 6-9 but the final three layers formed a uniform line, shown in Figure 6-10.

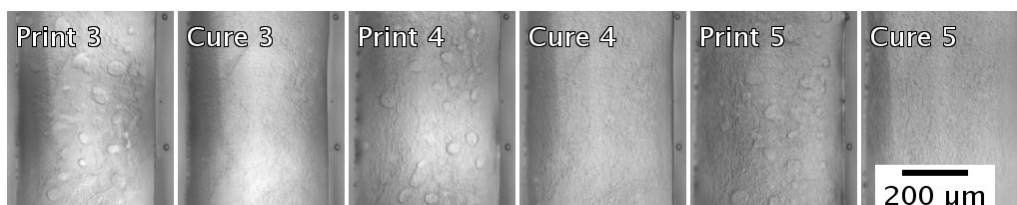


**Figure 6-10** - The last three layers of a five layer print of H<sub>12</sub>MDI and PEG BDO. Printed at 30 °C. Drop spacing set to 40 μm. Print, refers to image capture immediately after printing; while Cure, is an image taken immediately before printing the next layer.

It was found that after printing and curing the printed lines would undergo a further change. The nucleation and growth of the phase separation was observed around 18 minutes after printing, which continued for over 10 minutes (Figure 6-11). This occurred with no change in substrate heating or environment.

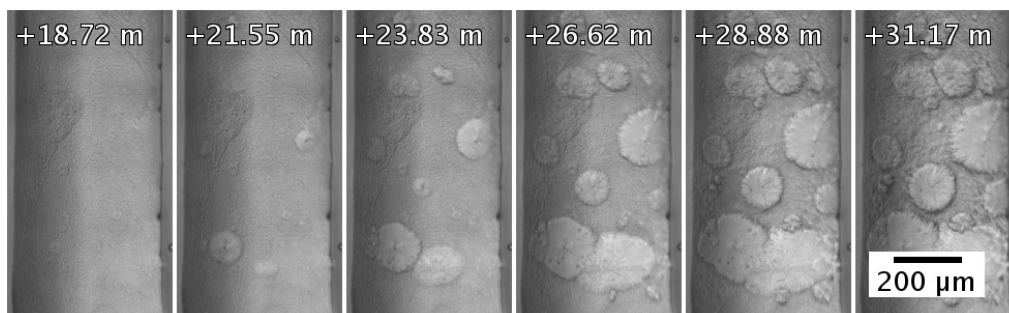


**Figure 6-11 - Nucleation and growth of a phase separation was observed in the printed lines. A three layer print of H<sub>12</sub>MDI and PEG BDO. Printed at 30 °C. Drop spacing set to 40 μm.**

### 6.1.3 Printed Sample Microscopy

The analysed samples were printed in 4x4 mm and 3x5 mm rectangles, where the later shape was selected for the PEG based samples. The change in pattern was carried out to increase printing speed, whilst yielding similar printed volumes for bulk chemical analysis.

#### *Layer vs Line: H<sub>12</sub>MDI and BDO*

A sample was produced using both layer and line based printing, the results shown in Figure 6-12 highlight the differences between the two techniques. In the line based scan reactions can occur as lines are printed and liquid on liquid pinning limits monomer transport in the line. This leads to small droplets that are well dispersed in the sample, resulting in short mixing lengths and high surface areas. The layer based scheme, printing layers of monomers, causes much larger droplets to form which increases the average mixing length. On the layer based sample considerable cracking and large pores were observed. In the line based sample pores were also observed, but these were smaller. Neither sample is an ideal case, however, it is clearly visible that there is increased uniformity, reduced pore size, and no cracking in the line strategy.

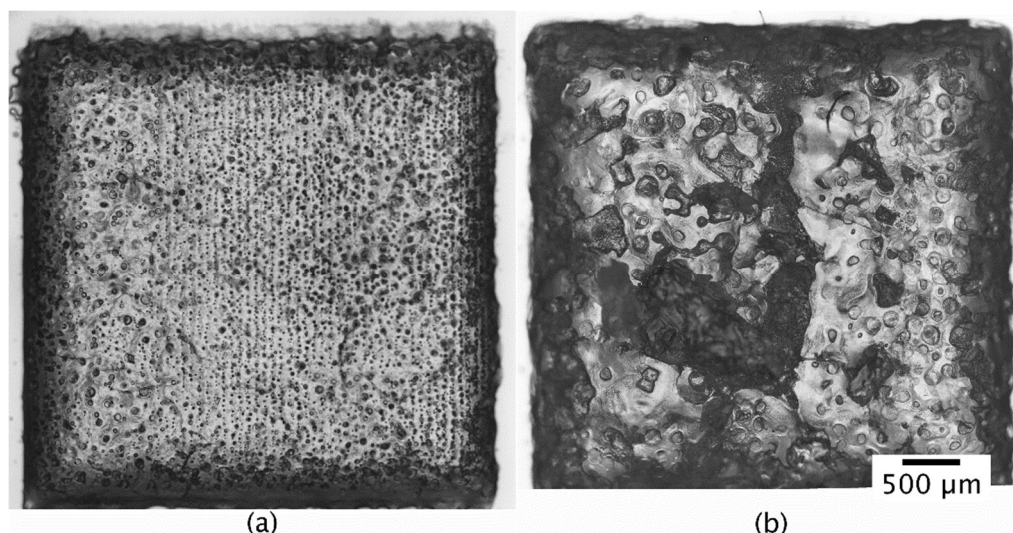


**Figure 6-12 - Difference between printing a) line by line and b) layer by layer. The line stability is increased due to the reaction between each deposited line. Printed at 30 °C, with H<sub>12</sub>MDI and butanediol.**

### *H<sub>12</sub>MDI and BDO*

Three printing cases were examined: a lower than stoichiometric ratio, stoichiometric ratio, and stoichiometric ratio at low printing speed. The result in Figure 6-12a, and Figure 6-13a compare the lower than stoichiometric, and stoichiometric respectively. The increased drop spacing in the first case led to increased monomer dispersion as seen in the images. Substrate heating was employed and the result shown in Figure 6-13, it was found that in all the printing conditions increased heating reduced pore size, and at 70 °C pores were no longer visible.

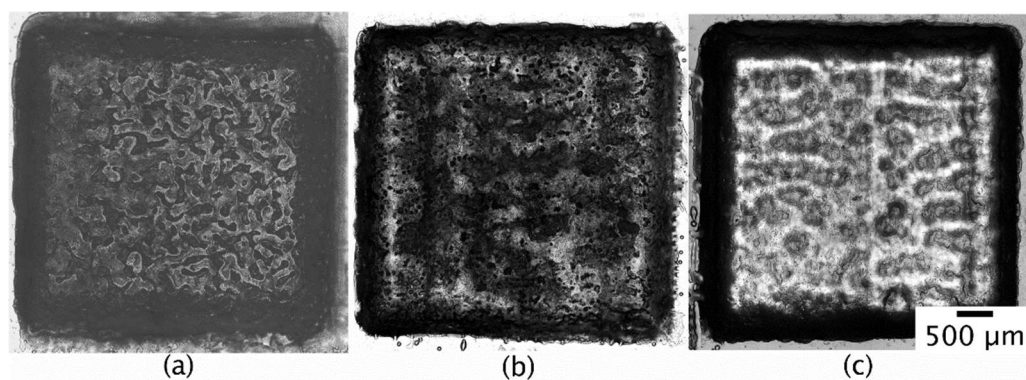


**Figure 6-13 - Comparison of printing H<sub>12</sub>MDI and BDO at different substrate temperatures. a) 30 °C, b) 50°C, c) 70 °C. Pore size is seen to reduce and disappear on increased heating.**

### *H<sub>12</sub>MDI and PEG BDO*

When printing the PEG based ink, it was found that small deposits of residual PEG would remain unmixed on the top surface of the samples. The decreased vapour pressure of PEG versus butanediol may mean that the evaporation of the hydroxyl ink which was observed in the previous printing does not occur. Despite these residual deposits, further chemical information obtained and discussed later shows a high isocyanate conversion. This high degree of conversion would not have been possible if these pockets of unreacted monomers were distributed throughout the sample, therefore, these are likely caused by nozzle miss fire, or an artefact only found on the top layer. This effect is also likely constrained to the top layer because if an additional layer were to be printed these deposits would then mix and react.

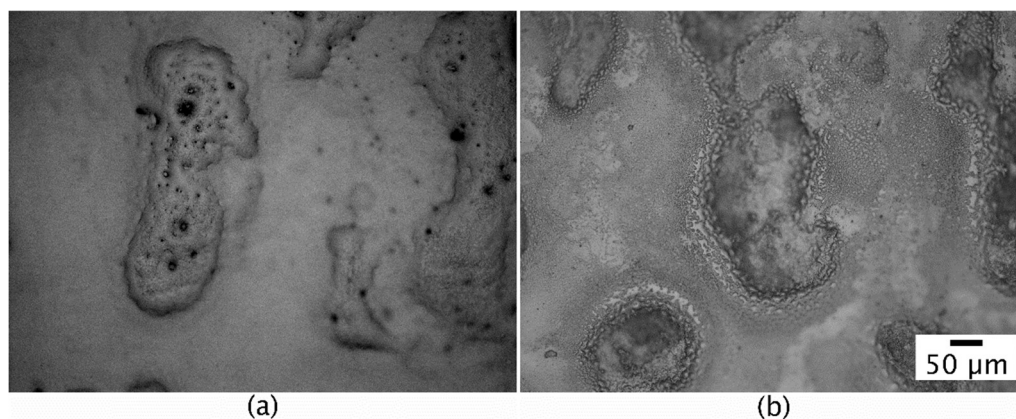


**Figure 6-14 - Residual unmixed monomer on top of the printed PU. a) unwashed printed sample, b) sample washed with IPA. Sample printed at 30 °C.**

When printing a sample at 70 °C it was found that the nozzle calibration had changed, either due to change in Dimatix seating or nozzle deviation. The printed samples had an offset between the two lines in both the X and Y direction. This meant that instead of mixing and reaction occurring in one line, around five lines were printed before multiple inks coalesced. Increasing the mixing time, and allowing for more instability in the liquid on liquid pinning.

The misalignment can be seen in Figure 6-15 where cross polarisation has been used. It was found from previous tests that the PEG has

polarises the light as it readily crystallises,<sup>120</sup> whereas the H<sub>12</sub>MDI with its isomers does not.<sup>105</sup>

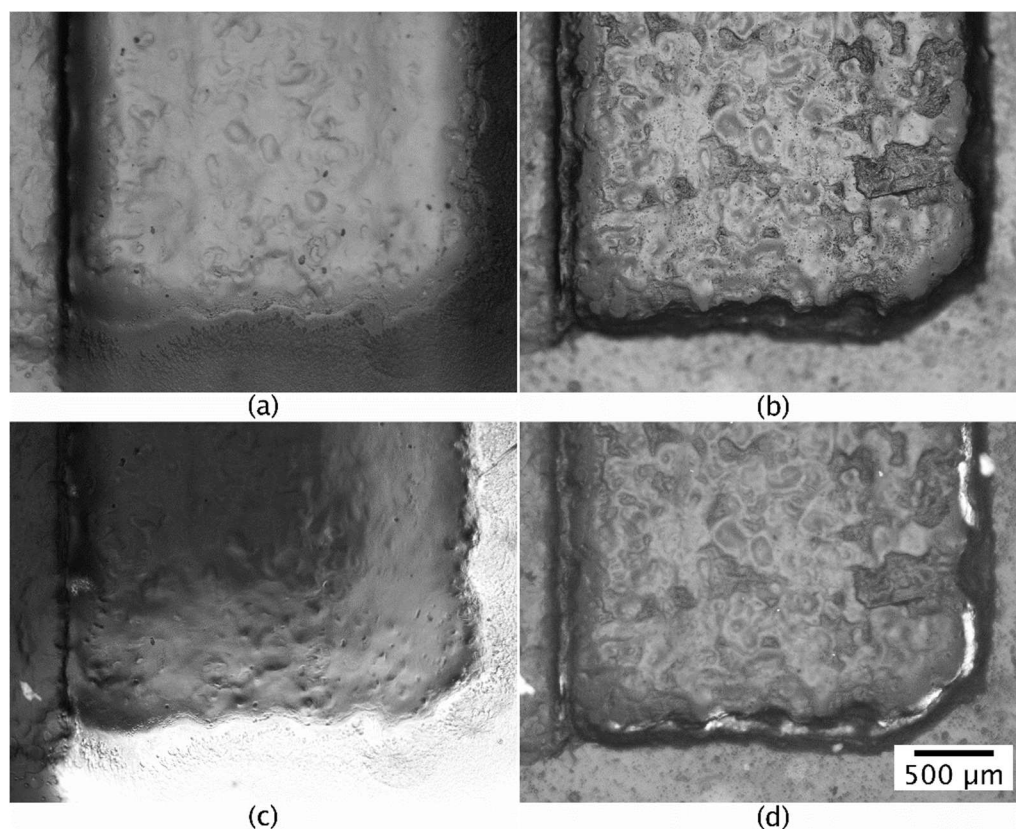


**Figure 6-15** – Cross polarisation imaging of printed PEG based PU. Sample was printed at 70 °C, a) unwashed - unpolarised, b) washed – unpolarised, c) unwashed - polarised, d) washed - polarised. It was found that only the PEG polarised light, whilst the PEG-PU did not.

#### 6.1.4 Profile Analysis

The surfaces of the printed samples were scanned to determine if there was any redistribution of material during printing. As the samples were printed in lines the curing rate can be estimated by the degree of movement across lines. The scans have also been used to determine the volume of the printed sample to understand the degree of evaporation; if any occurred.

#### *H<sub>12</sub>MDI and BDO*

The profile analysis of the butanediol based samples shows that printing at 70 °C reduced the volume remaining to 53% of the 30 °C print. This agrees with the findings of printed lines through the LP50

camera, where pores formed from the evaporation of the components before reaction. The profile data, Figure 6-16, shows the presence of the pores caused by the evaporation of butanediol. However, at the highest temperature 70 °C (Figure 6-16b) the printed profile is no longer porous but instead has an increased roughness and unpredictable profile. The 30 °C case can be seen to have an almost constant profile across the printed lines, this is indicative of reduced fluid transport until curing and is not present in the higher temperature print. The reduced movement is likely due to the higher viscosity of the H<sub>12</sub>MDI and BDO at the lower temperature. H<sub>12</sub>MDI and BDO have viscosities of 25 and 50 mPa.s respectively at 30 °C, at 60 °C these viscosities reduce to 12 and 22 mPa.s with further reduction when printing at 70 °C. Thompson<sup>50</sup> highlighted how the viscosity of the ink resists the transport in printed lines, this would also be true for printed films.

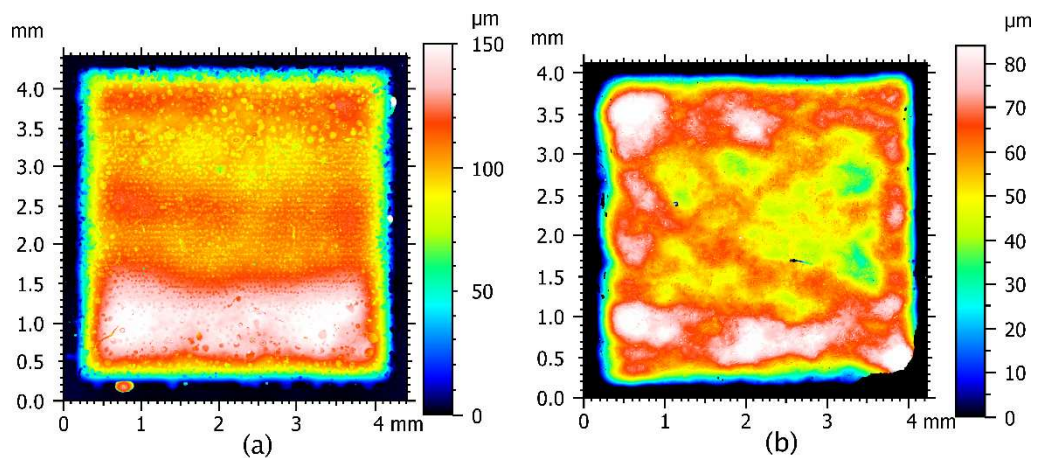


**Figure 6-16 - Surface profile data from the printed H<sub>12</sub>MDI and butanediol, substrate temperatures were (a) 30 °C, (b) 70 °C. The elevated substrate temperature reduced pore formation but resulted in large volume reduction. Samples were printed in the positive Y direction.**

*H<sub>12</sub>MDI and PEG BDO*

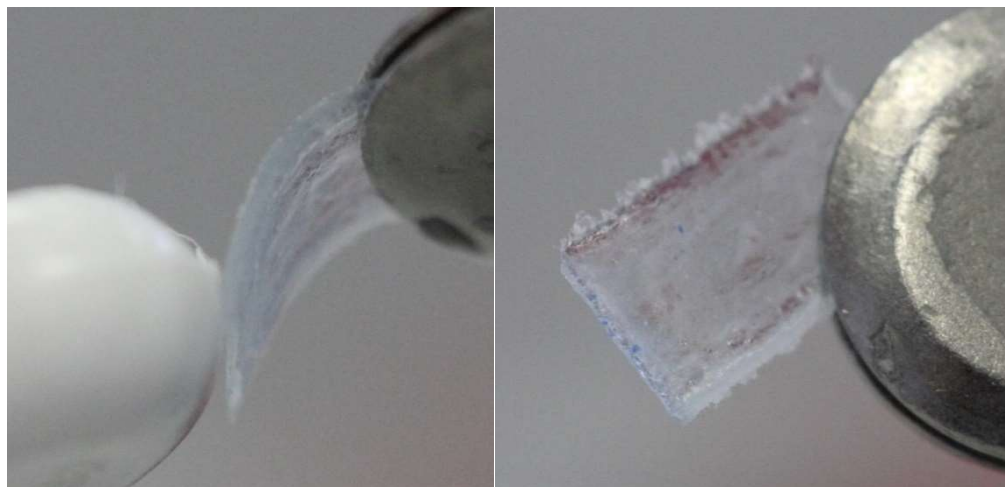


**Figure 6-17** – The samples of PEG-BDO-PU were the only samples which could be removed from the substrate. They were also shown to be flexible.

The profile analysis in Figure 6-18 shows the effect of the increased substrate temperature. It is apparent that increasing the substrate temperature to increase the reaction rate has some effect on the fluid transport, but the reduction of the component viscosities competes to increase fluid flow. The 50 °C case, Figure 6-18b, has an apparent increase in uniformity across printed lines, whereas the 30 °C case, Figure 6-18a, a low reaction rate allowed for a large movement of liquid across printed lines. This trend cannot be tracked into the higher temperature case due to nozzle misalignment, the effect of the misalignment is apparent in Figure 6-19, where the washed(b) and unwashed(a) samples are compared.

Interestingly this nozzle misalignment showed the possibility of using one component of a FRIJP ink for two purposes. The first reaction and production as intended, the second a material which confines the printed samples and is structurally supportive. The solvent and BDO in the PEG based ink eventually evaporates. When printed at high temperatures without the polymerisation reaction this evaporation leaves behind a high viscosity ink (45 mPa.s), which is apparently sufficient as a support.

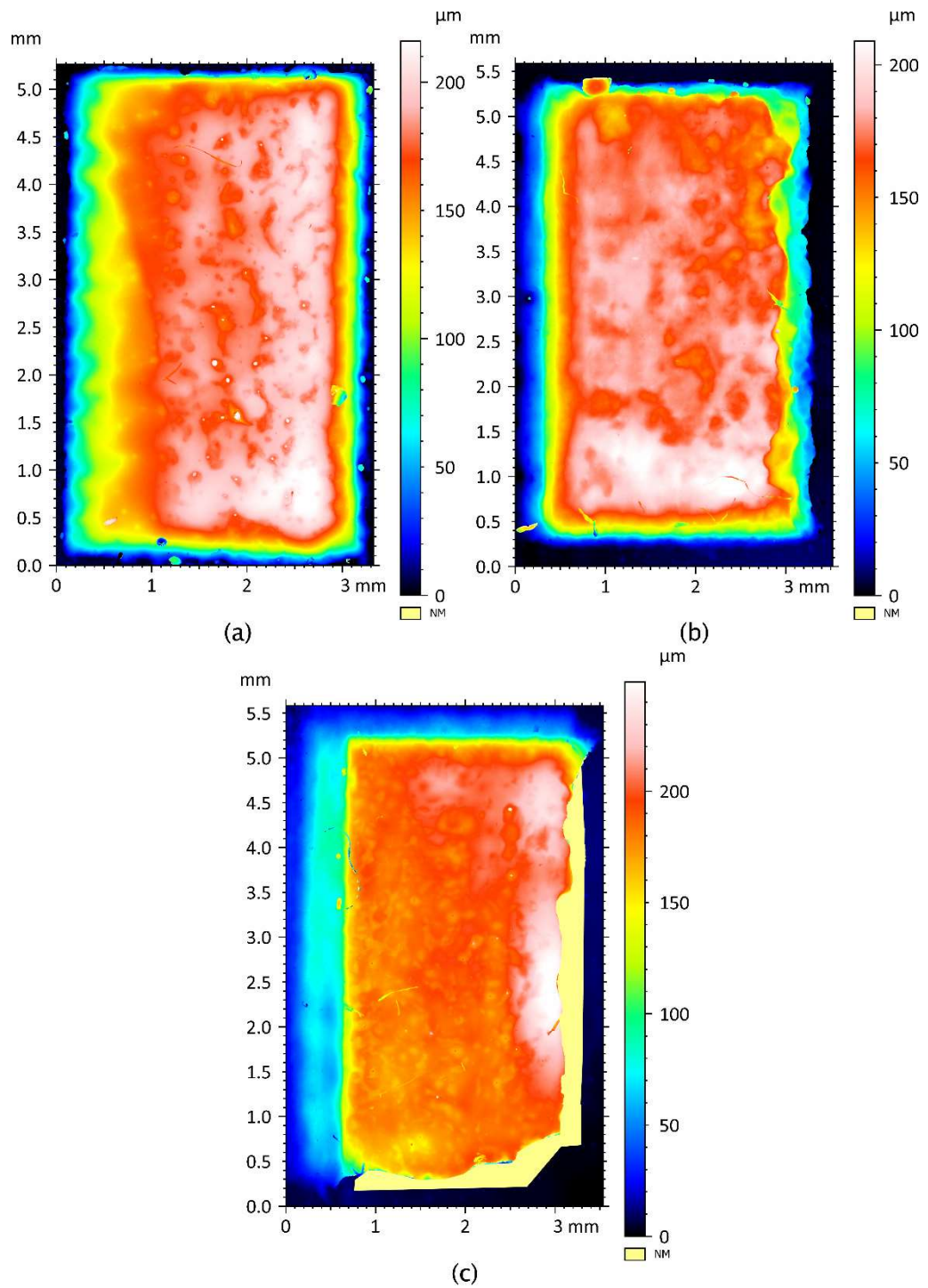
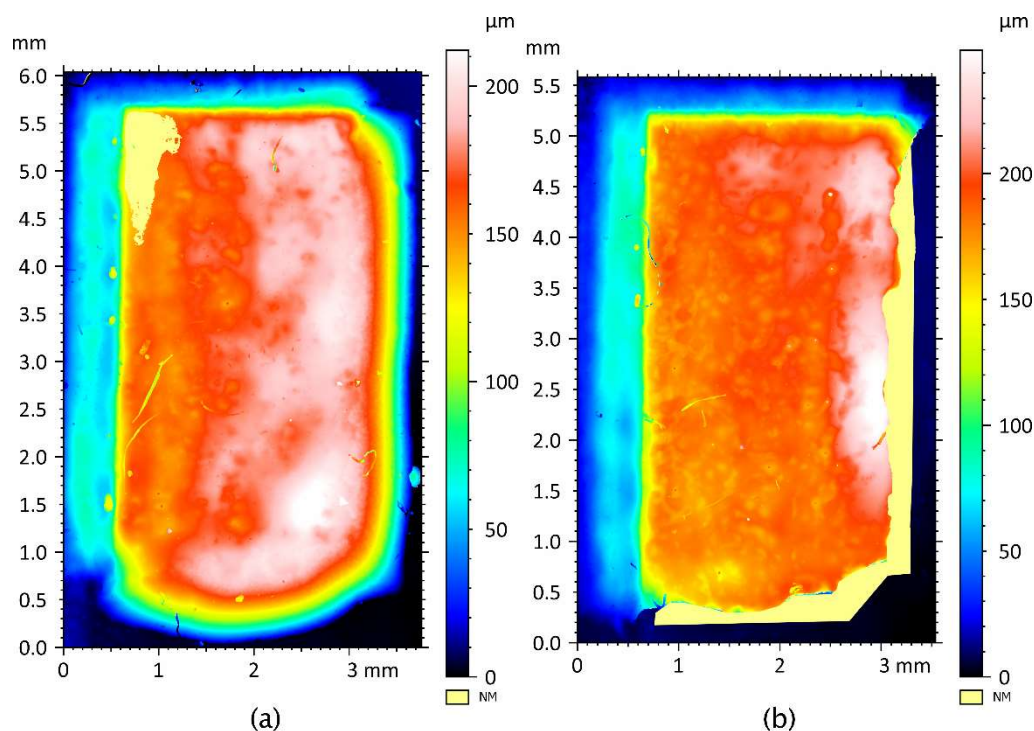


Figure 6-18 – Surface profile data from the printed H<sub>12</sub>MDI and PEG-BDO, substrate temperatures were (a-c) 30 °C, 50 °C, and 70 °C. Samples were washed to remove any residual unreacted components.



**Figure 6-19 - Surface profile data from the printed H<sub>12</sub>MDI and PEG-BDO, samples were unwashed (a) and washed (b), printed at 70 °C. NM stands for not measured, and was caused by bubble formation in the replica, for the case of the washed sample the NM data was 0 μm height.**

### 6.1.5 SEC and NMR-FTIR Data

#### SEC

All printed samples were analysed using SEC, a bulk method by which the degree of mixing can be estimated. In the literature it was found that number average molecular weights above 20 kDa are where most desirable mechanical properties are found. At this chain length polymer properties become a function of the repeating unit instead of the chain length. The number average weight is a function of the number of repeating units and average mass of a repeating unit. The results from the SEC analysis are shown in Table 6-3, where the number average, weight average and degree of polymerisation are shown. The results show that the PEG based ink obtained higher weights number and mass average weights than the other formulations. However, this is expected due to the greater weight of the component monomers. To more directly compare the mixing in

systems with different monomers the degree polymerisation is more useful. The degree polymerisation uses the average mass of the repeating unit to instead provide the average number of isocyanate and diol units in the chains. From the degree of polymerisations results it is clearer to say that the PU formulated from the PEG based ink printed at 30 °C is the best result, with greater than 99% conversion in all three samples.

The chromatograms show that in samples printed only with BDO, as shown in Figure 6-20, the mass distribution suggests unreacted monomer. Whereas in chromatograms with PU including PEG, as shown in Figure 6-21, a statistically normal distribution is shown. This result agrees with what was seen in the microscopy, in that samples without PEG could not readily mix. Further, the samples where substrate heating was elevated, Figure 6-22, and Figure 6-23, show a secondary peak around 2000 Da. This secondary peak, not found in the 30 °C sample, was likely caused by imbalance of reactants caused by the nozzle misalignment and confirms that the 30 °C sample only had minor surface deposits of PEG.

In the PU-PEG samples printed at 70 °C there is a corresponding increase in mass average molecular weight and polydispersity. This is indicative of imbalanced mixing ratios likely caused by both the misalignment and evaporation of the butanediol.

**Table 6-3 - Comparison of SEC results for the immiscible polyurethane formulations. Showing chemical components, substrate temperature, number average molecular weight, weight average molecular weight, and degree of polymerisation.**

<i>Sample</i>	<i>-CNO</i>	<i>-OH</i>	<i>T</i> (°C)	$\overline{M}_n$ ( $\frac{g}{mol}$ )	$\overline{M}_w$ ( $\frac{g}{mol}$ )	<i>Xn</i> (%)
<i>HDI</i>	HDI	BDO	30	4.4890E+03	4.7800E+03	97.12
<i>Low DPI</i>	H <sub>12</sub> MDI	BDO	30	4.0590E+03	4.7550E+03	95.66
<i>Low DPI</i>	H <sub>12</sub> MDI	BDO	50	5.4200E+03	7.1460E+03	96.75
<i>Low DPI</i>	H <sub>12</sub> MDI	BDO	70	6.4580E+03	8.9670E+03	97.27
<i>Slow Printing</i>	H <sub>12</sub> MDI	BDO	30	4.0100E+03	5.1760E+03	95.61
<i>Slow Printing</i>	H <sub>12</sub> MDI	BDO	50	5.7350E+03	7.0780E+03	96.93
<i>Slow Printing</i>	H <sub>12</sub> MDI	BDO	70	5.7870E+03	8.9780E+03	96.95
<i>Fast Printing</i>	H <sub>12</sub> MDI	BDO	30	3.3460E+03	4.4860E+03	94.73
<i>Fast Printing</i>	H <sub>12</sub> MDI	BDO	50	4.7960E+03	6.0690E+03	96.33
<i>Fast Printing</i>	H <sub>12</sub> MDI	BDO	70	5.9500E+03	7.9520E+03	97.04
<i>PEG 1</i>	H <sub>12</sub> MDI	PEG BDO	30	3.4962E+04	8.8041E+04	99.06
<i>PEG 1</i>	H <sub>12</sub> MDI	PEG BDO	50	1.1133E+04	3.2757E+04	97.05
<i>PEG 1</i>	H <sub>12</sub> MDI	PEG BDO	70	2.0089E+04	1.0876E+05	98.37
<i>PEG 2</i>	H <sub>12</sub> MDI	PEG BDO	30	3.9218E+04	9.7149E+04	99.16
<i>PEG 2</i>	H <sub>12</sub> MDI	PEG BDO	50	1.1555E+04	3.3951E+04	97.16
<i>PEG 2</i>	H <sub>12</sub> MDI	PEG BDO	70	1.8024E+04	9.4218E+04	98.18
<i>PEG 3</i>	H <sub>12</sub> MDI	PEG BDO	30	3.7280E+04	9.7446E+04	99.12
<i>PEG 3</i>	H <sub>12</sub> MDI	PEG BDO	50	1.1716E+04	3.3981E+04	97.2
<i>PEG 3</i>	H <sub>12</sub> MDI	PEG BDO	70	1.9770E+04	9.6901E+04	98.34

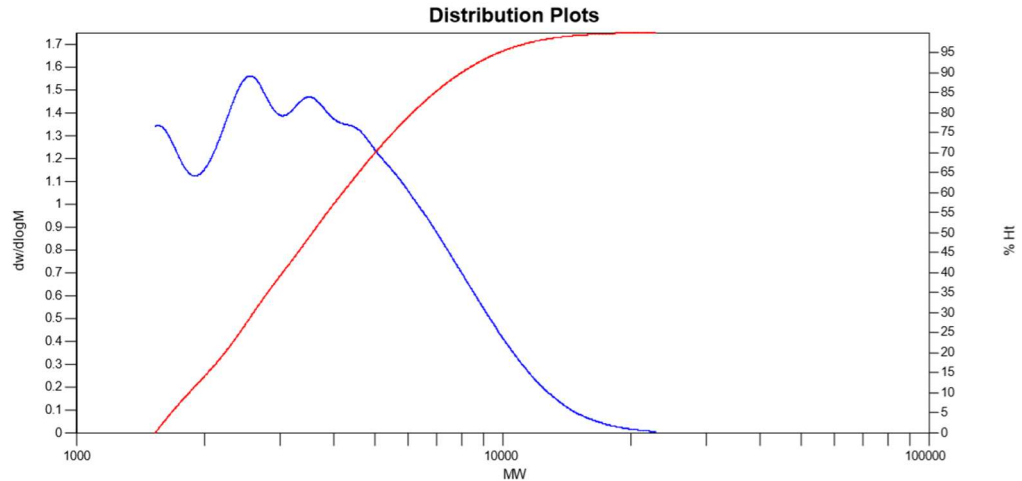


Figure 6-20 - Chromatogram from the SEC analysis of the inkjet printed polyurethane sample. Specific sample was Fast Printing 70 °C.

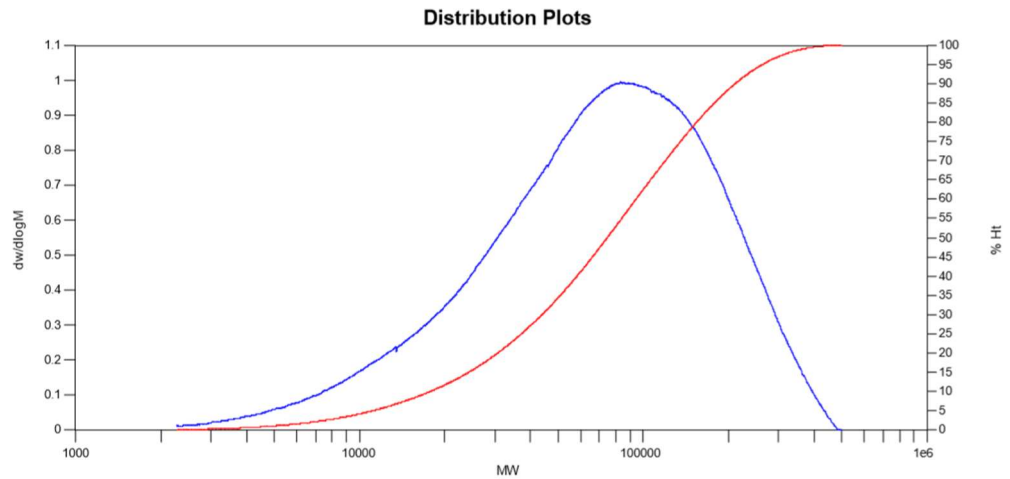


Figure 6-21 - Chromatogram from the SEC analysis of the inkjet printed polyurethane sample. Specific sample was PEG 1 30 °C.

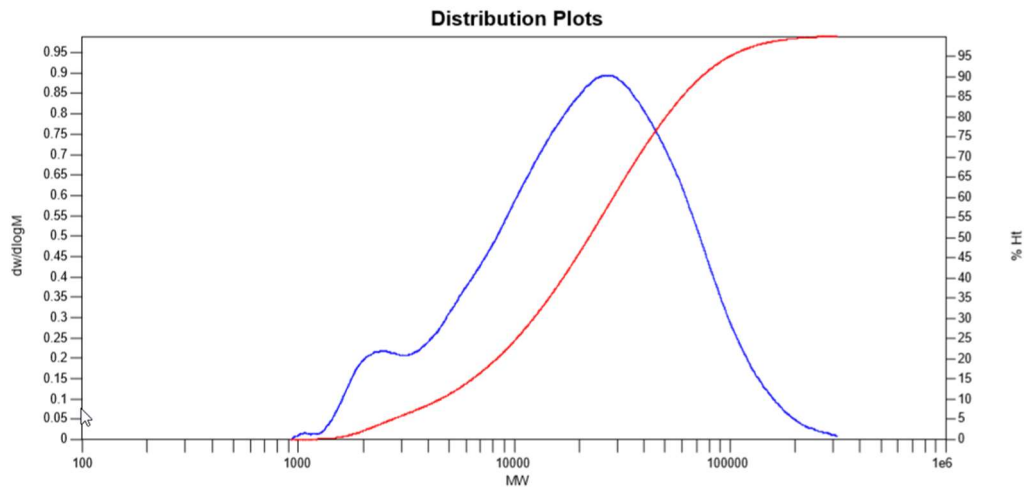
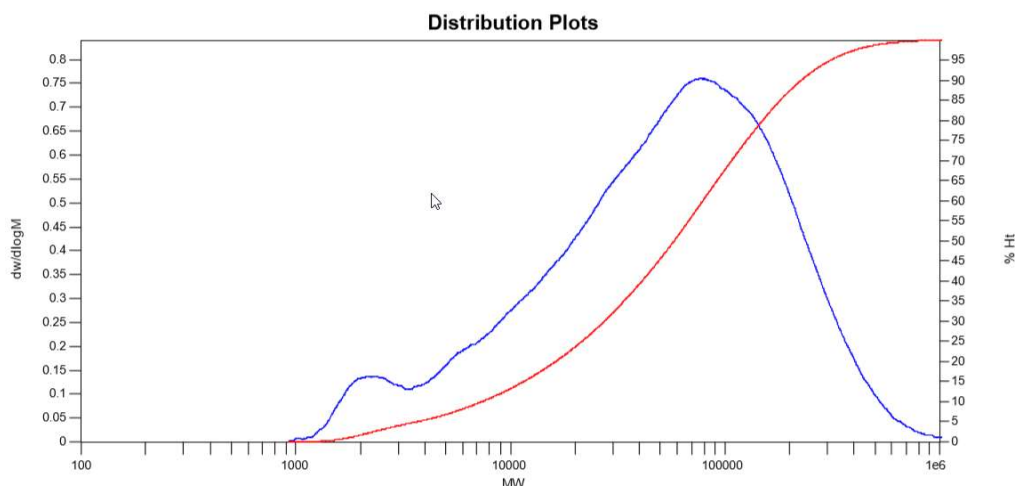


Figure 6-22 - Chromatogram from the SEC analysis of the inkjet printed polyurethane sample. Specific sample was PEG 1 50 °C.



**Figure 6-23 - Chromatogram from the SEC analysis of the inkjet printed polyurethane sample. Specific sample was PEG 1 70 °C.**

### *NMR and FTIR*

The confirmation of polymerisation of polyurethane was conducted with NMR and FTIR techniques. For the initial samples of polyurethane printed with butanediol the FTIR-ATR apparatus was used. Later in the PhD the confirmation of the polyurethane was conducted through NMR.

FTIR was used to determine if the samples printed with butanediol produced polyurethane. All samples printed at different temperatures showed peaks at  $3320\text{ cm}^{-1}$  (-N-H),  $1685\text{ cm}^{-1}$  (-C=O), and  $1528\text{ cm}^{-1}$  (-N-H), with a reducing peak at  $2259\text{ cm}^{-1}$  (-N=C=O). As FTIR-ATR technique was used only the surface of the sample was analysed and this resulted in spectra incorrectly showing almost complete isocyanate conversion. The results of the SEC and optical microscopy agree that this is only a surface feature.

NMR was used to confirm the presence of the polyurethane proton (N-H  $\delta$ :7.00 ppm, 7.15 ppm) for both the *trans* and *cis* isomers in all PEG-BDO polymers. The presence of two triplets ( $\delta$ :4.44 ppm, 4.60 ppm) were attributed to the hydroxyl groups of both the BDO and PEG. These signals in reference to the polyurethane bond were found

to have a total intensity of 0.01, 0.20 and 0.14 for the 30 °C, 50 °C, and 70 °C respectively. These values agree with the results from the SEC in that the lowest temperature case shows the greatest conversion of components. There is also some correlation between residual hydroxyl component and degree conversion. This correlation points to an increased evaporation effect in the samples printed at 70 °C, which caused the low weight polymer and unreacted monomers to evaporate more than the 50 °C case. This increased purification through evaporation would then show on the SEC results as a higher  $M_w$  produced with increased chain length distribution over the unevaporated correct mixing ratio.

## 6.2 Discussion

Three formulations were successfully used to FRIJP linear polyurethane samples. This was achieved by exploiting the innate dispersion of reactants in the inkjet printing method. Once droplets were dispersed mixing through diffusion could be achieved.

This method of mixing has been found to be dependent on the chemistry used, and with the original formulation of H<sub>12</sub>MDI (and HDI) and BDO only low degrees of conversion were obtained. The cause for this limited conversion is likely because the polyurethane was produced from only hard segments. Once polymerisation occurred the flexibility of the polymer reduced and the rate of reactive group interaction decreased. The increasing rigidity of the polymer resulted in a reduced the rate of diffusion of the monomers, until transport through the interfaces no longer occurred. Heating the substrate increased the polymer molecular weight limit on diffusion, but eventually diffusion still stopped. The order of the printing was isocyanate and then hydroxyl, with the hydroxyl component evaporating before complete reaction to leave exposed the interfacial polyurethane region. The results of the line microscopy showing

pores, the sample microscopy showing cells, and the SEC reporting low degree conversion all agree with this hypothesis.

Mixing increased by changing the components of the FRIJP ink to include soft segments. The soft segment was a polyethylene glycol (PEG) with an  $M_w$  of 1000. The PEG was selected as being the highest molecular weight whilst still being printable with minimal solvent. It was found that the formulation required solvent, but only at a concentration of 15 wt%. The increased flexibility of the PEG and the introduction of soft segments led to greatly increased mixing with no perceivable limit. This resulted in high degrees of conversion, as seen in the SEC analysis. The ability of the PEG based FRIJP to mix highlighted a second issue with the process. Printing at elevated temperatures in a dried atmosphere increased the evaporation rate of the inks. This effect could have been present in previous printing attempts, but due to the low degree of conversion it did not lower the  $M_w$  of the product.

Despite the reaction being observed and polyurethane produced in all cases, only the H<sub>12</sub>MDI and PEG-BDO printed at 30 °C produced a plastic sample with a suitable molecular weight. The molecular number over 20 000 Da indicates that the reaction proceeded to a sufficient degree, thus proving that FRIJP can be used to build 3D linear polyurethane structures. Notably, this value is higher than seen in the work by Cassagnau,<sup>103</sup> in which a reactive extrusion method was used with the same chemicals.

## ***7 FRIJP of Polyurethane: Miscible Components***

From the work presented in the previous chapters it was hypothesised that using components that were miscible would produce polyurethane with higher degrees of conversion. In theory, instead of producing a reaction interface, as described in the literature,<sup>89</sup> the mixing could occur separately to the reaction, and at a higher rate. Exchanging the interfacial reaction with bulk reaction the scheme would shift to that which was observed with the PDMS printing. The previously used H<sub>12</sub>MDI was combined with Tripropylene Glycol, a hydroxyl functional chemical which was predicted to be miscible using the partition coefficient. The printing was conducted using the single reactive line scheme described in 4.1.4 Line Printing. The samples were analysed in the same manner as the immiscible component inks using: profilometry, SEC, and NMR.

### **7.1 Results**

A polyurethane formulation was created for FRIJP that contained miscible monomer components. Miscibility was first predicted for Tripropylene Glycol (TPG) using the partition coefficient, it was later experimentally confirmed using a H<sub>12</sub>MDI and TPG solution without a catalyst. The solution was stirred and it was found that the components did not separate with minimal change to viscosity (no reaction). The lack of separation and reaction confirmed experimentally that the chemicals were miscible. As these two chemicals were miscible the reaction was no longer purely interfacial and instead bulk mixing could occur facilitating bulk reaction. This process was chosen as a method to obtain high degrees of cure after the results of the BDO and H<sub>12</sub>MDI, from Chapter 6, were analysed.

TPG was also chosen as it had a lower vapour pressure than the BDO. Where a reduced vapour pressure would reduce the evaporation of the ink and facilitate a more complete reaction through increased substrate temperatures.

### 7.1.1 Ink Development

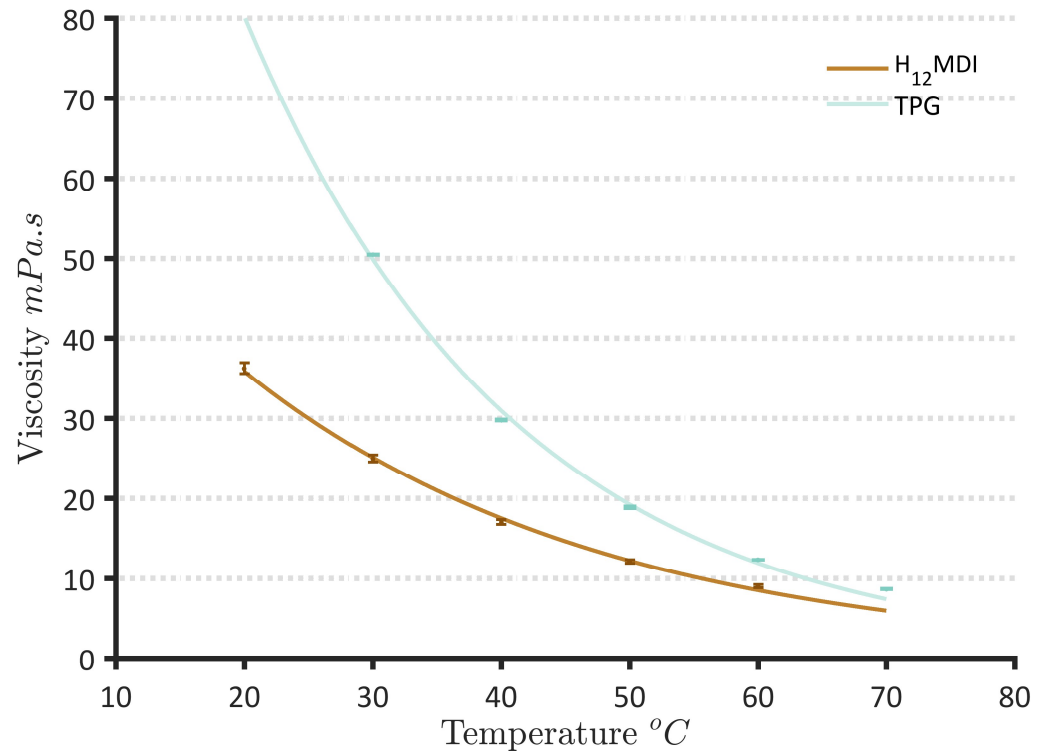


**Figure 7-1 - Viscosities of the inks used in printing the miscible polyurethane polymer. Both inks required only thermal modification to achieve a printable viscosity. The data was selected from the stable shear rate range and the exponential model was used to fit the points (as described in 3.2.1 Material Rheology)**

The previously developed H<sub>12</sub>MDI ink with the 3% DBDT catalyst was used. The hydroxyl component ink was pure TPG, and it was found that through thermal modification it was directly printable. The viscosities of these two inks are shown in Figure 7-1. Once printable the waveform for printing was developed. The printed mass of each ink, the values for the selected printing temperature, viscosity at that temperature, and Ohnesorge number are shown in Table 5-1.

Table 7-1 - The material properties used to calculate the printability, and the measured droplet volume.

Ink	Temp. (°C)	Viscosity (mPa.s)	Surface Tension (mNm <sup>-1</sup> )	Ohnesorge	Mass (ng)
H <sub>12</sub> MDI	50.00	12.14 ±0.44	37.84 ±0.15	0.43	8.21 ±0.17
TPG	60.00	12.38 ±0.09	35 †	0.46	4.84 ±0.15

† - Value found in literature

### 7.1.2 Printed Line Microscopy

Previously the printed line microscopy was used to track the mixing of the inks, however, with miscible components no interface change can be seen. What is observed in Figure 7-2, is that during curing the pre-polymer solution has different wetting characteristics to either the isocyanate or the diol phase. It was previously shown that the H<sub>12</sub>MDI could form continuous films in a single layer Figure 6-6a, but the pre-polymer in a range of drop spacings could not. Typically drop spacing is determined in this manner, but it was found that across a large range of drop spacings a continuous first layer could not be achieved. As the correct drop spacing could not be determined in this manner a best guess approach was adopted. From experience of other printing conducted with a single ink a drop spacing around 30 μm is typical for Dimatix printing. As this system involved two inks which were both liquid on the substrate the drop spacing needed to be adjusted. In this case it is the volume in an area which is controlled by the drop spacing, it was then decided to select a drop spacing that would achieve a theoretical volume identical to a single ink printed at 30 μm. The relation was identified as;

$$DPI_{dual}^2 = 0.5 * DPI_{single}^2 \quad (7-1)$$

where DPI is the dots per inch, a conventional term in printing which is useful as the reciprocal of the drop spacing. This equation leads to a drop spacing of 42.42 μm, which was rounded to 44 μm.

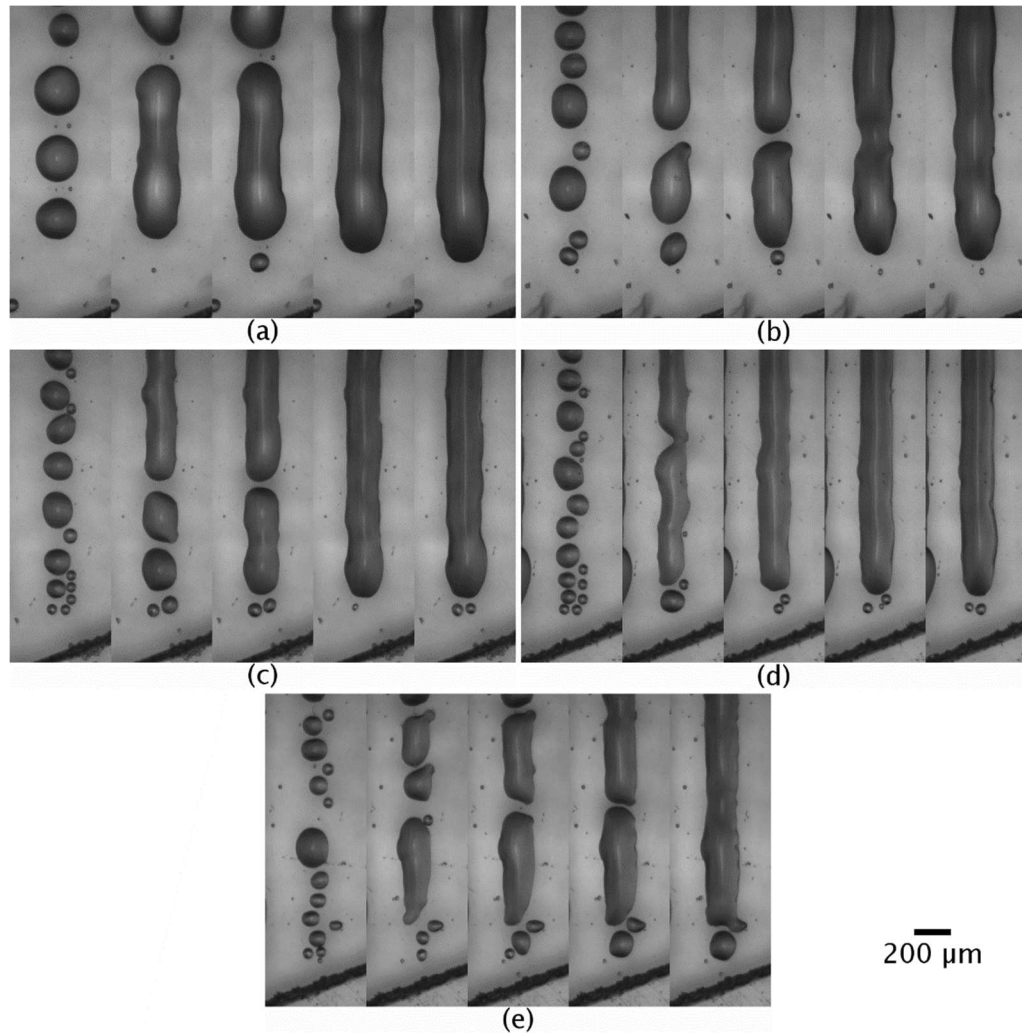


Figure 7-2 - Determination of suitable drop spacing for the H<sub>12</sub>MDI and TPG polyurethane on glass. (a-e) 35, 50, 65, 80, 95 μm.

### 7.1.3 Droplet volume microscopy

In this package of work there were three strategies relating to the volumes of each droplet. Initially, the work conducted neglected the effect of varying droplet volumes. Later droplet volumes were suspected as a cause for low degrees of curing, as such an optical method for determining volume was used. Lastly it was determined that the optical method was not reliable, and instead the weight based method discussed in 3.2.3 FRIJP Printing was used.

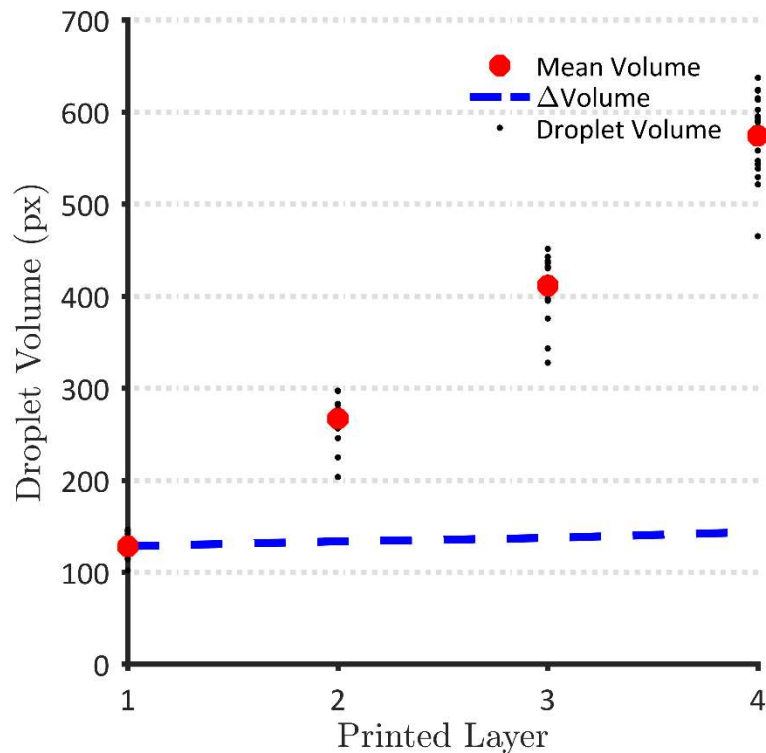


Figure 7-3 - Result of optical droplet volume analysis conducted on TPG. Multiple layers of TPG were printed in a grid on glass.

Although unreliable the method for drop volume determination did result in increased polyurethane conversion leading to higher molecular weights and solid samples. The process was based on the known profile of a micron scale droplet on a substrate, which is described by a spherical cap as discussed in 2.2.4 Ink Deposition. The profile of a spherical cap can be described by the contact angle and diameter of the droplet, therefore, the volume can be determined from top down microscopy providing the contact angle is known. Through the use of drop shape analysis the contact angle of both the H<sub>12</sub>MDI and the TPG was determined. When printing grids of droplets software was used to determine the average diameter of the circular profile, once determined the volume was calculated. The method used image processing in MATLAB with the following steps;

1. Removing the background
2. Thresholding
3. Detecting connected areas

4. Calculate diameter based on known area
5. Calculate droplet volume

Results of the analysis on printed TPG is shown in Figure 7-3. The issues with the optical method for determining droplet volume are shown in Figure 7-4. The TPG and glass contact angle is varying due to some unknown contamination. As such it is not possible to know if the contact angle determined through DSA is applicable in any specific area of the glass slide.

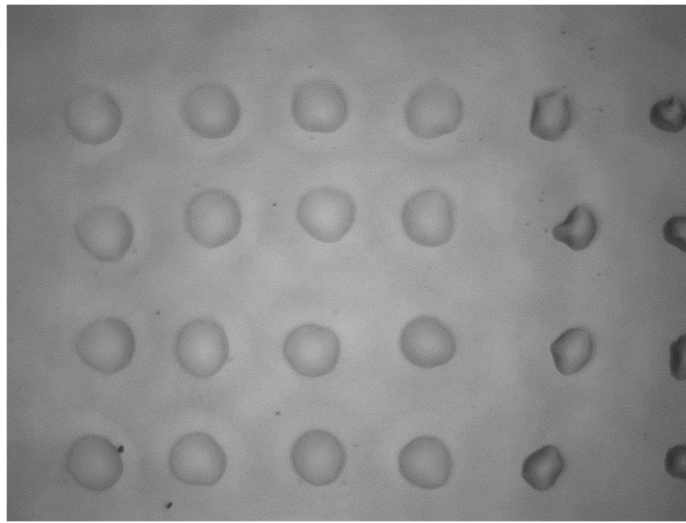


**Figure 7-4 - Example image of a grid of TPG printed onto glass slides. On the right of the glass the contact angle is different, this causes issues in optical drop volume determination.**

#### 7.1.4 SEC and NMR Data

The results in Table 7-2 summarise the SEC analysis for the miscible formulation. The method for droplet volume (if conducted) is identified through the letter A, B and C, respectively representing no volume determination, optical volume determination, mass based determination. In the previous chapter it was found that higher substrate temperatures produced high degrees of curing in the case of the H<sub>12</sub>MDI and BDO. In the study of the TPG a comparison of heating during printing and heating post printing was conducted.

Therefore, the results under category C are split into “printing temperature + post treatment temperature” (if conducted).

The results before finding the correct mixing ratio then highlight the need for the process control. As this specific chemistry was capable of completely mixing the monomers; the ratio between reactants became increasingly important. The results with no mass calculation, “A” show how the uncontrolled droplet volumes resulted in low degrees of conversion compared to the completely controlled mass based results.

**Table 7-2 - Comparison of SEC results for the miscible polyurethane formulations. Showing substrate temperature, treatment temperature, number average molecular weight, weight average molecular weight, and degree of polymerisation.**

Sample	Substrate $T (^{\circ}C)$	Treatment $T (^{\circ}C)$	$\overline{M}_n$ $(\frac{g}{mol})$	$\overline{M}_w$ $(\frac{g}{mol})$	$X_n$ (%)
A	30	NA	3.0250E+03	7.3020E+03	92.49
A	70	NA	5.2020E+03	5.8450E+03	95.63
A	100	NA	2.9590E+03	6.3040E+03	92.32
A	30	NA	2.4820E+03	4.4960E+03	90.84
A	70	NA	4.8620E+03	1.0005E+04	95.32
A	100	NA	6.7950E+03	2.6210E+04	96.65
B	30	NA	3.6620E+03	7.8970E+03	93.79
B	70	NA	4.5300E+03	1.3880E+04	94.98
B	100	NA	1.2770E+04	3.6100E+04	98.22
C	50	NA	4.0760E+03	6.5390E+03	94.42
C	50	NA	3.0560E+03	6.4570E+03	92.56
C	50	100	5.8730E+03	1.0070E+04	96.13
C	50	100	5.6880E+03	9.9220E+03	96.00
C	100	NA	1.0880E+04	2.2620E+04	97.91
C	100	NA	1.1350E+04	1.9880E+04	98.00
C	100	NA	9.8290E+03	2.0500E+04	97.69
C	100	100	1.2450E+04	2.0340E+04	98.17
C	100	100	1.2530E+04	2.2690E+04	98.19
C	100	100	9.4560E+03	1.9480E+04	97.60

The printing with the optical based measurement process incorrectly predicted a wt:wt of 1:2.4 (H<sub>12</sub>MDI:TPG) instead of the correct 1:1.69. This meant that samples A were printed with excess H<sub>12</sub>MDI and

samples B were printed with excess TPG. It is known that the TPG was evaporating significantly faster than the H<sub>12</sub>MDI during the reaction, and this could explain how excess TPG had a reduced effect over final sample properties compared to excess H<sub>12</sub>MDI.

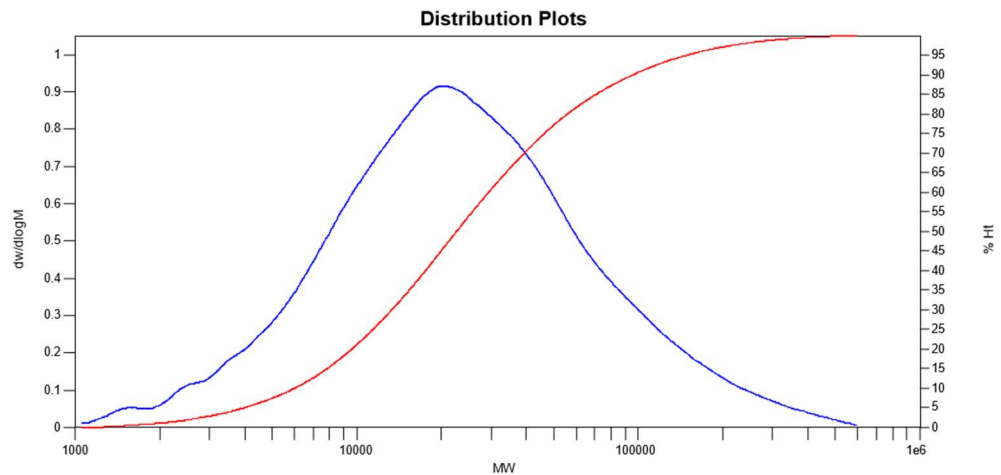


**Figure 7-5 - Chromatogram from the SEC analysis of the inkjet printed polyurethane sample. Specific sample was B 100 °C.**

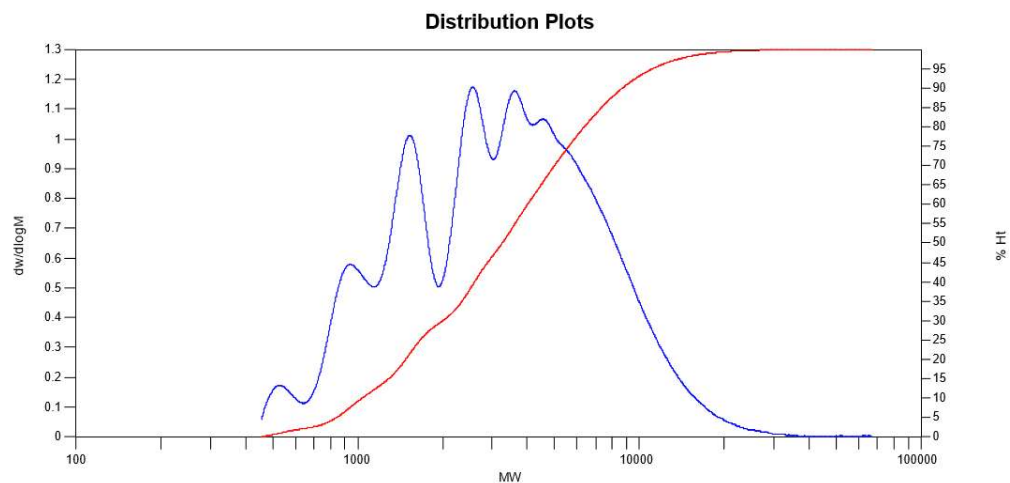


**Figure 7-6 - Chromatogram from the SEC analysis of the inkjet printed polyurethane sample. Specific sample was A 30 °C.**

It was found that samples printed at a higher substrate temperature had an increased polymerisation degree, however, this increased temperature caused problems during printing. It was found that the heated platform increased the print head temperature during printing, which led to uncontrolled ink viscosities. This led to ink

leaking and nozzle blockage. To solve this, a smaller platform heater was used which greatly reduced the print head heating.

The printing of samples at lower substrate temperature which were then post treated with higher temperature were analysed. In theory, this process would achieve high curing degrees without excessive thermal loading. This method would also decrease the chance of monomer evaporation affecting the mixing ratios. Seven 4 x 4 mm squares were printed consisting of 20 reactive layers, and this was carried out at 50 °C and 100 °C. Once printed, four samples from each series were post treated on the substrate at 100 °C for three hours. One of each sample was analysed using NMR, and the remaining twelve were analysed through SEC. For unknown reasons two of the samples (50 °C and 50 °C + 100 °C) produced no signal for SEC analysis, this was thought to be an issue with sample preparation.

The results of the post heat treatment analysis show only a moderately increased molecular number over the untreated samples. This increase is consistent with the evaporation of low weight chains and monomers in the sample, and not further polymerisation of the chains. Despite the improvement in polymer weight after post treating, the results are still lower than if printing was conducted at the higher substrate temperature. It also shows that the post treatment had no effect on the samples already printed at a higher temperature.

### *NMR Results*

NMR was used to confirm the presence of the polyurethane proton (N-H  $\delta$ : 7.01 ppm, 7.07 ppm, 6.75 ppm, 6.66 ppm) for both the *trans* and *cis* isomers in all TPG based polymers. NMR was also used to determine if any polyurea was formed when using substrate heating, an indicator of excess H<sub>12</sub>MDI. The following results for polyurea signal (N-H  $\delta$ : 5.87 ppm, 5.78 ppm, 5.58 ppm, 5.50 ppm) are quoted

in reference to the polyurethane bond signal. It was found that in the samples printed at 50 °C with and without heat treatment only trace amounts ( $\ll 1\%$ ) of polyurea was produced. The sample printed at 100 °C had a concentration of 2% and the post treated sample showed a 4% concentration of the polyurea. The increasing presence of polyurea as more heating is used confirms there is an evaporation effect even in the miscible bulk reaction. This evaporation creates an imbalance between reactants due to the difference in evaporation rates.

#### 7.1.5 Profile Analysis

The samples produced for the post treatment investigation were analysed with the Alicona Inifite Focus G5 following the method in 3.2.5 Profile Analysis. Analysis was conducted to determine what uniformity could be achieved through inkjet printing. Figure 7-7bd shows how after thermal treatment the profiles of the printed films were highly curved. The domed profile is like a spherical cap for a single droplet, as it is the lowest energy state a thin film can adopt. This result suggests softening and flow of the polymer at this temperature.

The comparison of the untreated samples shows that increasing the substrate temperature directly increased the print fidelity. Figure 7-7ac shows that the samples printed onto the high temperature substrate have increased uniformity and decreased edge thickness. This result shows that the printing of simple geometry could be achieved without the use of support material.

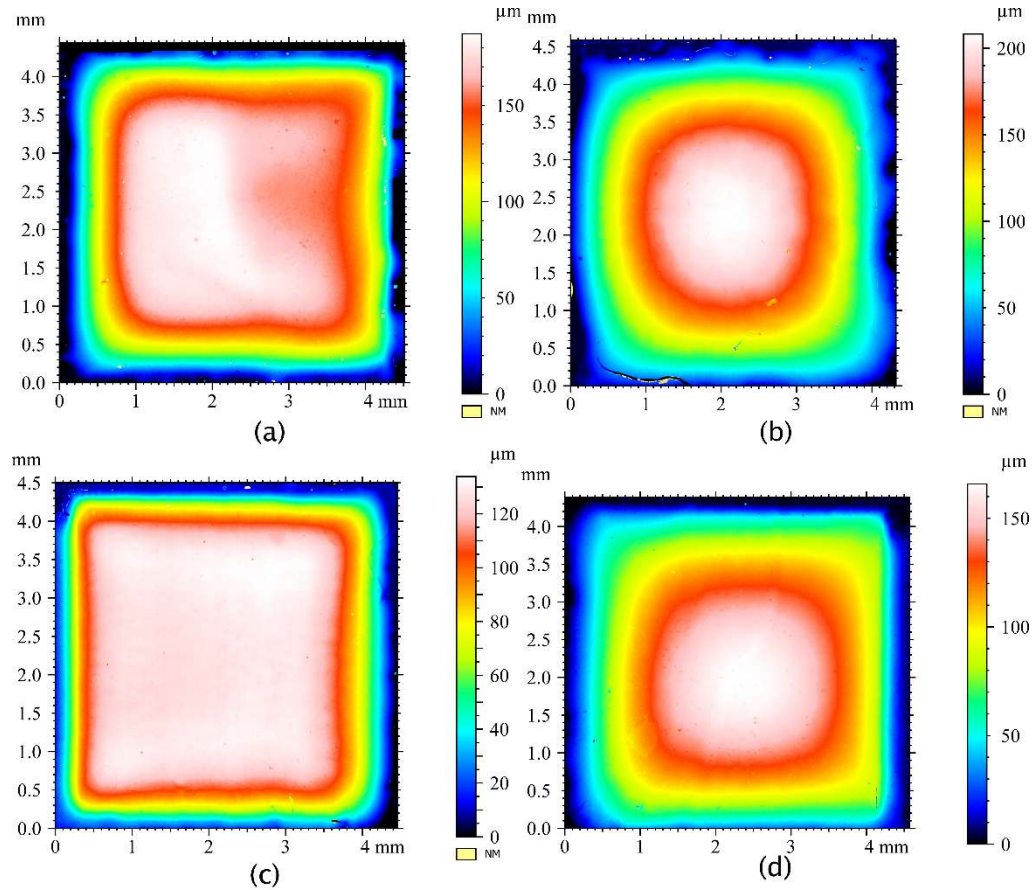


**Figure 7-7 - Printed miscible polyurethane sample profiles obtained through Alicona. Samples are: (a) 50 °C (b) 50 °C + 100 °C (c) 100 °C (d) 100 °C + 100 °C.**

The profile analysis was also used to determine the volume of the printed sample, and through this quantify the effect of evaporation. Figure 7-8 shows that there was considerable loss of volume when printing at the elevated temperature from 2.22  $\mu\text{L}$  to 1.78  $\mu\text{L}$ , a loss of 19.8%. Post heating of the sample printed at 50 °C also reflected this trend, but with a volume reduction of only 9.1 %. The increased volume loss of heating during printing was likely caused by the increased surface area. As the printing process exposes each printed layer to the environment instead of only the final top surface.

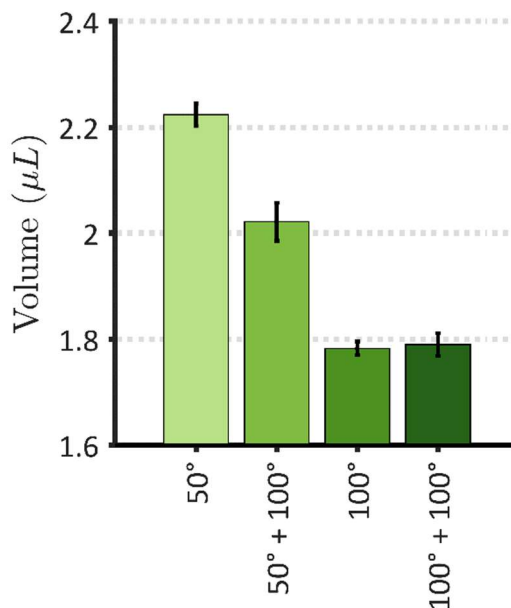


Figure 7-8 – Total volumes of printed samples for the miscible polyurethane profiles. Samples were printed onto a substrate of either 50 °C or 100 °C and post treatment at 100 °C was carried out on a subset.

## 7.2 Discussion

The focus of the miscible polyurethane work was to determine if by using miscible inks, and by having a mixing mechanism separate to the reaction, that higher conversion could be achieved. When selecting a suitable miscible monomer, vapour pressure was also considered, as an ink with reduced volatility would allow for greater substrate heating.

TPG was selected, as a monomer that was both miscible with the isocyanate, and offered a reduced vapour pressure compared to butanediol. The printing of pure TPG was achieved through thermal viscosity modification. The printable ink was highly reliable and no nozzle blockage occurred. TPG differed from the other hydroxyl group monomers used in this work because it has both a primary and secondary hydroxyl group. This structural difference would result in differing reactivities of the two groups which would have effects on overall reactivity and polymerisation.

With the miscibility of the inks, high degrees of mixing were achieved, and this highlighted an imbalance in the monomers. Initially an *in-*

*line* method for droplet volume determination was considered. This method used knowledge of the ink interaction with glass and the substrate camera to determine droplet volume. However, it was found that this method was unreliable due to the unpredictable wetting of the inks. Instead droplets were printed and weighed, although this method took longer, it was found to have increased reliability, with several results showing little variation. The results of droplet analysis found that the TPG ink was around 59% the mass of the isocyanate. Once the droplet ratio was corrected, and the substrate heating used, high degrees of conversion were possible. Polymers with  $M_n$  of over 10 000 Da were achieved. Through surface profile analysis it was found that increased substrate heating also increased the uniformity of the printed films. With the sample printed at 100°C showing only minimal edge effects.

There were issues from printing with a substrate temperature of 100°C, and to mitigate this an investigation of post thermal treatment was conducted. Samples were printed at a lower substrate temperature then post heated. It was found that although there was some effect of post treatment on the low temperature samples, the molecular weight was still lower. Also due to the high temperature of the substrate, polymer flow occurred which reduced the uniformity. These results suggest that a low substrate temperature cannot be used when high molecular weights are desired for this formulation.

NMR was conducted to confirm the presence of polyurethane bond and determine the degree of polyurea production. The presence of polyurea indicates that evaporation of the TPG occurred and the mixing ratio was imbalanced. The results were represented in relation to the signal of polyurethane protons to adjust for sample masses. In the samples printed at 100 °C polyurea was detected in increased amounts. The cause for the increase in polyurea after post

treating of the 100 °C is likely due to the evaporation of short chain polymers.

## 8 Discussion

In the chapters 4-6 the results of the investigation of Fully Reactive Inkjet Printing (FRIJP) were presented, involving firstly the crosslinking of polysiloxane based polymers (PDMS) and secondly the addition polymerisation of polyurethane. These two reactions schemes being chosen as they involve the combination of two different reactive species and produce no unwanted by-products. Although the general method for printing in all cases was FRIJP, differences were seen from the various chemistries, printing strategies, and process parameters investigated. In the following sections the critical process of mixing is firstly discussed for the various chemistries, followed by discussions of the effects of substrate heating, and in-process evaporation on the in-process reactions. As the ultimate aim of this work is to develop methods of printing precise 3D geometries, the final section in this chapter discussed the print profiles achieved.

### 8.1 Mixing in FRIJP

The main concern for FRIJP is achieving high mixing and curing degrees in the final part.<sup>64,97</sup> In FRIJP, with the absence of mechanical stirring, mixing is achieved through the dispersion of components and chemical diffusion. In this investigation mixing and curing were quantified in two different ways:

1. For the PDMS mixing was determined by the intensity of the residual hydride bond referenced to a calibration peak.
2. The polyurethane chemistry was assessed based on the chain lengths achieved during polymerisation.

Two different factors were analysed for the printing chemistries. With the PDMS, the printing strategy and print conditions were analysed,

whereas, with the polyurethane, investigations focused primarily on changing the monomers to achieve higher degrees of cure.

Initially it was found that the printed PDMS showed higher residual hydride than the calibration samples, showing peak Raman intensities of around 0.25 versus 0.175 (printed versus calibration Figure 5-10b). The droplet weights were analysed and it was found that the printed volume of ink A was lower than B. This result is in agreement with the findings of Reis<sup>40</sup>, as shown in Table 5-1, with the increased ink viscosity resulting in a reduced droplet volume. This resulted in a 14.6% excess of ink B, however, through changing the printing strategy and correcting for droplet volume (which increased hydride content) the excess hydride in the sample was reduced. The new, line based, strategy led to more complete mixing and, therefore, the hydride concentration was reduced. The final printed samples were found to closely match the hydride concentration found in mechanically mixed ones, with peak FTIR intensities around 0.20-0.25 versus 0.25 (printed versus calibration Figure 5-18). The reason this value was not zero is likely caused by the nature of reaction in crosslinked system, with the maximum limit not related to consumption of reactants, but due to the mobility of chains for further reaction.

It is known in the literature that typically polyurethane components are immiscible,<sup>14,89</sup> and that, without reaction, these components do not mix. In industrial and research polymerisation processes this is the reason for a pre-polymer method.<sup>86,100</sup> Such a prepolymer method is not suitable for inkjet printing as it would result in increased viscosities, instead it was found that selecting monomers suitable for reaction was crucial. The second limitation on mixing that was identified in this work was from the selection of short chain monomers that produced tightly packed and glassy polymer.

An attempt was made to print using the layer based approach, however, as shown in Figure 6-12b, it can be seen that in comparison to the line based strategy, much larger pores formed. It was apparent that the uncontrolled distribution of material, shown in Figure 5-5, that occurred with the PDMS samples was also present in this case. However, instead of the redistribution causing issues with the profile, the PU sample showed pores and cracking, a result of the volatile butanediol component not mixing, and instead evaporating.

Specifically, in the case of the butanediol printing it was found that pores were formed from the monomer separation and subsequent evaporation. This limitation is expected to be related to the molecular structure of the repeating units and due to the limited molecular diffusion. From the literature, and highlighted in Figure 2-18<sup>90</sup>, it was identified that in the immiscible case the monomers need to transport through the polymer interface to reach the reaction zone. The rate limiting step in this case would be the diffusion of monomers through the polymer. In the case of the butanediol based polymer it can be expected to be a very rigid and inflexible network that would greatly reduce diffusion rates. As the polymerisation continued and the thickness of this interface increased, the diffusion rate would be reduced and eventually diffusion would be too slow for reaction to proceed before evaporation. In these cases, it was found that pores formed. The removal of these pores when substrate heating was applied is likely caused by the rapid evaporation of the butanediol, as shown in Figure 6-16, where a volume loss of 47% was found.

The degree of polymerisation of the polyurethane was increased in this work through two different methods, the first method was to choose a formulation that was miscible before reaction, and the second was to choose a soft segment that had increased flexibility. In the first strategy, the mixing could occur before the reaction and facilitate a bulk scheme instead of an interfacial one. For the second

strategy, the increased flexibility of the polymer backbone would increase the flexibility of the polymer and at the molecular level increase the diffusion rates of the monomers.

Once increased mixing was achieved, issues were identified regarding the mixing ratio. Previously, in the butanediol printing the limit step was the mixing, but when the miscible tripropylene glycol was used (7 FRIJP of Polyurethane: Miscible Components) low molecular weights were the result of the incorrect mixing ratio. Through droplet volume determination the average molecular weight was increased, and once the ratio was corrected in this manner the formulation was again limited by the diffusion. In this case, however, it did not cause issues with mixing, but limited the maximum obtainable molecular weight. In this case, as the inks were readily mixing, substrate heating could be used with a reduced effect on the evaporation of the components, and through substrate heating to 100°C average molecular weights of over 10,000 were achieved. At this point, to increase the weight any further, either further heating or a change of formulation was required, and as there were printer issues with the substrate heating different formations were tested.

The most successful method for increasing the mixing and the molecular weight was using the longer chain polyethylene glycol. As well as producing the highest weight polymer it is also the formulation that was most similar to industrial chemistries, with the same formulation used in Cassagnau.<sup>102</sup> It was also the only polyurethane sample that was printed and able to be removed from the substrate without breaking, as shown in Figure 6-17. The increased flexibility of the polyethylene glycol in the formulation facilitated much greater degrees of cure, reaching a molecular number over 35,000. This value was achieved with only minimal substrate heating. With Carothers<sup>14</sup> equation, and assuming that the molecular weight was limited by the mixing ratio, we can calculate

that the two components were dispensed with less than 1% mass error.

As mentioned previously, in FRIJP there is no mechanical mixing of the printed samples, and initially this was a challenge that needed to be overcome. However, this work has shown that although there is not mixing after the components are brought together, the initial state at which the monomers mix is already a desirable arrangement. Through the use of inkjet printing heads with nozzle sizes around 21  $\mu\text{m}$  the in-flight drop sizes are also of the same order. This means for immiscible components an emulsion has already been created. In work relating to emulsion polymerisation of polyurethanes, Pearson<sup>89</sup>, showed that a stirring apparatus at 1800 and 2800 rpm produced monomer particles of 7 and 4.9  $\mu\text{m}$ . This work has shown that the distribution of components inherent in FRIJP can be suitable for complete mixing, but that it is highly dependent on the selected monomer.

## 8.2 Substrate heating

A factor that became apparent during course of the investigation was that of heating due to the exothermic PU reaction. Typical reactions of polyurethane in industry are conducted in either screw driven or single vessel stirred reactors.<sup>86</sup> In these cases, the mass of the reactants is similar or greater than the vessel, and they are often either heated or insulated to contain the heat from the reaction. In conducting FRIJP, individual droplets are printed in lines and in layers that react in stages, on either previously printed polyurethane or the glass substrate. These two cases are very different when considering the heat transfer in the process. In the manufacture of polyurethane, temperature rises of over 50  $^{\circ}\text{C}$  for the reaction vessel can be achieved, and in fact cooling is often employed to limit the reaction temperature to around 90-140  $^{\circ}\text{C}$ .<sup>86</sup> The printing in this investigation used only two nozzles, at around 3 kHz. At this rate,

with droplets of 10 ng in size, only 60  $\mu\text{g}$  of material is deposited in a second. This small amount of material coupled with a large contact area results in all the energy generated from the reaction quickly dispersing. Hence, there would be no expected heating of the sample.

This investigation found that in the case of the TPG-PU, substrate heating can increase the achieved weights of printed polyurethane. This effect has also been observed in BDO-PU, but as mixing was also temperature dependent the result is ambiguous. In this work the loss of the reaction energy to the surroundings led to the requirement of substrate heating to reach high degrees of polymerisation. However, there are many reactions which require careful control due to their exothermic nature, in these chemistries there is the possibility for increased control using FRIJP.

As stated previously, substrate heating was also used as a method to improve film formation through the increase of solidification rates. The PDMS chemistry contained a cross-linker, so that once reacted it would not re-melt. The polyurethanes were purposefully not thermosets, and included no cross-linking chemistry. As stated before this was done so that SEC and NMR could be conducted, and to demonstrate FRIJP processing of linear polymers. The substrate heating affected these two chemistries in different ways. In the PDMS the heating only increased the reaction rate, directly reducing the time to solidification. The polyurethane was however, more complex. Although the heating increased the reaction rate, there was no sharp liquid – solid transition. Instead the melt viscosity of the polyurethane was proportional to the molecular weight, and as the reaction proceeded the viscosity also increases. This meant that despite the reaction proceeding far enough for a solid at room temperature the polymer was still a viscous liquid at the printing temperature. Thompson,<sup>50</sup> showed how the viscosity of the liquid

affects line formation. This effect can be seen in the printed results of the PU-PEG-BDO, and the post treated results of the TPU-PU.

### 8.3 Evaporation

FRIJP has been called a process involving micron scale reaction vessels<sup>8</sup>, there is some truth in this but also particular issues with the process. Typical reaction vessels contain walls to keep the reactants contained, whereas, in this investigation considerable evaporation occurred at increased substrate temperatures. There are several factors that combine to exasperate the evaporation problem:

- Small scale droplets – high surface area to volume ratio.
- Heat losses – further substrate heating required.
- Monomers – typically low molecular weight leading to volatility.
- Reaction with moisture – requiring the drying of the printing environment, lowering the partial vapour pressure.

These factors combine to produce a high evaporation rate. This has a number of effects: in the PDMS it was, the desirable, evaporation of solvent; in PU-BDO it was the formation of pores; and in the printed PU-PEG-BDO a large polydispersity from the evaporation of the butanediol component.

One issue not encountered in the polyurethane printing that is present in bulk polyurethane polymerisation is reaction between water and isocyanate producing carbon dioxide. In this work, there was some evidence of polyurea formation in the NMR results from Chapter 7, however, no bubbles were identified in these samples. It may be possible that only a low amount of carbon dioxide was produced which was dissolved in the sample. However, it is more likely that due to the thin layers, around 4-7  $\mu\text{m}$ , that any gas produced was able to leave the liquid before solidification. Although the presence of polyurea is unwanted, the effect of this gas removal

means it would not greatly change the mechanical performance of the material.

#### 8.4 Printed Profiles

In this work the material has been deposited in reactive lines, where both components are printed at once. This allows for curing to occur in lines, which facilitates profile control through accelerated solidification. This printing strategy reduced the formation of pores in the BDO-PU, and reduced the residual hydride in the PDMS. However, the initial intention for this printing strategy was that it would allow greater three-dimensional profile control of the printed samples.

In material jetting for additive manufacturing, photo-curable and phase change inks are able to achieve controlled shapes because they have very short times to solidification.<sup>7</sup> For FRIJP to be used as a process without support structures, it also needs to show this. However, in cases where support structures are required, it would likely be a phase change or photo-curable ink, as used in Projet (wax support) or Objet (acrylate support).

In this work it was shown with the PDMS ink that controlled three dimensional geometries could be achieved using the line printing strategy. With the stepped ziggurat design (Figure 5-16) the profile variation using this strategy was greatly reduced compared to the layer method (Figure 5-9). This points to the line curing speed occurring at a similar rate to the printing speed. Throughout this work the profile has been used to estimate the curing speed in this way, i.e., a constant profile across printed lines has been interpreted as a curing speed greater than the printing speed. This has been demonstrated in the TPU-PU results, where printing at a substrate temperature of 100 °C produced a sample with a constant profile.

The PEG-PU profile results were dependent on the temperature the sample was printed at, as shown in Figure 6-18. For the low temperature case, there was significant profile asymmetry. Increasing the substrate temperature improved the uniformity of the profile, but this solution had limited applicability due to the printing issues previously discussed (Chapter 5). The asymmetric profiles seen at low temperature shows the material leading toward the edge that was last printed, this is similar to the case discussed and highlighted in Thompson<sup>50</sup> where a line that is printed will initially bulge and redistribution of the material will centre around this bulge. This is driven by the minimisation of energy through the increase of surface curvature, similar to how a single bubble with a greater radius is lower energy than two bubbles of the same total volume.

### 8.5 Unexpected Challenges

There were a number of challenges that were not considered at the beginning of this work, but became apparent through the course of the investigation. The three main challenges are listed below, of the three the last one has already been discussed.

1. **Low profile stability** *due to extended mixing times resulting from printing strategy*
2. **Incorrect mixing ratios** *due to differing droplet volumes caused by fluid viscosity*
3. **Incomplete mixing** *due to the chain flexibility of monomers*

The low-profile stability is a specific reference to the PDMS work that was printed in a layer strategy. Shown in Figure 5-5, is the result of printing a film of PDMS in two layers. The lack of curing led to uncontrolled redistribution of material. This challenge was solved in two ways, firstly by changing the printing pattern for the initial layers, termed microstructuring, as shown in Figure 5-6, and secondly by switching to a line based printing strategy. In this project the line based strategy showed improved results in all the FIRJP printing for

both the printed profiles and the chemical results. However, the microstructuring printing pattern that increased liquid pinning could be a useful strategy in other cases, typically where there is printing of only one material, or a material with a slow curing speed is used.

The incorrect mixing ratios were a result of the uncontrolled droplet volumes resulting from inkjet printing. Before chemical analysis was conducted and it was understood that there were printed imbalances, the differing droplet masses were not considered. However, due to the highly precise metering of reactants required for successful polyurethane printing this challenge became apparent. An optical strategy was trialled for droplet volume determination, but this method was too susceptible to measurement errors of surface contact angle. An ideal method would be droplet volume measurement using the drop watcher camera, but the modified printer could not conduct this. The method successfully used in this work involved printing 100 000 to 1 000 000 droplets into a DSC pan and weighing the result. However, once the actual droplet volume was calculated the printing pattern needed to be adjusted. In the printer used there was a resolution of 1 micron in both the X and Y direction. To achieve the accurate droplet ratios required for this project a supersampling method was employed which achieved an average fractional drop spacing by varying the spacing between two integer values. The details of this process are given in 4.1.4 Line Printing.

## 8.6 Summary and Novelty

This PhD aimed to use fully reactive inkjet printing to produce polymers on the substrate, with the goal of increasing the material choices available for material jetting. Two materials were chosen, PDMS and PU, due to their specific reaction chemistries. The addition reactions with no by-products are well suited for FRIJP, as

there is not method currently for purifying the samples during printing.

The novelty of this work is shown in how the initial aims were completed, the aims of this PhD were;

1. Advance the FRIJP process
2. Research FRIJP formulations
3. Demonstrate the capability of FRIJP
4. Characterise printed specimens

In covering the first aim a research focused multi-material printer was designed, the two primary features were; multi-material disposable print head cartridges, and the ability to select arbitrary mixing ratios not dependent on the printer's resolution. The developed printer facilitated rapid experimentation and process improvements throughout the investigation. Without this printer, and due to the costs associated with conventional piezo heads, the work in this project would have proceeded much slower. It would have likely revolved around a proxy analysis method for printing, that would require a further step to judge printability. A number of printing related process challenges would have likely not been encountered.

The second aim was completed when the formulations were developed based on the results from the FRIJP studies. Specifically when it was found that the polyurethane created from butanediol was forming brittle and hard samples, with low degrees of cure, alternative formulations were investigated. This work looked at two methods, increasing the miscibility of the two components, and increasing chain mobility during polymerisation. Although both methods showed increased curing, only the latter method produced the high chain lengths desirable in industry.

Until now, the literature has no examples of printed material jetted PDMS structures, or high molecular weight linear polyurethane. This is despite the fact that PDMS printing is theoretically possible through UV modification, and the polyurethane printing is possible through solvent based printing. For the case of the PDMS, the UV modification would reduce the optical clarity of the PDMS and reduce its chemical resistance. Based on previous work by Van Den Berg<sup>94</sup>, who printed polyurethane with 40% loading and a molecular weight of 1800, to print polyurethane with molecular weight of over 20,000 a decreased loading is to be expected and possible non-Newtonian printing effects. Through the use of FRIJP, chemically unmodified PDMS was possible which has the same optical clarity and chemical resistance as the non-printed formulation. The polyurethane was also possible with limited printing issues from the ink viscosity and with only 7.5% solvent (average of ink A and ink B).

The final aim was related to the current lack of analysis directly on printed samples. In previous work which suggested printed cross-linked polyurethane, Kröber<sup>9</sup>, there was no analysis on the sample that was printed, or proof that the solid was indeed polyurethane. In this work all chemical analysis was conducted on printed samples, including the NMR, FTIR, Raman, and SEC. Specifically interesting was the evidence from the NMR that only trace amounts of the polyurea was found in the printed samples. This was also backed by the result from SEC showing a molecular weight that was only possible if over 99% of the sample reacted. These chemical results on the printed samples are needed to show the capability of FRIJP, and to prove that FRIJP is a valid manufacturing method for multi-component inks.

## ***9 Conclusions and Future Work***

### **9.1 Conclusions**

The following points are taken from the total of this work, they are the conclusions of the FRIJP process, the specific conclusions of PDMS printing, and finally the conclusions from the work involving the polyurethane printing.

#### **9.1.1 Conclusions: FRIJP**

- FRIJP has been shown to increase the range of materials processable by material jetting, demonstrating for the first time both PDMS and linear polyurethane printing.
- FRIJP inks are typically slower to solidify than UV or solvent based inks, this means that the print strategy needs to be modified so that the desired profiles can be achieved.
  - In this work that meant changing the printing strategy so that two nozzles were aligned during a single pass.
  - This resulted in mixing of two components in around 0.3 seconds.
  - The decreased time to mixing had a direct effect over the printed PDMS sample, which resulted in improved layer uniformity and decreased residual crosslinker.
- Substrate heating or exothermic reactions resulted in droplet evaporation before curing.
  - Evaporation in FRIJP is very important issue, different components in each ink result in different evaporation rates.
  - Differing evaporation rates then result in changes in mixing ratio, which can directly reduce the maximum achievable molecular weight.

- Prior to conducting this research, the mixing in FRIJP was seen as the greatest challenge, however in this work it has found that this issue is related to the chosen inks, and not the printing process.
  - The use of the line based strategy meant that reaction could occur in lines, reducing monomer transport.
  - Reduction in monomer transport resulted in increased control of the mixing ratio across the sample.
  - The greatest increase in degree of mixing, and therefore the molecular weight of polyurethane samples, was achieved by changing the ink components.
  - The ejected drops from the print head were around 20  $\mu\text{m}$ , this was found to be suitable for full mixing to occur in the PDMS, TPG and PEG based polyurethane prints.

### 9.1.2 Conclusions: PDMS

- A stable FRIJP ink based around a two-part PDMS chemistry was developed and used for the first time to print PDMS with material jetting.
  - The catalyst and the cross-linker components were in separate inks to delay reaction until printing.
  - 40% loading was achieved with Octyl Acetate used as a solvent.
- Low degree of interaction between ink and substrate was encountered due to the long times to cure (layer strategy), however, these were solved using a microstructuring pattern.
  - Only the first layers with the microstructuring pattern were required for successive ink pinning.
  - The microstructuring method was carried out on the printer, removing the need for a secondary process or over coating as utilised in Kröber<sup>9</sup>.
- The long times to mixing in the layer printing method meant that printed films were non-uniform.

- Films showed a large degree of height variation.
- This variation was reduced with substrate heating.
- It is apparent that ink flow in the 2D plane resembled the line printing simulation and experiment found in Thompson<sup>50</sup>.
- The improved printer with the line based printing method greatly reduced the sample reflow.
  - This was achieved by reducing the time to mixing from around 120s to 0.3s.
  - The improved strategy resulted in constant height profiles on the printed ziggurat design.
  - It removed the need for the microstructuring pattern required in the layer printing process.
- It was found that with confocal Raman microscopy there were no material concentration gradients that would be indicative of mixing issues.
  - Only in one case was there a slight dependence of residual crosslink component on axial direction. This dependence was not found in the samples with elevated substrate heating.
- Through the use of FTIR it was determined that the samples printed with the line based strategy showed the lowest degree of residual cure.
  - Printed samples were found to have residual crosslink component which is the same as conventionally fabricated samples.
  - The improved distribution of material, and the facilitation of reaction in lines is likely the cause for the reduce hydride component.
  - The mass adjustment carried out resulted in samples with decreased residual crosslink component.

### 9.1.3 Conclusions: PU

- Despite other research in this area, this is the first time it has been proven that polyurethane can be manufactured using FRIJP.
  - Other research produced solid samples<sup>9</sup>, but it did not determine whether these were primarily monomers or contaminants (polyurea).
- This is the first time linear solid polyurethane samples were printed with the FRIJP method.
  - Through NMR and SEC the samples were confirmed to be polyurethane, crucially it was shown that a high degree of polymerisation was achieved.
  - In the case of the TPG polyurethane, NMR was used to determine low degrees of polyurea contamination.
- It was found that the selection of the monomers greatly affected the maximum achievable molecular weight.
  - Through the addition of PEG compared to purely BDO polyurethane, the molecular weight of samples was increased from less than 7000 to over 35000 M<sub>n</sub>.
- Through the use of substrate heating the molecular weights of the polymers could be varied.
  - Through sample heating a moderate increase in molecular weight was achieved with the BDO based polyurethane.
  - This method resulted in very high amounts of sample evaporation, which was determined by profile measurement.
- Issues in mixing of immiscible components has been observed *in-situ* with an optical camera.
  - With low molecular weight components the issues with immixing were apparent.

- The interface between the two monomers could be observed.
- Over time it was possible to see how the monomers reacted and how, in some cases, evaporation occurred.
- Two methods were trialled to increase the amount of mixing in FRIJP. These were; using a higher molecular weight ink, and by using miscible components.
  - The increased molecular weight of the monomer resulted in increased mixing of the samples. This is likely due to the increased diffusion possible with the flexible soft segment.
  - Monomers could be selected to be miscible before reaction, and in the case of the TPG based polyurethane this resulted in bulk reaction scheme as opposed to a interfacial one.

## **9.2 Future Work**

This PhD is one of the first works to investigate FRIJP in the robust manner required, not only determining printability but starting to interrogate the printed parts. Throughout this PhD improvements were made to the formulation or process dependent on the previous results. As such there is a lot of investigation still required.

### **9.2.1 Investigation of other poly-addition reactions**

Polyurethane is widely used in industrial applications, and every formulation is tailored to the application. This PhD has used relatively simple formulations, but more specific focus on an end product would allow for specific tuning of the component monomers. This process could also be extended to other poly-addition reaction schemes, one obvious choice is polyurea, however there are many more chemistries that could be trialled.

Polydimethylsiloxane and polyurethane are popular addition reactions, but there are a lot more chemistries out there that could be

investigated. These other systems are likely to have their own challenges, for example polyethylene is produced from the polymerisation of ethylene, a gas at room temperature. Whereas, polycarbonate is commonly produced from bisphenol A and a chloride or carbonate, the issue being that bisphenol A is a solid at room temperature with a melting point over 140 °C.

Despite this, further work to find FRIJP compatible inks is a good step toward further increasing the range of processable materials for material jetting additive manufacture.

### **9.2.2 Conduct mechanical analysis**

In this study the developed printer focused on minimising the cost of investigating inks. The printer only used two printing nozzles with relatively low speeds. The formulations of PDMS and PU-PEG-BDO are ideal candidates for further mechanical tests. However, to fabricate larger parts with these formulations machines with higher throughputs are recommended. Print heads with 128 or more nozzles are available and would facilitate larger samples printed at a faster rate.

### **9.2.3 Droplet diameter**

It was argued in this study that the only mixing mechanism in FRIJP is molecular diffusion, meaning that the mixing length is the most crucial parameter. With the Dimatix nozzle size of 21  $\mu\text{m}$  the dispersion of monomers was achieved. However, with the PU-BDO formulation this dispersion was not adequate for complete mixing. Industrial material jetting heads typically have nozzles that are twice as large. This could have a negative effect on the mixing and curing of the formulations, as an increased droplet size would increase the mixing length. This would need investigation before commercial adoption.

#### **9.2.4 Monomers as a support**

Due to nozzle failure or misalignment PEG ink was deposited in the incorrect area during printing. It was possible to selectively clean only the PEG from the printed sample using IPA as a solvent. Looking at the profile results of samples cleaned and not cleaned it was determined that the PEG component acted as a supporting material to the surrounding polyurethane. For the industrial production of polymers, and the fabrication of complex objects it is undeniable that a supporting material is required. If this supporting material is also used as part of the build material, then this would reduce the number of print heads required, or used for non-build production. This would then offset the need for multiple print heads of multi-ink printers over the conventional UV material jetting inks which have a print head for build material and a print head for support material.

#### **9.2.5 Functional grading**

In this study only two inks were printed together. Using the same process, with an increased number of heads, could facilitate the functional grading of the polymer. Possible grading could be conducted with cross-linker, multiple isocyanates, multiple diols, or even the combination of other soft segments. In essence you could print a part that was rigid and flexible, that was both a thermoplastic and thermoset, or that had both a hard shell and durable internal volume.

A multi-shot injection moulding process can achieve multiple plastic materials in a single part, however each component is moulded and cured before the next is added. If jetting was used, not only binary mix, but continually graded concentrations with complex boundaries could be created. In a single process a part could be printed with a rigid backbone which transitions to a softer more tactile grip. As it is an AM process these could be bespoke designs at no added cost.

## CHAPTER TEN

**10 References**

1. Sturgess, C., Tuck, C. J., Ashcroft, I. A. & Wildman, R. D. 3D reactive inkjet printing of polydimethylsiloxane. *J. Mater. Chem. C* **5**, 9733–9743 (2017).
2. Hart, L. R. *et al.* 3D Printing of Biocompatible Supramolecular Polymers and their Composites. *ACS Appl. Mater. Interfaces* **8**, 3115–3122 (2016).
3. Zhang, F. *et al.* Inkjet printing of polyimide insulators for the 3D printing of dielectric materials for microelectronic applications. *J. Appl. Polym. Sci.* **133**, 43361 (2016).
4. Xaar, T., Technology, T. F. & Xaar, T. Xaar 2001+. (2001).
5. Hopkinson, N., Hague, R. & Dickens, P. *Rapid Manufacturing: An Industrial Revolution for the Digital Age.* (Wiley, 2005).
6. ASTM International. *ASTM International Technical Committee F42 on Additive Manufacturing Technologies.* (2013).
7. Gibson, I., Rosen, D. W. & Stucker, B. *Additive Manufacturing Technologies.* (Springer US, 2010). doi:10.1007/978-1-4419-1120-9
8. Smith, P. J. & Morrin, A. Reactive inkjet printing. *J. Mater. Chem.* **22**, 10965 (2012).
9. Kröber, P., Delaney, J. T., Perelaer, J. & Schubert, U. S. Reactive inkjet printing of polyurethanes. *J. Mater. Chem.* **19**, 5234 (2009).
10. Sung, Y., Jeang, J., Lee, C. & Shih, W. Fabricating optical lenses by inkjet printing and heat-assisted in situ curing of

- polydimethylsiloxane for smartphone microscopy. *J. Biomed. Opt.* **20**, 47005 (2015).
11. Wijshoff, H. The dynamics of the piezo inkjet printhead operation. *Phys. Rep.* **491**, 77–177 (2010).
  12. Derby, B. Inkjet Printing of Functional and Structural Materials: Fluid Property Requirements, Feature Stability, and Resolution. *Annu. Rev. Mater. Res.* **40**, 395–414 (2010).
  13. İçten, E., Giridhar, A., Taylor, L. S., Nagy, Z. K. & Reklaitis, G. V. Dropwise additive manufacturing of pharmaceutical products for melt-based dosage forms. *J. Pharm. Sci.* **104**, 1641–1649 (2015).
  14. Charles E. Carraher, J. *Polymer Chemistry*. (2006).
  15. Gunasekera, D. H. A. T. *et al.* Three dimensional ink-jet printing of biomaterials using ionic liquids and co-solvents. *Faraday Discuss.* (2016). doi:10.1039/C5FD00219B
  16. He, Y., Wildman, R. D., Tuck, C. J., Christie, S. D. R. & Edmondson, S. An Investigation of the Behavior of Solvent based Polycaprolactone ink for Material Jetting. *Sci. Rep.* **6**, 20852 (2016).
  17. Park, B. K., Kim, D., Jeong, S., Moon, J. & Kim, J. S. Direct writing of copper conductive patterns by ink-jet printing. *Thin Solid Films* **515**, 7706–7711 (2007).
  18. Torrisi, F. *et al.* Inkjet-printed graphene electronics. *ACS Nano* **6**, 2992–3006 (2012).
  19. Lee, H.-H., Chou, K.-S. & Huang, K.-C. Inkjet printing of nanosized silver colloids. *Nanotechnology* **16**, 2436–2441 (2005).
  20. Chen, X., Ashcroft, I. A., Wildman, R. D. & Tuck, C. J. An

- inverse method for determining the spatially resolved properties of viscoelastic–viscoplastic three-dimensional printed materials. *Proc. R. Soc. A Math. Phys. Eng. Sci.* **471**, 20150477 (2015).
21. Kim, K., Ahn, S. Il & Choi, K. C. Direct fabrication of copper patterns by reactive inkjet printing. *Curr. Appl. Phys.* **13**, 1870–1873 (2013).
  22. Fathi, S. Fundamental Investigation on Inkjet Printing of Reactive Nylon Materials. *Journal 3* (2011).
  23. El-Molla, M. M. Synthesis of polyurethane acrylate oligomers as aqueous UV-curable binder for inks of ink jet in textile printing and pigment dyeing. *Dye. Pigment.* **74**, 371–379 (2007).
  24. He, Y. An Investigation of Inkjet Printing of Polycaprolactone Based Inks By. (2016).
  25. van der Bos, A. *et al.* Velocity Profile inside Piezoacoustic Inkjet Droplets in Flight: Comparison between Experiment and Numerical Simulation. *Phys. Rev. Appl.* **1**, 14004 (2014).
  26. Ohnesorge, W. Anwendung eines kinematographischen Hochfrequenzapparates mit mechanischer Regelung der Belichtung zur Aufnahme der Tropfenbildung und des Zerfalls flüssiger Strahlen. (University of California, 1937).
  27. Ohnesorge, W. ~V. Die Bildung von Tropfen an Düsen und die Auflösung flüssiger Strahlen. *Zeitschrift Angew. Math. und Mech.* **16**, 355–358 (1936).
  28. Munson, B. R., Okiishi, T. H., Huebsch, W. W. & Rothmayer, A. P. *Fundamentals of Fluid Mechanics*. (Wiley, 2012). doi:978-0-470-39881-4
  29. Fromm, J. E. A numerical study of drop-on-demand ink jets. *2d*

- Int. Colloq. Drops Bubbles* 54–62 (1982).
30. Fromm, J. E. Numerical Calculation of the Fluid Dynamics of Drop-on-demand Jets. *IBM J. Res. Dev.* **28**, 322–333 (1984).
  31. Reis, N. & Derby, B. Ink Jet Deposition of Ceramic Suspensions: Modeling and Experiments of Droplet Formation. *MRS Proc.* **625**, 117 (2000).
  32. Dong, H., Carr, W. W. & Morris, J. F. An experimental study of drop-on-demand drop formation. *Phys. Fluids* **18**, (2006).
  33. Basaran, O. A. Small-scale free surface flows with breakup: Drop formation and emerging applications. *AIChE J.* **48**, 1842–1848 (2002).
  34. Jang, D., Kim, D. & Moon, J. Influence of fluid physical properties on ink-jet printability. *Langmuir* **25**, 2629–2635 (2009).
  35. Wang, X., Carr, W. W., Bucknall, D. G. & Morris, J. F. High-shear-rate capillary viscometer for inkjet inks. *Rev. Sci. Instrum.* **81**, (2010).
  36. Reis, N., Ainsley, C. & Derby, B. Viscosity and Acoustic Behavior of Ceramic Suspensions Optimized for Phase-Change Ink-Jet Printing. *J. Am. Ceram. Soc.* **88**, 802–808 (2005).
  37. Hoath, S. D. *et al.* Links Between Ink Rheology, Drop-on-Demand Jet Formation, and Printability. *J. Imaging Sci. Technol.* **53**, 41208 (2009).
  38. Hoath, Stephen, D. *Fundamentals of Inkjet Printing*. (Wiley-VCH Verlag GmbH & Co. KGaA, 2016). doi:10.1002/9783527684724
  39. Tjahjadi, M., Stone, H. a. & Ottino, J. M. Satellite and

- subsatellite formation in capillary breakup. *J. Fluid Mech.* **243**, 297 (1992).
40. Reis, N., Ainsley, C. & Derby, B. Ink-jet delivery of particle suspensions by piezoelectric droplet ejectors. *J. Appl. Phys.* **97**, 94903 (2005).
  41. Morrison, N. F. & Harlen, O. G. Viscoelasticity in inkjet printing. *Rheol. Acta* **49**, 619–632 (2010).
  42. Hoath, S. D. *et al.* Inkjet printing of weakly elastic polymer solutions. *J. Nonnewton. Fluid Mech.* **205**, 1–10 (2014).
  43. A-Alamry, K., Nixon, K., Hindley, R., Odel, J. A. & Yeates, S. G. Flow-Induced Polymer Degradation During Ink-Jet Printing. *Macromol. Rapid Commun.* **32**, 316–320 (2011).
  44. McIlroy, C., Harlen, O. G. & Morrison, N. F. Modelling the jetting of dilute polymer solutions in drop-on-demand inkjet printing. *J. Nonnewton. Fluid Mech.* **201**, 17–28 (2013).
  45. Wheeler, J. S. R. *et al.* Effect of polymer branching on degradation during inkjet printing. *Polym. Degrad. Stab.* **128**, 1–7 (2016).
  46. Rioboo, R., Tropea, C. & Marengo, M. Outcomes From A Drop Impact On Solid Surfaces. *At. Sprays* **11**, 12 (2001).
  47. Mundo, C., Sommerfeld, M. & Tropea, C. Droplet-wall collisions: Experimental studies of the deformation and breakup process. *Int. J. Multiph. Flow* **21**, 151–173 (1995).
  48. Yarin, a. L. Drop Impact Dynamics: Splashing, Spreading, Receding, Bouncing.... *Annu. Rev. Fluid Mech.* **38**, 159–192 (2006).
  49. Oliver Brand (Editor), Gary K. Fedder (Editor), Christofer

- Hierold (Editor), Jan G. Korvink (Editor), Osamu Tabata (Editor), Patrick J. Smith (Series Editor), D. H. S. (Series E). *Inkjet-Based Micromanufacturing. Journal of Chemical Information and Modeling* **9**, (2012).
50. Thompson, A. B., Tipton, C. R., Juel, A., Hazel, A. L. & Dowling, M. Sequential deposition of overlapping droplets to form a liquid line. *J. Fluid Mech.* **761**, 261–281 (2014).
51. Stringer, J. & Derby, B. Formation and stability of lines produced by inkjet printing. *Langmuir* **26**, 10365–72 (2010).
52. Soltman, D. & Subramanian, V. Inkjet-printed line morphologies and temperature control of the coffee ring effect. *Langmuir* **24**, 2224–31 (2008).
53. Castrejón-Pita, J. R., Betton, E. S., Kubiak, K. J., Wilson, M. C. T. & Hutchings, I. M. The dynamics of the impact and coalescence of droplets on a solid surface. *Biomicrofluidics* **5**, 14112 (2011).
54. Roisman, I. . *et al.* Drop impact onto a dry surface: Role of the dynamic contact angle. *Colloids Surfaces A Physicochem. Eng. Asp.* **322**, 183–191 (2008).
55. Duineveld, P. C. The stability of ink-jet printed lines of liquid with zero receding contact angle on a homogeneous substrate. *J. Fluid Mech.* **477**, 175–200 (2003).
56. Deegan, R. D. *et al.* Capillary flow as the cause of ring stains from dried liquid drops. *Nature* **389**, 827–829 (1997).
57. de Gans, B.-J. & Schubert, U. S. Inkjet Printing of Well-Defined Polymer Dots and Arrays. *Langmuir* **20**, 7789–7793 (2004).
58. Hu, H. & Larson, R. G. Marangoni effect reverses coffee-ring depositions. *J. Phys. Chem. B* **110**, 7090–4 (2006).

59. de Gans, B. J., Duineveld, P. C. & Schubert, U. S. Inkjet Printing of Polymers: State of the Art and Future Developments. *Adv. Mater.* **16**, 203–213 (2004).
60. Kwakkel, M., Breugem, W.-P. & Boersma, B. J. Extension of a CLSVOF method for droplet-laden flows with a coalescence/breakup model. *J. Comput. Phys.* **253**, 166–188 (2013).
61. QIAN, J. & LAW, C. K. Regimes of coalescence and separation in droplet collision. *J. Fluid Mech.* **331**, 59–80 (1997).
62. Ashgriz, N. & Poo, J. Y. Coalescence and separation in binary collisions of liquid drops. *J. Fluid Mech.* **221**, 183 (1990).
63. Sellier, M. & Treluyer, E. Modeling the coalescence of sessile droplets. *Biomicrofluidics* **3**, 22412 (2009).
64. Castrejón-Pita, J. R., Kubiak, K. J., Castrejón-Pita, a. a., Wilson, M. C. T. & Hutchings, I. M. Mixing and internal dynamics of droplets impacting and coalescing on a solid surface. *Phys. Rev. E* **88**, 23023 (2013).
65. Dong, H., Carr, W. W., Bucknall, D. G. & Morris, J. F. Temporally-resolved inkjet drop impaction on surfaces. *AIChE J.* **53**, 2606–2617 (2007).
66. Jo, B. H., Van Lerberghe, L. M., Motsegood, K. M. & Beebe, D. J. Three-dimensional micro-channel fabrication in polydimethylsiloxane (PDMS) elastomer. *J. Microelectromechanical Syst.* **9**, 76–81 (2000).
67. Camou, S., Fujita, H. & Fujii, T. PDMS 2D optical lens integrated with microfluidic channels: principle and characterization. *Lab Chip* **3**, 40–45 (2003).
68. Cai, Z., Qiu, W., Shao, G. & Wang, W. Sensors and Actuators A :

- Physical A new fabrication method for all-PDMS waveguides. *Sensors Actuators A. Phys.* **204**, 44–47 (2013).
69. Chang-yen, D. A., Eich, R. K. & Gale, B. K. A Monolithic PDMS Waveguide System Fabricated Using Soft-Lithography Techniques. **23**, 2088–2093 (2005).
70. Kopetz, S., Cai, D., Rabe, E. & Neyer, A. PDMS-based optical waveguide layer for integration in electrical – optical circuit boards. **61**, 163–167 (2007).
71. Noll, W. Chemistry and Technology of Silicones. 716 (1968). doi:10.1016/B978-0-12-520750-8.50025-7
72. Friend, J. & Yeo, L. Fabrication of microfluidic devices using polydimethylsiloxane. *Biomicrofluidics* **4**, 1–5 (2010).
73. Kirikova, M. N. *et al.* Direct-write printing of reactive oligomeric alkoxy silanes as an affordable and highly efficient route for promoting local adhesion of silver inks on polymer substrates. *J. Mater. Chem. C* **4**, 2211–2218 (2016).
74. Sun, J. *et al.* Fabrication of Bendable Circuits on a Polydimethylsiloxane (PDMS) Surface by Inkjet Printing Semi-Wrapped Structures. *Materials (Basel)*. **9**, 253 (2016).
75. De Paz, M. V., Zamora, F., Begines, B., Ferris, C. & Galbis, J. A. Glutathione-mediated biodegradable polyurethanes derived from L-arabinitol. *Biomacromolecules* **11**, 269–276 (2010).
76. Begines, B., Zamora, F., Roffé, I., Mancera, M. & Galbis, J. A. Sugar-based hydrophilic polyurethanes and polyureas. *J. Polym. Sci. Part A Polym. Chem.* **49**, 1953–1961 (2011).
77. Zlatanovic, A., Lava, C., Zhang, W. & Petrovic, Z. S. Effect of Structure on Properties of Polyols and Polyurethanes Based on Different Vegetable Oils. *J. Polym. Sci. Part B Polym. Phys.* **42**,

- 809–819 (2004).
78. Guo, A., Demydov, D., Zhang, W. & Petrovic, Z. S. Polyols and polyurethanes from hydroformylation of soybean oil. *J. Polym. Environ.* **10**, 49–52 (2002).
79. Takahashi, T., Hayashi, N. & Hayashi, S. Structure and properties of shape-memory polyurethane block copolymers. *J. Appl. Polym. Sci.* **60**, 1061–1069 (1996).
80. Guan, J., Fujimoto, K. L., Sacks, M. S. & Wagner, W. R. Preparation and characterization of highly porous, biodegradable polyurethane scaffolds for soft tissue applications. *Biomaterials* **26**, 3961–3971 (2005).
81. Ionescu, M. *Chemistry and Technology of Polyols for Polyurethane*. (2008). doi:10.1002/pi.2159
82. Wu, Z. *et al.* The effects of polydimethylsiloxane on transparent and hydrophobic waterborne polyurethane coatings containing polydimethylsiloxane. *Phys. Chem. Chem. Phys.* **16**, 6787–94 (2014).
83. Young, R.J.; Lovell, P. A. *Introduction to polymers, third edition*. (2011).
84. Ebewele, R. *Polymer Science and Technology*. (CRC Press, 2000). doi:10.1201/9781420057805
85. Prisacariu, C. *Polyurethane Elastomers From Morphology to Mechanical Aspects*. (Springer Vienna, 2011). doi:10.1007/978-3-7091-0514-6
86. Clemitson, I. R. *Castable Polyurethane Elastomers, Second edition*. (2015).
87. Verhoeven, V. W. A. The reactive extrusion of thermoplastic

- polyurethane. *Int. Polym. Process.* **21**, 158 (2006).
88. Morgan, P. W. *Condensation polymers: by interfacial and solution methods.* **10**, (Interscience Publishers, 1965).
  89. Pearson, R. G. & Williams, H. L. Interfacial polymerization of an isocyanate and diol. *J. Polym. Sci.* **23**, 9–18 (1985).
  90. Dhumal, S. S., Wagh, S. J. & Suresh, a. K. Interfacial polycondensation-Modeling of kinetics and film properties. *J. Memb. Sci.* **325**, 758–771 (2008).
  91. Fields, S. D., Thomas, E. L. & Ottino, J. M. Visualization of interfacial urethane polymerizations by means of a new microstage reactor. *Polymer (Guildf).* **27**, 1423–1432 (1986).
  92. Wickert, P. D., Ranz, W. E. & Macosko, C. W. Small scale mixing phenomena during reaction injection moulding. *Polymer (Guildf).* **28**, 1105–1110 (1987).
  93. Machuga, S. C., Midje, H. L., Peanasky, J. S., Macosko, C. W. & Ranz, W. E. Microdispersive interfacial mixing in fast polymerizations. *AIChE J.* **34**, 1057–1064 (1988).
  94. van den Berg, A. M. J. *et al.* Inkjet printing of polyurethane colloidal suspensions. *Soft Matter* **3**, 238 (2007).
  95. Hung, K. C., Tseng, C. S. & Hsu, S. H. Synthesis and 3D Printing of biodegradable polyurethane elastomer by a water-based process for cartilage tissue engineering applications. *Adv. Healthc. Mater.* **3**, 1578–1587 (2014).
  96. Hernández-Córdova, R. *et al.* Indirect three-dimensional printing: A method for fabricating polyurethane-urea based cardiac scaffolds. *J. Biomed. Mater. Res. - Part A* 1912–1921 (2016). doi:10.1002/jbm.a.35721

97. Fathi, S. & Dickens, P. Challenges in drop-on-drop deposition of reactive molten nylon materials for additive manufacturing. *J. Mater. Process. Technol.* **213**, 84–93 (2013).
98. Lai, Y.-H., Hsu, M.-H. & Yang, J.-T. Enhanced mixing of droplets during coalescence on a surface with a wettability gradient. *Lab Chip* **10**, 3149–3156 (2010).
99. Cai, D., Neyer, A., Kuckuk, R. & Heise, H. M. Raman , mid-infrared , near-infrared and ultraviolet – visible spectroscopy of PDMS silicone rubber for characterization of polymer optical waveguide materials. *J. Mol. Struct.* **976**, 274–281 (2010).
100. Seneker, S. D., Born, L., Schmelzer, H. G., Eisenbach, C. D. & Fischer, K. Diisocyanato Dicyclohexylmethane - Structure Property Relationships of Its Geometrical-Isomers in Polyurethane Elastomers. *Colloid Polym. Sci.* **270**, 543–548 (1992).
101. Desmodur W, Product Datasheet.
102. Puaux, J. P., Cassagnau, P., Bozga, G. & Nagy, I. Modeling of polyurethane synthesis by reactive extrusion. *Chem. Eng. Process. Process Intensif.* **45**, 481–487 (2006).
103. Cassagnau, P., Nietsch, T. & Michel, A. Bulk and Dispersed Phase Polymerization of Urethane in Twin Screw Extruders. *Int. Polym. Process.* **14**, 144–151 (1999).
104. Nigar, M., Blackwell, J., Seneker, S. D. & Schmelzer, H. G. The structure of the hard domains in frans,frans-HMDI-based polyurethane elastomers. *Acta Polym.* **47**, 48–54 (1996).
105. Saralegi, A. *et al.* Effect of H12MDI isomer composition on mechanical and physico-chemical properties of polyurethanes based on amorphous and semicrystalline soft segments. *Polym.*

- Bull.* **70**, 2193–2210 (2013).
106. Rosthauser, J. & Haider, K. Mechanical and dynamic mechanical properties of polyurethane and polyurethane/polyurea elastomers based on 4,4'-diisocyanatodicyclohexyl methane. *J. Appl. Polym. Sci.* **64**, 957–970 (1997).
  107. Tsui, Y. K. & Gogolewski, S. Microporous biodegradable polyurethane membranes for tissue engineering. *J. Mater. Sci. Mater. Med.* **20**, 1729–1741 (2009).
  108. Sids, O., Glycol, T. & Publications, U. TRIPROPYLENE GLYCOL CAS N ° : 24800-440. 1–35
  109. Magenau, A. J. D., Richards, J. A., Pasquinelli, M. A., Savin, D. A. & Mathers, R. T. Systematic Insights from Medicinal Chemistry To Discern the Nature of Polymer Hydrophobicity. *Macromolecules* **48**, 7230–7236 (2015).
  110. Sharmin, E. & Zafar, F. Polyurethane : An Introduction. 3–16 (2012).
  111. Niyogi, S., Sarkar, S. & Adhikari, B. Catalytic activity of DBTDL in polyurethane formation. *Indian J. Chem. Technol.* **9**, 330–333 (2002).
  112. Li, Z. F. *et al.* Investigation of effects of dibutyltin dilaurate on reaction injection molding polyurethane-urea kinetics, morphology and mechanical properties by in situ FTIR. *Front. Mater. Sci. China* **2**, 99–104 (2008).
  113. Solis-Correa, R. E. *et al.* Synthesis of HMDI-based segmented polyurethanes and their use in the manufacture of elastomeric composites for cardiovascular applications. *J. Biomater. Sci. Polym. Ed.* **18**, 561–578 (2007).

114. Jettable Fluid Formulations Guidelines. Jettable Fluid Formulations Guidelines. Available at: [https://www.fujifilmusa.com/shared/bin/Dimatix\\_Materials\\_Printer\\_Jettable\\_Fluid\\_Formulation\\_Guidelines\\_05-13.pdf](https://www.fujifilmusa.com/shared/bin/Dimatix_Materials_Printer_Jettable_Fluid_Formulation_Guidelines_05-13.pdf). (Accessed: 1st April 2016)
115. Stauffer, C. E. The Measurement of Surface Tension by the Pendant Drop Technique. *J. Phys. Chem* **69**, 1933–1938 (1965).
116. Ambwani, D. S. & Fort, T. in *Surface and Colloid Science: Volume 11: Experimental Methods* (eds. Good, R. J. & Stromberg, R. R.) 93–119 (Springer US, 1979). doi:10.1007/978-1-4615-7969-4\_3
117. Dimatix Materials Printer, FUJIFILM, Operator's Manual.
118. Sreenivasan, K. Crosslinking effect of hard segment domains on the diffusion of lipids through polyurethanes based on H12MDI. *J. Macromol. Sci. Part B* **32**, 125–129 (1993).
119. EDU170 Ndrive HP102030, Aerotech Ltd, Manual.
120. Pielichowski, K. & Flejtuch, K. Differential Scanning Calorimetry Studies on Poly ( ethylene Glycol ) with Different Molecular Weights for Thermal Energy Storage Materials †. **696**, 690–696 (2003).

